Monthly Scientific-Technical and Production Journal

The Paton WELDING JOURNAL

January 2003 # 1

English translation of the monthly «Avtomaticheskaya Svarka» journal published in Russian since 1948

Founders: *The E.O. Paton Electric Welding Institute of the NAS of Ukraine*
International Association «Welding»

Publisher: *International Association «Welding»*

Editorial and advertising offices:
E.O. Paton Electric Welding Institute,
International Association «Welding»,
11, Bozhenko str., 03680, Kyiv, Ukraine
Tel.: (38044) 227 67 57
Fax: (38044) 268 04 86
E-mail: journal@paton.kiev.ua
http://www.nas.gov.ua/pwj

State Registration Certificate
KV 4790 of 09.01.2001

Subscriptions:
$460, 12 issues per year,
postage and packaging included.
Back issues available

CONTENTS

To 100th birthday anniversary of Professor Georgy A. Nikolaev

Georgy Aleksandrovich Nikolaev was born in 1903. In 1925 he graduated from the Institute of Transportation Engineers and in 1928 from the Mechano-Mathematical Department of the Moscow State University. In 1934 he was advanced to the academic title of Professor, in 1939 he was given the degree of Doctor of Science (Eng.).

G.A. Nikolaev began the engineering and scientific work from 1925, and pedagogical activity from 1930. In 1938 he became Dean of Mechano-Technological Department. From 1939 to 1964 he was Pro-Rector for Research, and from 1964 to 1985 — Rector of N.E. Bauman Moscow Higher Engineering College (MHEC). In 1940–1947 he was Head of the Chair of Materials Resistance, and from 1947 to 1989 — Head of the Chair of Machines and Automation of Welding Processes.

G.A. Nikolaev is an outstanding scientist, who contributed fundamental theoretical and experimental investigations to the progress of science. He gave a lot of attention to problems of strength and performance of welded structures, as well as development of codes for their design. His profound studies of inherent stresses and strains of welded structures formed the base for a number of new areas of welding science and a theoretical and practical base for broad acceptance of welding in various sectors of national economy. The first welded railway bridges were constructed with his participation.

During the Second World War G.A. Nikolaev made a great contribution into application of welding in arms manufacturing.

Starting from 1946, G.A. Nikolaev began developing welding and brazing technologies, in particular, advanced processes of joining metals and non-metals. Under direct leadership of G.A. Nikolaev and with his participation outstanding results were achieved in development of fundamentally new processes of vacuum welding, ultrasonic welding and cutting of non-metallic materials. In 1972 G.A. Nikolaev was awarded the State Prize and Inventor's Diploma for his work on welding and cutting biological tissues, in particular ultrasonic cutting which became widely accepted in surgery.

For outstanding achievements in development of material processing technology G.A. Nikolaev was elected in 1970 the Corresponding Member and in 1979 the full Member of the USSR Academy of Sciences in the Division of Physical Chemistry and Technology of Inorganic Materials.

G.A. Nikolaev is the founder and leader of a major scientific school of welders. In the period from 1935 and 1982 more than 90 theses of Candidate of Science and 20 theses of Doctor of Science were prepared and successfully defended under his leadership. In the scientific area, led by G.A. Nikolaev, 20 monographs and manuals were written and published over the last 15 year by just the staff of the Chair of Welding of N.E. Bauman MHEC.

G.A. Nikolaev has more than 350 publications. These include handbooks and manuals for colleges on design of welded structures, monographs on strength and advanced welding processes. A number of publications have been translated into English, French, German, Check, Polish, Hungarian, Rumanian and Chinese languages.

G.A. Nikolaev gave a lot of his attention to development of the technology of joining metallic materials, strength of welded structures and automation of welding processes. Work, performed by the Chair, headed by him, was awarded Lenin and other State Prizes, six Prizes of USSR Soviet of Ministers and two Lenin Komsomol Prizes.

Scientific areas, initiated by G.A. Nikolaev, such as ultrasound application for treatment of biotissues and laser systems were the basis for establishing two new chairs at MHEC.

In 1967 he was elected Deputy of the Supreme Soviet of the Russian Federation. He was Deputy Chairman of the Commission on Public Education, Science and Culture of the Supreme Soviet of the Russian Federation. Since 1965 he was several times elected a member of Moscow City and Bauman District Communist Party Committees. He was elected delegate to several congresses of the Communist Party of the Soviet Union.

G.A. Nikolaev was awarded three orders of Lenin, order of October Revolution, four orders of Labour Red Banner, Order of Merit and five medals of the USSR. In 1969 G.A. Nikolaev was awarded the title of Hero of Socialist Labour for his great contribution to development of Soviet science.

Editorial Board of «The Paton Welding Journal»

FAMOUS SCIENTIST, ENGINEER, TEACHER*

Prof. Boris E. PATON

The beginning of scientific and teaching activity of Prof. Georgy Nikolaev coincided with the historical period of transition to the industrializing of the USSR and welding implementation in the industrial construction. Some methods of arc, resistance, gas and thermal welding started their use in small volumes, however, the problem of development of reliable weldments as a final aim of the welding industry had not been yet solved successfully.

G.A. Nikolaev became one of the founders of science of strength of welded structures, carrying out research works in welding stresses and strains in particular. The scientific achievements of the young scientist were based on his interest to welding and good engineering education, which he received at Moscow Institute of Transport Engineers, where Prof. Evgeny O. Paton was a teacher earlier, and then at Moscow State University, where G.A. Nikolaev studied the theory of strength. His research works cleared the way for welding application in manufacture of such critical engineering constructions as railway bridges.

Since the 1930s G.A. Nikolaev was developing the methods of design of strength and designing of welded structures, and also methods of calculation and determination of welding stresses and strains which were included into standardized documentation, manuscripts and manuals. Even at the beginning of the scientific activity G.A. Nikolaev carried out a lot of works on testing welded joints and sub-assemblies, study of distribution of stresses in welds, strengthening of worn-out bridges by welding, designing of welded spans of bridges, compiling of the first technical specifications for designing spans of railway bridges in the USSR.

A great attention was paid by G.A. Nikolaev to the analysis of causes of failure and to the solution of problems of assurance of welded structure reliability by the parameter of a probability of a failure-free operation in service until reaching the limiting state. G.A. Nikolaev was the first who came to the conclusion that these problems should be solved not only taking into consideration the technologies of manufacture, but also with account for achievements in

Delegation of specialists-welders of the USSR in Austria, 1958. At the top 5th on the left — Prof. G. Nikolaev

* From the speech at the opening of the All-Russian Conference on Welding at the Transition of Centures, Jan. 20–21, 2003. N.E. Bauman MHTC, Moscow.

Prof. G. Nikolaev is consulting students, 1940

science in the field of metallurgy, metals science, strength, theory of elasticity and plasticity, fracture mechanics. These trends of investigations found their development in works of numerous pupils and successors of G.A. Nikolaev.

G.A. Nikolaev and his pupils paid also a great attention to the solution of problem of strength of welded joints at alternating loads. Investigations and generalizations made under his supervision reflected general regularities in change of fatigue resistance of welded joints, included approaches to applying rates of allowable stresses in fatigue life calculations and analyzed the ways of improving fatigue resistance of the joints.

Moreover, the name of G.A. Nikolaev is associated with a number of successful works on vacuum welding, ultrasonic welding and cutting of non-metallic materials, in particular biological tissues.

The works of Prof. Nikolaev have a great importance also for the solution of modern problems of evaluation and extension of service life of welded structures. These problems acquired a special actuality due to the fact that many constructions, machines and equipment, being now under the service in CIS countries, have already exhausted their design period of life.

G.A. Nikolaev was also a talented and well-known teacher, who made a great contribution to the education of highly-qualified specialists. Exactly 70 years ago he was given his first post-graduate student, and, in total, more than about hundred of candidate's and more than 20 doctor's scientific theses were made under his supervision. The well-known scientific school of G.A. Nikolaev was created. Among his pupils, there are outstanding scientists, leaders of enterprises, research institutions, high educational institutions and chairs in many countries. And, if to take into account that during decades all the future welding engineers were educated by his manuals, and again in many countries, then the contribution of Georgy Nikolaev is extremely valuable.

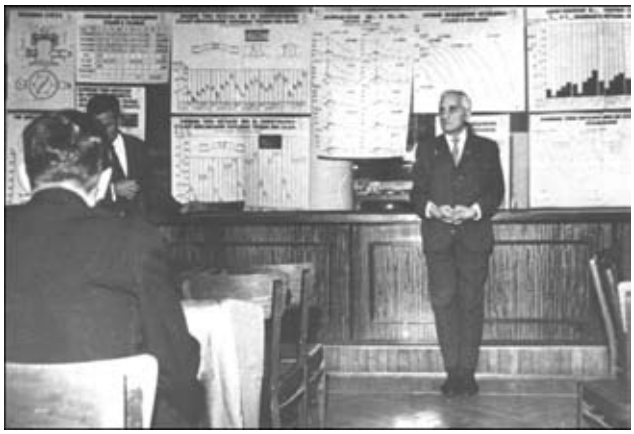

Prof. G. Nikolaev at the defense of thesis, 1975

His work in the Higher Attestation Commission, in Commission on People's Education of the Supreme Soviet of Russian Federation, in the Council of Rectors of high educational institutions of Moscow can be added to all the above-mentioned.

All the people, communicating with him, were conquered by his intellectuality, refinement, genuine interest to the history. During every visit to Kiev he was having a walk in the historical streets, visited museums. Once, he spent the whole day in the museum under the open sky — Museum of Architecture and Mode of Life in Ukraine. Those, who accompanied him and did not know about his passion for mounting-skiing and climbing, were surprised of his endurance and indomitable energy. Every time, when Georgy Aleksandrovich came to Kiev, he was met at the railway terminal and he refused always to take the Institute's car and, passing several kilometers to the E.O. Paton Electric Welding Institute, he climbed on foot to the 10th floor («Director's floor»), even being ahead of those who met him at the entrance. Many patonovites knew Georgy Aleksandrovich as a fervent follower of a healthy, sporting way of life, an antagonist of alcohol and smoking. I think it is no mere chance that among the graduates of N.E. Bauman Moscow Higher Technical College (MHTC) there are several cosmonauts and famous sportsmen, i.e. people who received not only education in one of the most «difficult» and prestigious higher educational institutions of the country, but possessed also an excellent health. Among these graduates, cosmonaut Svetlana Savitskaya, is the woman who could master the technology of welding and spraying in open space using a versatile hand tool.

It is necessary to outline specially a great contribution of Georgy A. Nikolaev to the establishment and strengthening of interstate and international cooperation of scientists and specialists working in the field of welding and related technologies. He was a member of the National Committee of the USSR on Welding and represented it with dignity at the International Institute of Welding.

Several decades Prof. Nikolaev was a member of bureau of the Scientific and Coordination Councils on Welding at the USSR State Committee on Science and Technology, participated in organizing, creating and fulfillment of a number of national integrated programs for development of welding industry, sci-

ence and technology in the field of welding in the country. It is nice to outline that owing to the efforts of G.A. Nikolaev the close scientific-technical relations were established between N.E. Bauman MHTC and scientists and specialists of Ukraine, and first of all, the fruitful cooperation with the E.O. Paton Electric Welding Institute of the National Academy of Sciences of Ukraine.

G.A. Nikolaev knew well main European languages. It is remembered, for example, that at the opening of the International Conference devoted to the jubilee of Evgeny Paton, Georgy Aleksandrovich made a speech in Russian, English, German and French. His emotional speech was met by continuous applause and set the pitch of the conference. His scientific papers at symposia, congresses and conferences were welcomed, characterized by argumented and at the same time simple interpretation. He was born a lecturer, scientist-popularizer of science. Several times, by my request, he made reports like the educational lectures for the staff of the PWI. These lectures, delivered in an over-crowded conference-hall were very lively, and I think, very useful for our staff.

Results of research and pedagogical activity of G.A. Nikolaev continue to be used for the development of welding science and the school, based by him will, undoubtedly, continue to enrich the welding science and technology with new remarkable achievements, promote the scientific-technical progress in the new XXI century, passing the threshold of centuries.

In the last century, we, representatives of leading scientific-technical schools, managed to solve many complicated scientific, engineering and organizing problems. However, the science, technology and production are facing now the more and more new problems. It would be necessary for us, welders, to explore the space and sea depths, to manufacture structures operating at superhigh pressures, ultralow and superhigh temperatures in vacuum and aggressive media, to create and use the new materials. It is better to solve all these problems together by exchanging experience and opinions, by uniting efforts of creative teams. In this connection, the earnest scientific conferences are very useful which can not only summarize and present the results of investigations and developments, but also outline the future trends.

PROSPECTS FOR APPLYING PHOSPHORUS IN IRON-BASE SURFACING CONSUMABLES (REVIEW)

I.I. RYABTSEV and **Yu.M. KUSKOV**
The E.O. Paton Electric Welding Institute, NASU, Kyiv, Ukraine

Analysis of literature data on the effect of phosphorus on mechanical and service properties of steels and cast irons has been conducted. It is shown that phosphorus is a candidate alloying element for surfacing consumables intended for repair and hardening of parts operating under metal against metal friction conditions.

Key words: *steel, cast iron, phosphorus alloying, phosphide eutectics, mechanical properties, surfacing consumables*

Phosphorus is rather common in nature — it takes up about 0.04 % of the total mass of the earth's crust. The main raw material to obtain phosphorus and its compounds are phosphites and apatites. Ferrophosphorus and ferromanganophosphorus are produced on industrial scale by blast furnace melting. These alloys are used in metallurgy for alloying and deoxidation of special steels and cast irons.

Data on phosphorus solubility in iron are contradictory. Author of [1] states that at room temperature the weight fraction of phosphorus, dissolved iron with solid solution formation, may be up to 1.2 %. According to other works [2] at room temperature phosphorus practically does not dissolve in iron, forming FeP, Fe_2P, Fe_3P phosphides, and only at high temperatures the weight fraction of phosphorus dissolved in iron may be up to 0.6 %. In [3] it is noted that at solidification of steels and cast irons with this element content of 0.05–0.50 % a ternary phosphide eutectic usually forms, which has a melting temperature of 950 °C and consists of cementite, Fe_3P phosphide and austenite (ferrite). At a higher content of phosphorus, a double phosphide eutectic (phosphide–ferrite, phosphide–austenite) may form, alongside the ternary eutectic.

This review presents data on phosphorus influence on the properties of steels and cast irons, and analyzes the prospects for its use as an alloying element in surfacing consumables.

Phosphorus influence on the properties of steels. Phosphorus in small amounts is contained practically in all the commercial steels and cast irons, where it almost always is an undesirable impurity. It is prone to intercrystalline segregation, leading to deterioration of ductile characteristics of steels, particularly at lower temperatures. For this reason, the weight fraction of this element in high-quality Fe-base alloys is limited by 0.03 % [4]. Nonetheless, it is known [5–7] that phosphorus increases the strength of iron and steel to a greater extent than silicon, manganese, molybdenum, chromium, vanadium and some other elements (Figures 1 and 2). Steels with a higher content of phosphorus also have anticorrosion properties [6, 8] and quite good magnetic characteristics [9, 10].

On the other hand, when the simultaneous influence of phosphorus and carbon on impact toughness

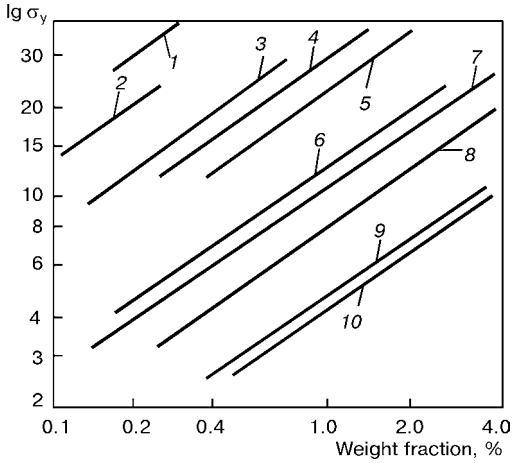

Figure 1. Influence of the content of various alloying elements on α-iron yield point σ_y: *1* — Be; *2* — P; *3* — Cu; *4* — Si; *5* — Ti; *6* — Mn; *7* — Ni; *8* — V; *9* — Co; 10 — Cr

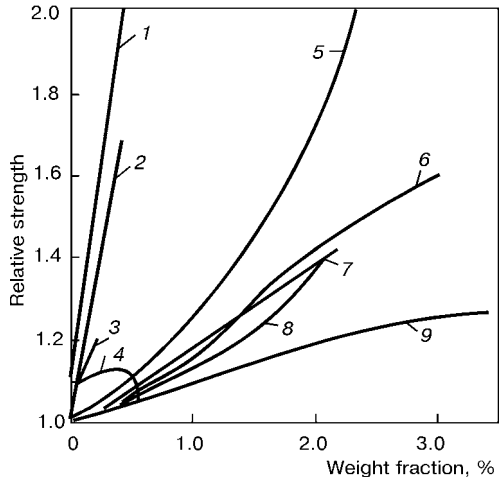

Figure 2. Influence of the content of various alloying elements on relative strength of normalized steel: *1* — C; *2* — Mo; *3* — P; *4* — V; *5* — Mn; *6* — Cu; *7* — Si; *8* — Cr; *9* — Ni

Table 1. Composition and hardness of the studied alloys

Alloy	Weight fraction of elements, %				Alloy hardness HRC	
	C	Cu	S	P	cast	quenched
1	0.19	7.92	0.42	0.34	26	20
2	0.26	7.94	0.72	0.45	28	59
3	0.70	7.94	0.72	0.48	37	26
4	0.86	8.00	0.70	0.52	32	54
5	1.03	7.76	1.36	0.60	38	54

of some steels was studied, it was established [7] that this index drops markedly at phosphorus content of ≥ 0.3 % (Figure 3). Phosphorus also has an adverse influence on brittle transition temperature of pearlitic steels with 0.3 wt.% C. Adverse influence of phosphorus on impact toughness and brittle transition temperature of steel can be neutralized through its alloying by aluminium [11, 12]. A favourable influence of the latter it attributed by some authors [13] to lowering of excess energy of metal grain boundaries, enriched with phosphorus.

Possibility of using phosphorus to improve the high-temperature properties of steel was studied. It was established [7] that addition of 1.0 % P to steel with 0.10 % C, 5.0 % Cr, 0.5 % Mo increases the high-temperature ultimate strength and yield point with a slight loss of ductility. In [14] it is noted that at phosphorus content of 0.2 % in 12Kh18N9T (304SS) steel its high-temperature resistance rises 5 to 10 times without lowering of the intercrystalline corrosion resistance.

There is an opinion that phosphorus increases the wear resistance and lowers the coefficient of sliding friction of Fe-base alloys [15]. This is confirmed by the data of [16–19], in which Fe-base cast alloys were studied, which contained up to 10 % Cu, 0.3–1.6 % P, 0.42–1.36 % S and up to 1.03 % C. It is shown that eutectic phases, acting as solid lubricants, form in the structure of alloys of Fe–Cu system with 1.0–1.6 % P and 0.3–0.8 % S. Tribotechnical characteristics of these alloys under the conditions of sliding friction at boundary lubrication are on the level of those for bronze Br.OF10-1.

Thus, presence in the composition of these alloys of components, based on phosphorus and sulphur compounds, should markedly lower the friction losses.

Work [18] gives the results of studying the influence of carbon on the structure of antifriction Fe-base alloys, alloyed with copper, sulphur and phosphorus in the as-cast and quenched condition (Table 1). It is established that wear resistance of test alloys with the weight fraction of carbon above 0.3 % is higher than that of bronze Br.AZhMts10-3-1.5 three and more times. Structure of the studied alloys changes from the ferrite-pearlite structure (alloy No.1) to pearlite-carbide structure (alloy No.5). Microhardness of the phosphide eutectic varies from 2840 (alloy No.1) up to 7840 MPa (alloy No.5). The alloys have

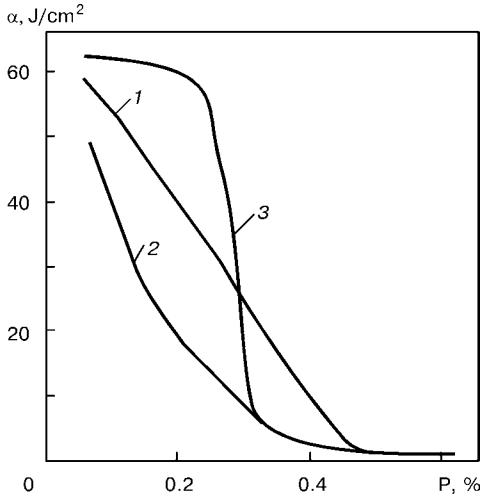

Figure 3. Influence of phosphorus content on impact toughness α of steel at the following weight fraction of carbon, %: *1* — 0.040–0.090; *2* — 0.12–0.18; *3* — 0.25–0.35

a high wear resistance and good antifriction properties, which may be varied in certain ranges by changing the alloy composition.

Influence of phosphorus on scale resistance, specific electric resistance and magnetic characteristics of steels has been studied [7]. Phosphorus essentially lowers steel oxidation at high-temperature heating (Figure 4). Increase of phosphorus weight fraction up to approximately 0.60 % leads to a linear growth of the specific electric resistance. Further increase of phosphorus content practically does not influence this characteristic. Magnetic properties of steel also change with the increase of phosphorus weight fraction. Phosphorus also promotes reduction of the coercive force, increase of the maximal magnetic permeability, but practically does not influence the residual induction.

Phosphorus influence on cast iron properties. Phosphorus is added to cast irons in much greater amounts (up to several percent) than to steel. Presence of an alloyed phosphide eutectic improves the fluidity of cast irons and allows producing sound castings from them (for instance, centrifugal pipes, art castings). Phosphorus cast irons are further characterized by rather high wear-, high temperature- and corrosion-resistance [20]. However, low strength, de-

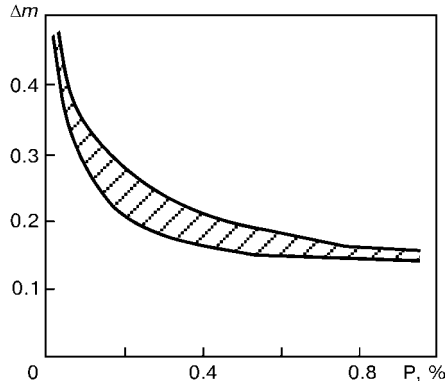

Figure 4. Influence of phosphorus content on relative weight loss Δm (hatched area) at heating of low-carbon steels in air at T = = 760 °C

spite the good antifriction properties, restrains their commercial application.

In [21] the authors studied the nature of brittleness of aluminium cast iron with phosphorus, containing (wt.%) 2.26–2.31C; 1.50–1.65Al; 0.20–0.26Mn, 0.18–0.21Si. Phosphorus weight fraction was varied in the range of 0.07 to 0.36 % in different melts. Phosphide eutectic was detected in all the samples of test melts, its distribution changing with the increase of phosphorus content from individual uniformly distributed inclusions up to coarse clusters in the form of a broken net along the boundaries of metal grains. X-ray diffraction analysis showed that a P-saturated layer of the thickness of just 18 to 20 μm forms in the matrix regions, bordering on the phosphide eutectic. A feature of this element distribution in aluminium cast iron is the small width of the transition layer near the phosphide eutectic, which should be favourable for the indices of toughness and ductility of cast iron. This assumption was confirmed by the results of mechanical tests: lowering of brittleness under the influence of phosphorus, characteristic of cast irons of Fe–Si–C system, is significantly reduced at partial or complete replacement of silicon by aluminium in them. Silicon and aluminium influence on ductile properties of phosphorus cast irons is explained by the authors of [21] as follows. Phosphorus atoms, present in the solid solution, are not only weakly bonded to the atoms of iron and silicon, but also weaken the forces of interaction of the atoms of the main component with each other. Silicon replacement by aluminium should be accompanied by redistribution of the forces of interatomic bonds. In this case stable bonds of the type of Al–P may form in the solid solution. Their appearance should neutralize the adverse influence of phosphorus on the processes of interaction of the atoms of the main component. Thus, aluminium promotes a qualitative and quantitative change of the nature and mechanism of phosphorus influence on cast iron brittleness, creating favourable prospects to produce high-quality alloys.

In modern mechanical engineering P-containing (0.3–0.4 %) grey cast irons (PCGCI), alloyed with various elements, are ever wider applied for fabrication of critical parts, operating under the conditions of lubricated friction [22]. Structure of PCGCI castings should contain uniformly distributed lamellar graphite of medium size, finely dispersed pearlite matrix, continuous net of fine inclusions of ternary phosphide eutectic and fine eutectic grain [22]. Presence of ternary phosphide eutectic, particularly in the form of a continuous or broken net, leads to less wear and better tearing resistance of the metal.

Table 2. Enthalpy of formation of certain metal carbides [28]

Carbide	ΔH^0_{298}, *kJ/(C atom)*	*Carbide*	ΔH^0_{298}, *kJ/(C atom)*
ZrC	−196.6	SiC	−71.9
Nb_2C	−188.2	Cr_3C_2	−48.9
TiC	−183.6	Mo_2C	−46.0
NbC	−139.7	WC	−40.5
VC	−100.8	Fe_3C	−25.1
$Cr_{23}C_6$	−98.2	Mn_3C	−15.0

It is known [22] that phosphorus, similar to silicon, increases the reactivity of carbon in Fe–C alloy, this leading to graphitization of cast iron. Therefore, phosphorus, similar to silicon, should have a modifying action in cast iron melting. Application of P-containing master alloys, as graphitizing modifier, improves PCGCI structure, which, in the opinion of the authors of [22], should increase the wear resistance and strength properties of parts, operating at friction and lubrication.

In [23] strength of cast iron with phosphorus content of 0.05–0.50 % was studied after various heat treatment modes (samples were subjected to normalizing or ferritizing annealing). It is established that with the increase of phosphorus content up to the specified limits, cast iron hardness rises by 20 %, and ultimate strength decreases 2 times, compared to cast iron, unalloyed with phosphorus. This is, apparently, related to formation of a phosphide eutectic in the cast iron structure.

Antifriction properties and wear resistance of cast iron were determined in friction machine MT-66 [24], at sliding rate of 1–3 m/s and up to 50 kPa pressure with limited feed of I-20 lubricant. Quenched steel 45 was used as the mating body. Phosphorus alloying in the range of 0.05–0.50 % leads to 5 times increase of wear resistance of cast iron at normalizing and 2 times at ferritizing annealing, compared to unalloyed cast iron. No phosphorus influence on the change of cast iron friction coefficient was found [23].

In order to improve the performance of wheel chocks of railway and industrial transport, the possibility was studied [25] of modifying with (wt.%) 0.1–0.5 % Ce additives the hypoeutectic cast irons with 2.6–3.2C; 1.4–1.6Si; 0.5–0.7Mn; 0.3–3.5P. With the increase of phosphorus content the graphite plates first become thinner, then coarse lamellar graphite forms, and the number and quantity of eutectic inclusions change, accordingly. Dendrite branching is enhanced, and dendrite number and dimensions become smaller. At weight fraction of phosphorus of 2.5–3.5 % the amount of excess austenite becomes smaller, and that of phosphide eutectic rises. It is established that small additives of selenium are effective modifiers. In cast irons with phosphorus content of 2.5 % and more, the effectiveness of selenium as modifier is enhanced. Wear resistance and friction properties of cast iron are improved with the increase of phosphorus content. So, at phosphorus content of 1.4 %, the wear resistance and coefficient of friction of cast irons are by 10–15 % smaller than in cast irons with 2.5 % P.

One of the most promising methods to improve wear resistance of cast iron for brake assemblies is its alloying with phosphorus in combination with vanadium, titanium and other alloying elements [26].

Table 3. Enthalpy of formation of phosphides of some metals [28]

Phosphide	ΔH^0_{298}, *kJ/(P atom)*	*Phosphide*	ΔH^0_{298}, *kJ/(P atom)*	*Phosphide*	ΔH^0_{298}, *kJ/(P atom)*
Zr_2P	−513	MoP	−192	Ni_2P	−162
ZrP	−426	Cr_3P	−252	NiP	−108
Ti_2P	−456	CrP	−168	Co_2P	−174
TiP	−265	MnP	−186	CoP	−158
Nb_2P	−405	Mn_3P	−181	Fe_3P	−163
NbP	−320	Mn_2P	−172	Fe_2P	−147
V_2P	−327	WP	−172	FeP	−119
VP	−238	W_2P	−171	AlP	−150
Mo_2P	−255	Ni_3P	−197	SiP	−69

Bench and operating tests of brake blocks of phosphorus cast iron showed that an increased content of phosphorus, alloying and modifying elements is favourable for the structure of phosphide eutectic and structural base of cast iron, which results in wear resistance of parts increasing by 2–3 times, compared to wear resistance of parts of unalloyed cast iron.

Prospects for application of phosphorus in surfacing consumables. Analysis of published data, given in this review, shows that phosphorus alloying improves the tribotechnical properties of steels and cast irons. This is indicative of good prospects for its application in materials, used for surfacing various shafts, axles, roller conveyor rollers, and rollers and track links of industrial and agricultural tractors and other components, operating under the conditions of metal friction over metal. Some researchers also believe phosphorus to improve the tearing resistance of steel [22]. This may be used in material alloying for surfacing the deep heading dies and other parts, operating under similar conditions.

In unalloyed steels phosphorus forms low-melting brittle eutectics of FeP–Fe_3P type. Iron phosphides do not have a high hardness or thermodynamic stability. Therefore, it is intended to bind phosphorus into high-melting phosphide phases of Al–P, B–P or $(Fe, Cr)_3P$ and $(Fe, Mo)_3P$ type, instead of the low-melting and brittle eutectics of FeP–Fe_3P type [27]. In this case the Fe-base phosphide phase will be in thermodynamic equilibrium with the ternary phosphide phase. Heat treatment allows bringing these phosphide phases into a finely dispersed state, strengthening the steel similar to carbides [27]. In view of the fact that in surfacing alloys strong carbide-forming elements are usually used for alloying, it is important to establish an equilibirum between the carbides and phosphides of alloying metals, which depends on their thermodynamic characteristics (Tables 2 and 3). So, proceeding from these data, titanium carbide should form before its phosphide does.

Phosphorus greatly improves the fluidity of Fe-base alloys, lowering their surface tension. Phosphorus influence on fluidity of pure iron was studied in [29]. At the temperature of about 1000–1200 °C complete spreading of liquid P-containing alloy is observed. Thus, phosphorus demonstrates surface activity in liquid iron, promoting a drop of surface tension. Lowering of the latter should be favourable for formation of the deposited layers. Better formation of the deposited metal permits reducing the allowances and simplifying the machining of the surfaced parts, which, in the long run, will improve the economics of the surfacing process.

In surfacing the negative influence of phosphorus may be neutralized by that in the surfaced part the strength is ensured by the base metal, and the deposited layer improves the performance (resistance to different kinds of wear, corrosion, etc.).

It is intended to use phosphorus in surfacing consumables as an alloying element — its content may reach several percent. Therefore, the primary objectives in development of such consumables will be determination of the coefficient of phosphorus transition into the deposited metal with different processes of arc surfacing, evaluation of welding-processing properties and formation of deposited metal, as well as its susceptibility to hot and cold cracks.

CONCLUSIONS

1. Phosphorus alloying at up to 0.6 % content improves the steel strength. Its ductility characteristics, namely impact toughness, relative elongation and reduction in area deteriorate simultaneously with increase of phosphorus content.

2. Phosphorus improves the wear resistance and lowers the coefficient of friction of Fe-base alloys. The structure of such alloys, containing phosphorus and sulphur with weight fraction of 1.0–1.6 and 0.3–0.8 %, respectively, forms eutectics, which may act as hard lubricant.

3. Increased wear resistance of surfacing alloys, containing phosphorus, can be achieved by forming in the structure the compact phosphides of alloying elements (primarily, molybdenum, niobium, titanium, zirconium), whose formation is the most probable in terms of thermodynamics. Better results on

wear resistance with phoshpide eutectic arrangement along the grain boundaries can be obtained, when it forms as a thin continuous or broken net.

4. Addition of even small amounts of phosphorus to low-alloyed surfacing alloys should be favourable for formation of deposited layers, which is related to lowering of surface tension of molten metal.

5. Use of phosphorus as alloying element allows development of a new class of low-alloyed wear-resistant surfacing consumables for surfacing items, exposed to metal friction over metal in service.

The authors are grateful to Dr. V. Chernogorenko (Institute for Problems of Materials Science of the NAS of Ukraine) for assistance in selection of published sources and valuable advice in writing this review.

1. Doroshek, S.I. (1959) Influence of phosphorus on structural transformations and properties of low-alloyed electric steel. *Fizika Metallov i Metallovedenie*, **5**, 770–776.
2. Goudremont, E. (1966) *Special steels*. Moscow: Metallurgiya. Vol. 2.
3. (1977) *Encyclopedia of inorganic materials*. Vol. 2. Kyiv: Ukr. Sov. Ents.
4. Muchnik, S.V. (1979) Chemistry and technology of phosphorus-bearing alloys. Phosphorus-bearing alloys. In: *Chemistry and technology of phosphides and phosphorus-bearing alloys*. Kyiv: IPM AN USSR.
5. Stitzig, W.A., Sober, R.I. (1977) Effect of phosphorus on the mechanical properties of hot-rolled 0.1–1.0 Mn steel strip. *Met. Trans.*, **10**, 1585–1590.
6. Kusaka, K., Fukase, T. *Phosphorus-bearing high-manganese steel designed for valves*. Pat. 48-9689 Japan. Publ. 27.03.73.
7. Spretiniak, J.W. (1961) *Phosphorus in metallurgy. Phosphorus and its compounds*. Vol. 2. Technology, biological functions and application. Ed. by R. John van Wazer. Interscience.
8. Gulyaev, A.P., Tsulkova, V.M. (1974) Influence of phosphorus on corrosion properties of stainless steels. In: *Corrosion-resistant metallic structural materials and their application*. Moscow: Mashinostroenie.
9. Schubert, H. (1973) Neue Dauermagnetwerkstoffe. *Int. J. Magn.*, **1–3**, 215–222.
10. Takayanagi, K., Negishi, A. *Wear-resistant alloys with magnetic permeability*. Appl. 2539582 FRG. Publ. 07.04.77.
11. Keiz, S.L., Van-Gorn, K.R. (1959) *Aluminium in cast iron and steel*. Moscow: Metallurgizdat.
12. Svechnikov, V.N., Trush, I.Kh. (1958) Influence of nitrogen on mechanical properties of medium-carbon phosphorus steel. *Izv. Vuzov, Chyorn. Metallurgiya*, **12**, 81–88.
13. Grdina, Yu.V., Glikman, E.E. (1964) On mechanism of influence of aluminium and phosphorus on brittle fracture susceptibility of high-phosphorus steel. *Ibid.*, **12**, 106–111.
14. Medovar, B.I., Pinchuk, N.I., Puzrin, L.G. (1962) Influence of phosphorus on long-term strength of Kh18N9T steel welded joints. *Metallovedenie i Term. Obrab. Metallov*, **8**, 24–25.
15. Bakfart, F.G., Daniel, S.G. (1967) New about lubricants. In: *Abstr. of pap. of Int. Conf. on Lubricants*, Washington, 1964. Moscow: Khimiya.
16. Markovsky, E.A., Kachko, N.A., Mashinetsky, N.Ya. (1993) Formation of surface structure of Fe–Cu system alloys alloyed by sulphur and phosphorus. *Protsessy Litia*, **4**, 15–18.
17. Kachko, M.O., Markovsky, E.A., Ilchenko, V.D. (1998) Antifriction iron alloys with phases of solid lubricant. *Metaloznavstvo ta Obrob. Metaliv*, **3**, 17–21.
18. Markovsky, E.A., Ilchenko, V.D., Butenko, L.I. et al. (1999) Influence of composition and structure of antifriction alloy on its wear resistance. *Protsessy Litia*, **2**, 60–64.
19. Ilchenko, V.D., Markovsky, E.A., Butenko, L.I. et al. (1999) Casting properties of antifriction alloys, depending on quantity of main alloying elements in alloy. *Ibid.*, **4**, 62–66.
20. Bobro, Yu.G., Savchuk, S.A. (1973) Sintegal — new structural cast iron from Fe–Al–C group of alloys. In: *Cast alloys*. Kyiv: Naukova Dumka.
21. Bobro, Yu.G., Savchuk, S.A., Sharkin, O.P. (1971) Nature of brittleness of aluminium cast iron with phosphorus. *Litejnoe Proizvodstvo*, **10**, 32–34.
22. Syrokvashev, A.V., Bauman, B.V. (2000) Modification of gray phosphorus cast irons, operating in friction conditions. *Ibid.*, **9**, 16–17.
23. Kralya, V.D., Pushkarev, V.V., Matvienko, A.I. et al. (1979) Antifriction properties and wear resistance of modified cast iron alloyed with ferromanganophosphorus and ferrophosphorus. In: *Chemistry and technology of phosphides and phosphorus-bearing alloys*. Kyiv: IPM AN USSR.
24. (1979) *Explanatory dictionary on friction, wear and lubrication of machine elements*. Kyiv: Naukova Dumka.
25. Esaulov, V.P., Yatsenko, A.I., Belaj, G.E. et al. (1977) Modified high-phosphorus cast irons. *Litejnoe Proizvodstvo*, **6**, 8–10.
26. Kunaev, A.M., Sukharnikov, Yu.I., Levintov, B.L. (1979) Prospects of production and application of high-phosphorus complex alloys, containing alloying metals. In: *Chemistry and technology of phosphides and phosphorus-bearing alloys*. Kyiv: IPM AN USSR.
27. Chernogorenko, V.B. (1979) Ways to develop the works concerning production, investigation and application of phosphides and phosphide-bearing alloys. *Ibid*.
28. Chernogorenko, V.B., Ershov, G.G., Gavrilyuk, G.V. (1998) Decrease of detrimental effect of phosphorus in iron-carbon alloys by alloying. *Metally*, **2**, 6–10.
29. Samsonov, G.V., Panasyuk, A.D., Borovikova, M.S. (1977) Influence of phosphorus on adhesion of liquid metals to refractory compounds. In: *Production, properties and application of phosphides*. Kyiv: Naukova Dumka.

SELECTION OF OPTIMAL METHODS FOR EXPLOSION LOADING OF WELDED JOINT BASED ON ESTIMATION OF HARDNESS

V.A. TITOV, Yu.I. FADEENKO and **V.G. PETUSHKOV**
The E.O. Paton Electric Welding Institute, NASU, Kyiv, Ukraine

Results of investigation into the effect of explosion treatment of welded joints using elongated explosive charges on distribution of residual stresses are given. Formulae relating parameters of residual stress fields in the explosion treated welded joints to parameters characterising explosion treatment conditions are presented.

Key words: *welded joints, explosion treatment, residual stresses, calculation of parameters, charge, explosives*

Explosion treatment (ET), being a mobile and low-cost operation, is one of the most promising methods increasing fatigue resistance of steel parts and welded metal structures [1–4]. Physical basis of this type of treatment employed to increase resistance to different kinds of fractures is formation of a stress-strain trace (SST) in local high-rate deformation of metal at the moment when a shock wave propagates through it [5–7]. Metal in the SST zone is characterised by an increased hardness (explosion or strain hardening), compared with the base metal, and biaxial compressive residual stresses (RS) present in the surface layer of the metal. The last factor prevents propagation of cracks usually initiated on the workpiece surface. Structure, intensity and size of SST depend upon the type of an explosive and its geometric peculiarities, as well as upon the strength characteristics of metal treated [7, 8].

A wide variety of commercially produced explosives allowed the authors of [1, 2, 4, 9–11] to investigate the effect of ET on cyclic strength of different types of welded joints by varying over wide ranges the intensity and geometry of explosive loading. The above efforts yielded both positive and negative results. However, no general theory has been developed as yet on their basis to explain the mechanism of increase in fatigue resistance of welded joints by ET. One of the reasons is the lack of understanding of the dependence of structure and parameters of SST upon the strength properties of metal and characteristics of an explosive charge. In turn, this lack of understanding is attributable to a cumbersome nature of analytical methods for investigations of even the simplest problems of formation of SST [12], as well as to considerable labour expenditures needed to reveal the desired experimental relationships. The latter can be explained proceeding from the below reasoning.

Consider the case of treatment of metal plate of an infinite length through an inert interlayer using an elongated cylindrical explosive charge with radius r_0, and characterise treatment conditions using the following parameters: ρ_0, $\rho 1$ and $\rho 2$ — density of an explosive, interlayer and metal plate, respectively; D and p — detonation velocity and pressure, respectively; c_0, c_1 and c_2 — velocity of sound in the detonation products, interlayer and plate, respectively; δ_0, δ_1 and δ_2 — thickness of the explosive charge, interlayer and plate, respectively; σ_y — yield stress of the metal; and M — its deformation modulus. Let x and z be coordinates of a plate element in which it is necessary to determine components of the RS field, $F_{1,2}$. Then, proceeding from the similarity theory and dimensions, the desired relationships should have the following form:

$$F_{1,2}(x, z) = f_{1,2}(x/\delta_2);\quad z/\delta_2;\quad p/\rho_0 D^2;\quad \rho_0 c_0/\rho_1 c_2;\quad \rho_1 c_1/\rho_2 c_2;\quad \delta_0/\delta_1;\quad \delta_1/\delta_2;\quad p/\sigma_y;\quad M/\sigma_y. \qquad (1)$$

This simplest case as it is does not yet allow for a sheath the cord charge has, for a common practice of application of the charge consisting of several sections of the detonating cords, as well as for the conditions of contact between the plate treated and a massive support. Distribution of RS through thickness of the plate is determined, for example, by using the N.N. Davidenkov method, which consists in layer-by-layer etching of metal, resulting in variations in residual stresses. Then the data obtained are recalculated using a special software.

It can be easily seen from the above-said that experimental measurements of the total RS field are a very labour-consuming operation, hardly suitable for a systematic use in routine practice of optimisation of the ET process parameters. Therefore, the practical optimisation procedure has to rely on simplified techniques. For example, in processing of the experimental data based on the available experience, some of the dimensionless parameters of the right part of (1) are often ignored, and the elongated concentrated charge is characterised only by weight of an explosive per its unit length, μ, specific calorific value (explosion heat) Q or explosion energy input $E = \mu Q$. However, the most efficient of the simplifying techniques is the use of a certain similarity of the RS fields and hardness increase fields (explosion hardening).

Obviously, in a general case no exact correspondence exists between these two fields, as strain hardening is determined by an overall plastic deformation and pressure under which it was realised. In addition, as opposed to the RS field, the strain hardening field

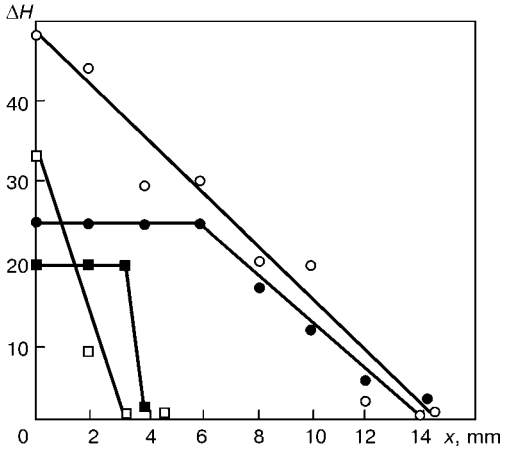

Figure 1. Distribution of increase in hardness, ΔH, in SST in a direction transverse to the charge axis at a depth of 0.5 mm after ET using a cord explosive charge: *1*, *2* — high-strength steel (σ_y = = 1000 MPa); *3*, *4* — low-strength steel 09G2S (σ_y = 360 MPa) (light signs — contact charge; dark signs — using a damping interlayer)

does not exceed the limits of the zone of marked residual plastic strains. At the same time, structure of the RS field is determined by gradients of residual (not overall) plastic strains. This field may extend far beyond the limits of the region of elastic strains.

However, as proved by many years of practice, in the majority of cases there are two main parameters of the RS field, i.e. thickness of the surface layer of compressive stresses and amplitude of residual stresses in it, which vary with variations in the treatment conditions, like thickness of the strain-hardened layer and amplitude of the strain hardening field do. Therefore, a labour-consuming procedure of measuring the RS diagrams at the first stage of optimisation of the technology can be replaced by a simple and fast measurement of distribution of hardness in the strain hardening region. This gives rise to a practically important problem of establishing general relationships between the strain hardening field parameters and ET parameters, which exactly is the purpose of this study.

Experimental procedure. Steels with low (σ_y = = 250 MPa, σ_t = 420 MPa), increased (σ_y = 350 MPa, σ_t = 500 MPa) and high (σ_y = 1000 MPa, σ_t = = 1100 MPa) strength were selected for the experiments.

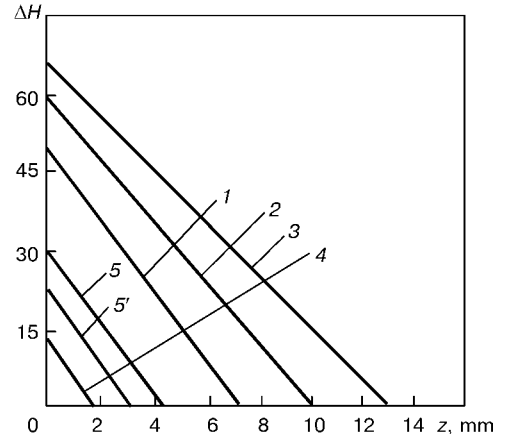

Figure 2. Distribution of increase in hardness, ΔH, through thickness of the low-strength steel 09G2S specimen after ET performed by different methods: *1* — using one contact cord charge; *2* — same using a plug with a density of 3.7 g/cm^3; *3* — using a cumulative effect; *4* — using an air interlayer; *5*, *5′* — using interlayers of a differing thickness

Analysis of the character of deformation of metal in ET was done by measuring hardness in sectional samples using procedure described in [13]. Residual stresses were evaluated by the magnetoelastic strain measurement method described in detail in [14].

Ductility of metal was studied by testing specimens with induced fatigue cracks 3 mm long to critical crack tip opening displacement δ_c using the tensile testing machine 2054-R5.

Fatigue limit of welded joints was evaluated using the dynamic pulser TsDM-200 PU with a test frequency of 7 Hz. Standard cord and thin plastic strip explosives, based on RDX, were used as the explosive charges for the experiments.

Treatment using cord charges. Placement of an explosive charge directly on metal leads to formation of the strain hardening zone, which has a pronounced maximum hardness value under the charge axis (Figure 1). A dramatic decrease in hardening down to an initial value is seen at a distance from this zone through thickness and in width (Figures 1 and 2). Absolute sizes of the deformed zone depend upon the strength properties of steel, such as the tensile strength to yield stress ratio, $k = \sigma_t/\sigma_y$, and weight of the charge per its unit length, m. The RS component in the surface layer of steel about 1 mm thick in a direction transverse to the charge axis, x (σ_{RS}), is compressive. Sizes of the surface zone of compressive residual stresses are close to those of the strain hardening zone (Figures 3 and 4). In all the cases residual dents covered by a network of scratches were seen on the treated surface of a steel specimen. Hardening of metal achieved in this case is a result of increase in the density of dislocations and twins. Specific data on relative contributions of these two mechanisms of deformation and hardening are available only for low-strength steels. According to the data of [15], in the concerned technological range of the maximum loading pressure values equal to 1–14 GPa for steel 20, an increase in pressure is accompanied by the gradual replacement of a dislocation slip by twinning.

In this case an increase in yield stress is expressed in terms of the density of dislocations N and twins β through the relationship of the following type:

$$\Delta\sigma_y = a_1\beta^{1/2} + a_2N^{1/2}, \qquad (2)$$

where a_1 and a_2 are some constant values, and increase in the yield stress is proportional to the maximum loading pressure (the strain hardening field almost coincides with the maximum loading pressure field).

Allowing for the fact that welded structures subjected to explosion treatment operate at different climatic temperatures, an investigation was conducted to study the effect of explosion hardening by the explosion loading method under consideration on ductile properties of steel. An increased-strength steel characterised by a substantial discontinuous decrease in fracture resistance during the tough to brittle fracture transition was chosen for the investigation.

The investigation results shown in Figure 5 are indicative of a negative effect exerted by explosion hardening on ductility of steel over a wide range of

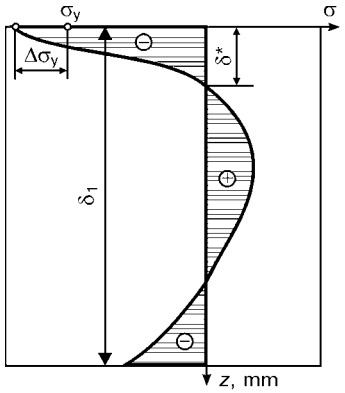

Figure 3. Diagram of distribution of residual stresses in SST through metal thickness: δ^* — thickness of the surface layer with compressive stresses

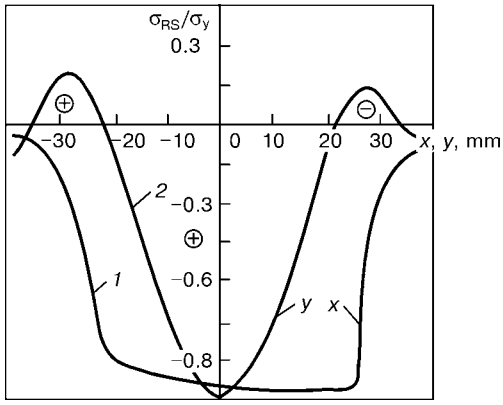

Figure 4. Distribution of residual stresses in the surface layer of metal about 0.5 mm thick after ET along (*1*) and across (*2*) the weld: y — distance from the weld axis

test temperatures. This is confirmed by the data of [9], which reports that fatigue tests of the cruciform-type welded joints in a similar steel revealed decrease in their fatigue life after ET performed by the method under consideration. The negative effect on fatigue resistance of welded joints is exerted also by the presence of a scratch network on the surface treated, especially in the case of welded joints in steels with an increased sensitivity to the concentration of stresses.

Fracture of welded structures subjected to alternating loads is always of a local character. It almost always occurs in the weld to base metal transition zone, i.e. in the zone of the highest concentration of stresses caused by external loading. The size of this zone depends upon the radius of the weld to base metal transition region and ranges from 0.01 (butt joint) to 0.10 mm (welding of different structural members to base metal). Considering high values of the gradients of hardness and residual stresses in SST in width (see Figures 1 and 4), as well as the fact that the cord charge axis can hardly be aligned with the zone of expected fracture because of geometric peculiarities of welded joints, there is no way to reproduce ET by using the method under consideration to the sufficient degree of accuracy.

Allowing for the above drawbacks of different ET methods which provide for a direct contact between an explosive and metal, in a series of the experiments conducted the damping interlayers of an inert material were placed between the treated surface of a welded joint and the cord explosive charge. At the presence of an interlayer the character of fracture changes, hardness diagrams (see Figure 1) take a П-like form with a wide plateau of maximum values, thus providing a good reproducibility of the ET results for the probability of shift of the charge axis from the expected fracture zone. The RS diagrams in the surface layer almost repeat the hardness distribution diagrams (see Figures 1 and 4). This coincidence seen more than once also with other ET methods can serve as the basis for using the above method for preliminary selection of the optimal treatment parameters.

Figures 1 and 2 show variations in hardness of an increased-strength steel after ET, depending upon the damping interlayer thickness. Ductile properties of the steel with such ET methods remain suitable for the problems to be handled (see Figure 5). Figure 6 shows results of fatigue tests of large specimens of steel increased strength 15KhSND, 16 mm thick, after ET using a special method. Positive results were obtained in all the cases. The fatigue life of welded joints at the stage of crack propagation increased 5–10 and more times, while the fatigue limit almost doubled, compared with the initial state.

Hardening using strip charges. The results obtained in using strip charges differ from those obtained in the case of using cord charges. Hardening of low- and increased-strength steels using strip explosive charges, in contrast to the cord charges, leads to formation of the uniformly hardened zones in metal under the entire surface area of the charge. Sizes of these zones depend upon the strength of steel. Residual strains are noted on the surface treated. ET of high-strength steels, in which the $k = \sigma_t/\sigma_y$ ratio is close to one, leads to a fundamental change in geometry of the hardened zone. In this case hardening occurs only at the ends of the charge (Figure 7), where the plastic displacement field in metal is similar to the mass velocity field formed in explosion of a strip captive charge on the surface of liquid or soil (see, e.g. [16]). Two assumptions can be made to explain causes of the abnormal distribution of strain hardening.

Firstly, marked residual strains are formed at the ends of a flat charge, while they are absent under the central part of the charge. This might be caused by the fact that the degree of strain hardening is somehow associated with residual strains.

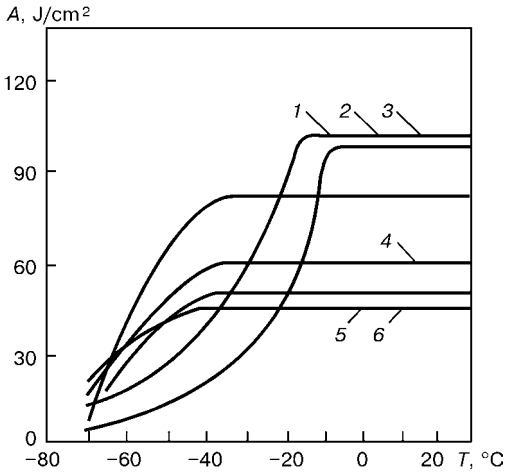

Figure 5. Energy of fracture of specimens, A, with a sharp notch: *1* — initial state; *2–6* — ET modifications

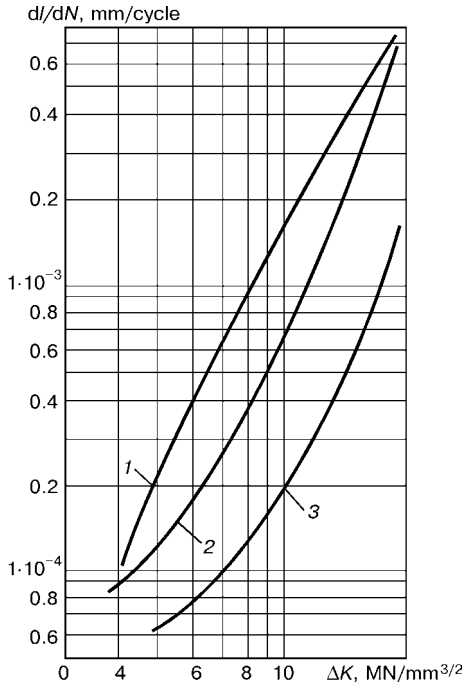

Figure 6. Dependence of the velocity of the fatigue crack, dl/dN, upon the amplitude of the stress intensity factor, ΔK, for the sharp-notched specimens: *1* — in the initial state; *2* — after one-sided ET using a strip explosive charge; *3* — same using a 1.5-fold charge (l — length of the fatigue crack; N — quantity of loading cycles)

Secondly, and this is more probable, this phenomenon is attributable to the dependence of mechanisms of multiplication of twins and dislocations due to a hydrostatic pressure (growth of a relative role of dislocation deformation, compared with the role of twinning, in the decreased-pressure zone near the free surface, i.e. the end zone).

Results of fatigue tests of welded joints in low- and increased-strength steels are indicative of the efficiency of using strip charges for increasing their fatigue fracture resistance. Here, like in the case of cord charges, it is indicated to use damping interlayers to prevent embrittlement of strain-hardened metal. In ET of welded joints in high-strength steels with a value of k close to one, the use of the strip charges, placed so that the expected fracture zone is located under the central part, is inefficient. Supposedly, the positive results in this case can be obtained if the strip charge is placed so that its end is located exactly over the fusion line. This provides residual deformation of metal in this location.

Principles of formation of the strain hardening zone. Configuration of shock-wave flows in an explosion-loaded solid is very complicated. This can be seen from Figure 8 [17], which shows structure of shock waves in metal loaded by the method analysed in this study. The results obtained indicate that in treatment under optimal technological conditions the first and most labour-extensive part of the experiments can be conducted without measuring residual stresses induced by the treatment, but by measuring just hardness. Further simplification can be achieved by establishing principles to relate sizes of the strain hardening zone to the treatment parameters. Indeed, it is enough to know two parameters of the strain hardening field to try out the process under optimal conditions: width of the strip with a constant hardness, $l_{c.h}$, and depth of the hardened zone, l, in this area.

The first of these values is determined by direct measurements of hardness on the surface treated, whereas measurement of the second is time consuming because of the need to make specimens.

In this study the authors investigated phenomenological principles relating increase in yield stress in the surface layer of steel treated (definitely related to increase in hardness) and the $l_{c.h}$ and l values to the cord charge and damping interlayer parameters, thus allowing the search for optimal treatment conditions to be substantially accelerated.

A series of experiments was carried out to establish these principles. Each of the experiments included variations in just one of the parameters characterising properties of the cord charge and interlayer, the rest of the parameters being kept unchanged. Processing of the results obtained allowed determination of the general form of relationships of the desired parameters, i.e. $l_{c.h}$ and maximum increase in yield stress (or

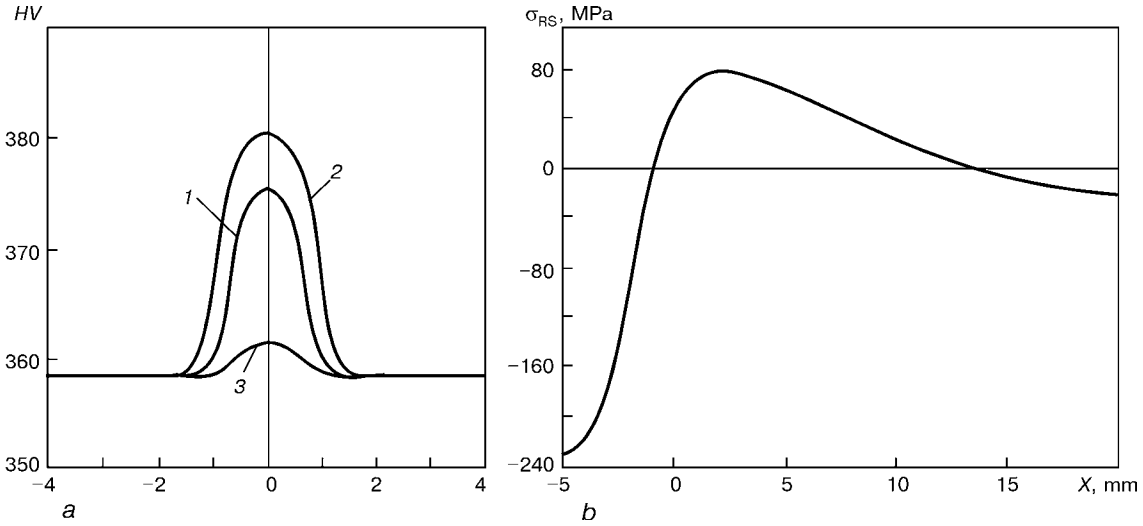

Figure 7. Distribution of hardness (*a*) and residual stresses (*b*) in surface layers of specimens of high-strength steel after ET using a flat linear high-explosive charge 1.5 mm thick and 10 mm wide at a depth of 2.5 (*1*), 1.0 (*2*) and 3.5 (*3*) mm (X — distance from the charge end)

hardness) on the metal surface, with the dimensionless parameters characterising treatment conditions:

$$l = A_1\left(\frac{E}{\sigma_d}\right)^{1/2}, \quad (3)$$

$$l_{c.h} = l\left[1 + A_2\left(\frac{\delta_1}{\delta_0}\right)\right]^{-1}, \quad (4)$$

$$\Delta\sigma = A_3 k\mu^{1/2}, \quad (5)$$

where E is the energy input of the explosive charge; σ_d is the dynamic yield stress of steel, substantially different from the static one [17]; A_1–A_3 are the coefficients depending upon the choice of an explosive and interlayer material; and values of $k = \sigma_t/\sigma_y$ characterise the grade of steel.

Relationships (3) through (5) are valid only for a limited range of parameters used particularly for ET to increase fatigue fracture resistance of welded joints (in particular, for interlayers with thickness sufficient to affect the $l_{c.h}$ value, but exerting no effect on the l and $\Delta\sigma_y$ values). However, the knowledge of these relationships is also of a more general significance, as it makes the procedure of searching for optimal conditions of any types of ET using concentrated elongated charges much shorter.

Therefore, knowing the initial RS fields in a welded joint and parameters of explosion loading using cord charges, the results obtained in this study allow the size and intensity of SST after explosion treatment to be approximately predicted and parameters of the treatment to be reasonably selected for a final development of the technology by measuring the induced RS fields.

It should be noted in conclusion that there are also other possibilities of employing the explosion energy to control parameters of the RS fields, e.g. using methods based on utilisation of a cumulative effect, increasing the intensity of compression waves in their reflection from acoustically hard screens, or using massive inert plugs capable of dramatically increasing duration of the phase of the high pressure effect, thus resulting in a substantial increase in parameters of SST.

CONCLUSIONS

1. Treatment of welded joints along the weld and base metal fusion lines using cord and thin strip explosive charges is an efficient method for formation of compressive residual stress fields in surface layers of metal and increase in fatigue fracture resistance of steel welded joints. Cord explosive charges (commercially produced detonation cords) offer the optimal solution for the above problems.

2. The above treatment should be performed through damping interlayers, allowing the ET results to be stabilised and embrittlement of hardened metal to be eliminated through varying parameters of the generated SST.

3. Techniques were selected on the basis of the experiments conducted, enabling labour consumption for trying out of optimal ET conditions to be reduced. In particular, at the first stage of the work it is indicated to control results by measuring the distribution of hardness, instead of labour-consuming measurements of distribution of residual stresses. Dependencies were derived to relate parameters of the hardened zone to parameters characterising ET conditions using cord explosive charges.

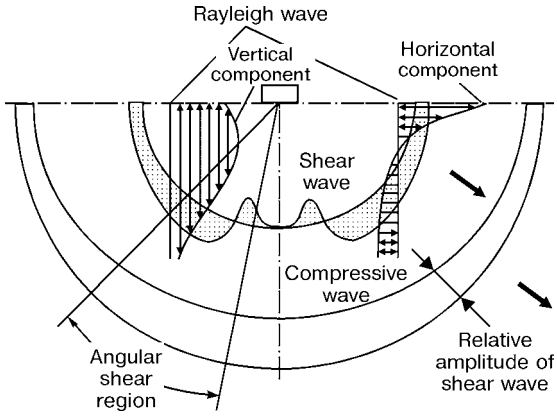

Figure 8. Structure of shock waves in a loaded solid using a narrow strip explosive charge

1. Trufyakov, V.I., Mikheev, P.P., Bushtedt, Yu.P. (1967) Application of pulsed treatment to increase the fatigue life of welded joints. *Avtomatich. Svarka*, **10**, 63–64.
2. Trufyakov, V.I. (1973) *Fatigue of welded joints*. Kyiv: Naukova Dumka.
3. Trufyakov, V.I., Mikheev, P.P., Kudinov, V.M. et al. (1974) Increase of welded joints fatigue resistance by explosion loading. *Avtomatich. Svarka*, **9**, 29–32.
4. Trufyakov, V.I., Kudinov, V.M., Mikheev, P.P. et al. (1977) Increase of fatigue resistance of steel parts by explosion treatment. *Vestnik Mashinostroeniya*, **5**, 63–65.
5. Petushkov, V.G., Fadeenko, Yu.I. (1980) On explosion treatment of welded joints. *Fizika Goreniya i Vzryva*, **5**, 64–68.
6. Petushkov, V.G. (1982) On mechanism of decrease of residual stresses by explosion treatment. *Avtomatich. Svarka*, **4**, 1–4.
7. Petushkov, V.G. (1986) Residual stresses formation in welded joints during explosion treatment. *Problemy Prochnosti*, **12**, 37–40.
8. Titov, V.A., Mikheev, P.P., Orekhov, G.T. et al. (1986) Distribution of residual stresses in surface layers of steel after explosion treatment. *Avtomatich. Svarka*, **1**, 69–70.
9. Titov, V.A. (1989) Increase in fatigue resistance of welded joints by explosion. In: *Proc. of 1st Int. Conf. of Young Sci. in Field of Welding and Related Technologies*, Kyiv, May 16–20, 1989. Kyiv: PWI.
10. Kasperovich, V.B., Naumovich, N.V., Titov, V.A. et al. (1990) Application of explosion treatment to increase reliability and service life of welded joints on large dump truck BelAZ. In: *Proc. of 8th All-Union Conf. on Explosion Welding, Cutting and Treatment*, Minsk, Sept. 25–27, 1990. Minsk.
11. Titov, V.A., Mikheev, P.P., Petushkov, V.G. et al. (1988) Application of explosion treatment to increase fatigue resistance of welded joints. In: *Proc. of 7th Int. Symp. on Application of Explosion Energy for Production of Metallic Materials with New Properties*, Gotvaldov, Oct. 25–27, 1988. Pardubitse.
12. Godunov, S.K., Sergeev-Albov, N.N. (1977) Equations of linear theory of elasticity with Maxwell point sources of stress relaxation. *Prikladn. Mekhanika i Tekhn. Fizika*, **4**, 140–152.
13. Petushkov, V.G., Kasatkin, S.B. (1979) Application of explosion energy to increase brittle fracture resistance of welded joints. In: *Proc. of 4th Int. Symp. on Application of Explosion Energy for Production of Metallic Materials with New Properties*, Gotvaldov, Oct. 1–5, 1979. Gotvaldov.
14. Petushkov, V.G., Bryzgalin, A.G., Titov, V.A. et al. (1992) Estimation of stress state of welded metallic structures by the method of magnetoelastic strain measurement. *Avtomatich. Svarka*, **5**, 16–18.
15. Efros, B.M., Zaika, T.P., Loladze, L.V. et al. (2000) Influence of shock-wave loading on structure and properties of carbon steels. *Fizika i Tekhnika Vys. Davleny*, **2**, 43–50.
16. Lavrentiev, M.A., Shabat, B.V. (1977) *Problems of hydrodynamics and their mathematical models*. Moscow: Nauka.
17. Petushkov, V.G., Kudinov, V.M., Fadeenko, Yu.I. (1993) *Explosion treatment of welded joints on metal structures*. Moscow: Metallurgiya.

LINK BETWEEN THE STRUCTURE AND STRENGTH PROPERTIES OF STEEL-ALUMINIUM JOINTS MADE BY FRICTION AND EXPLOSION WELDING

L.I. MARKASHOVA, E.N. BERDNIKOVA and **I.I. KHOMUTSKAYA**
The E.O. Paton Electric Welding Institute, NASU, Kyiv, Ukraine

Results of investigations of specifics of processes of structure and phase formation in joints of dissimilar metals with a limited mutual solubility (St.3 + aluminium), made by pressure welding using different temperature conditions of welding deformation (conventional and inertia friction welding and explosion welding) are presented.

Key words: *friction welding, explosion welding, steel-aluminium joints, structural parameters, strengthening, mechanical properties, phase precipitations, dislocations*

Among the new structural materials with special physical-chemical and service properties an important place is occupied by joints of difficult-to-weld dissimilar materials characterized by a limited mutual solubility, whose major part is welded using different methods of pressure welding. However, the joints of this type are typical of instability of mechanical properties. To clarify the reasons, the more comprehensive investigations of dependence of a dynamics of structure-phase state of metal in the zone of welding on technological parameters, and also a more detailed analysis of interrelation of structure state of joints and changes in their mechanical characteristics are required.

The use of the integrated procedure of investigations, including the quantitative optical metallography, analytical scanning and transmission electron microscopy, could give a clear idea of structure and phase composition of metals welded in all the zones of the joint including the interface. On this basis, a methodological approach was developed to a quantitative evaluation of effect of definite structure parameters of metals welded (chemical composition, size of grain and subgrain, density of dislocations, size, morphology and nature of distribution of phase formations, etc.) on changes in mechanical characteristics of dissimilar welded joints in the region located along a local zone of contact.

This evaluation on the example of changing the yield strength $\Delta\sigma_y$ was given earlier in [1] for St.3 + aluminium joints made by conventional and inertia friction welding, characterizing by different temperature of welding deformation.

In the present work we shall dwell more in detail on the causes of changes in strength properties, and also on the study of a principle of an analytical evaluation of changes in yield strength depending on structure parameters of a transition zone of dissimilar joints made by friction welding (inertia and conventional) and explosion welding.

Figures 1–3 show the changes in structures in the zone of contact of St.3 + aluminium joints, made by the conventional and inertia friction welding, as well as their contribution to the strengthening σ_y.

Thus, the strengthening in joints produced by the inertia friction welding from the steel side is provided mainly by increasing a total density of dislocations

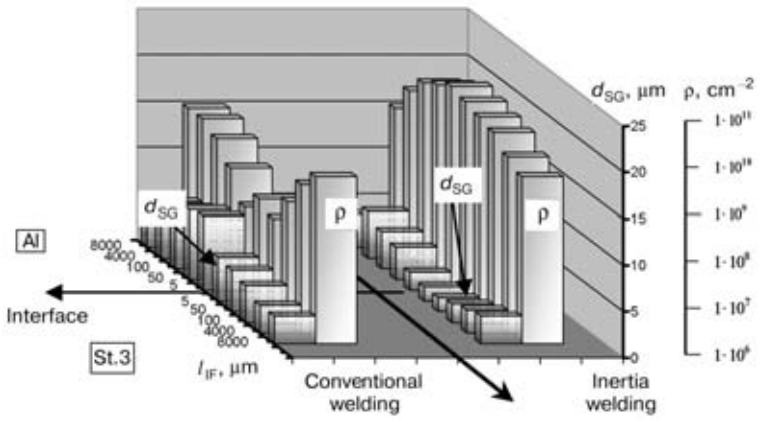

Figure 1. Change in sizes of subgrain d_{SG} and density of dislocations ρ in the zone of contact of St.3 + aluminium joints, made by friction welding (l_{IF} — distance from interface)

(≈ 22 % of contribution), and also by refining of a grain structure and substructure (≈ 35 % of total contribution). Here, in aluminium (softer metal as compared with steel) a significant increase in value of yield strength due to formation of the new dispersed intermetallic phases (about 15 %), and also increase in density of dislocations (about 12 %) is observed directly in the contact zone.

The quantitative evaluation of strengthening (increment of yield strength) stipulated by the contribution of each of structure parameters, was made as follows. The yield strength of the materials welded was considered as a sum of the following components [2]:

• lattice friction resistance σ_0 ($\sigma_0 = 2 \cdot 10^{-4} G$, MPa, where G is the shear modulus, equal for aluminium to 27300, for steel — 84000 MPa [3];

• strengthening of solid solution with alloying elements $\Delta\sigma_{SS}$ ($\Delta\sigma_{SS} = \Sigma k_i C i$, MPa, where k_i is the coefficient of strengthening [4], C_i is the concentration of alloying element in solid solution);

• strengthening at the expense of a pearlitic component $\Delta\sigma_p$ ($\Delta\sigma_p = 2.4P$, MPa, where P is the content of a pearlitic component, vol.%);

• strengthening at the expense of changing in sizes of grain $\Delta\sigma_g$ and subgrain $\Delta\sigma_{SG}$, evaluated by the known relationship of Hall–Petch ($\Delta\sigma_g = k_y D_g^{-1/2}$; $\Delta\sigma_{SG} = k_c d_{SG}^{-1}$, MPA, where k_c and k_y are the coefficients accounting for a barrier effect of subboundaries and boundaries [2, 5–7]; D_g, d_{SG} are the sizes of grain and subgrain, respectively);

• dislocation strengthening $\Delta\sigma_d$ ($\Delta\sigma_d = \alpha G b \rho^{1/2}$, MPa, where α is the coefficient, equal to 0.3 for aluminium and 0.5 for steel [8–10]; b is the Burger's vector equal to $2.2 \cdot 10^{-7}$ mm for aluminium and $2.5 \cdot 10^{-7}$ mm for steel [9, 10];

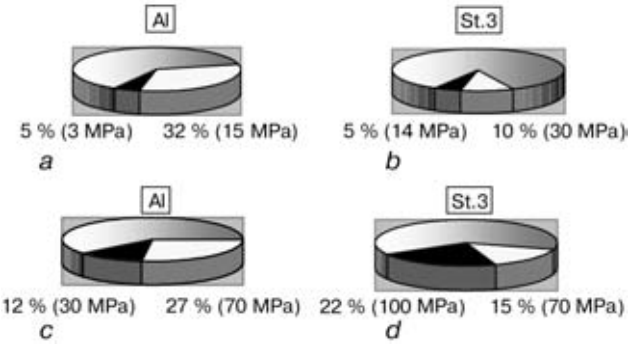

Figure 2. Contribution of structural parameters d_{SG} (❒) and ρ (■) to strengthening in the zone of contact of St.3 + aluminium joints made by friction welding: *a*, *b* — conventional; *c*, *d* — inertia welding

• dispersion strengthening with particles of forming phase precipitations, calculated by the Orowan's relationship $\Delta\sigma_{part}$ ($\Delta\sigma_{part} = 0.81 \frac{Gb}{4\pi} \varphi \ln \frac{l2r}{2b} \frac{2}{l - 2r}$, MPa, where φ is the coefficient characterizing the type of dislocations interacting with particles [11, 12]; r is the radius of particles; l is the distance between the particles). This resulting in

$$\sigma_y = \sigma_0 + \Delta\sigma_{SS} + \Delta\sigma_g + \Delta\sigma_p + \Delta\sigma_{SG} + \Delta\sigma_d + \Delta\sigma_{part}.$$

The examination of structure in the zone of welding and evaluation of change in properties were also made on the joints of a similar pair of metals (aluminium with steel), made by the explosion welding.

Changes in structure parameters, including intermetallic phases (their sizes, density of distribution), for the mentioned type of the joint are shown in Figure 4, *a*. Results of calculations of contribution of each of the structure parameters to the change in strength characteristics in different zones of welding are given in Figure 4, *b*, and a vector diagram (Fi-

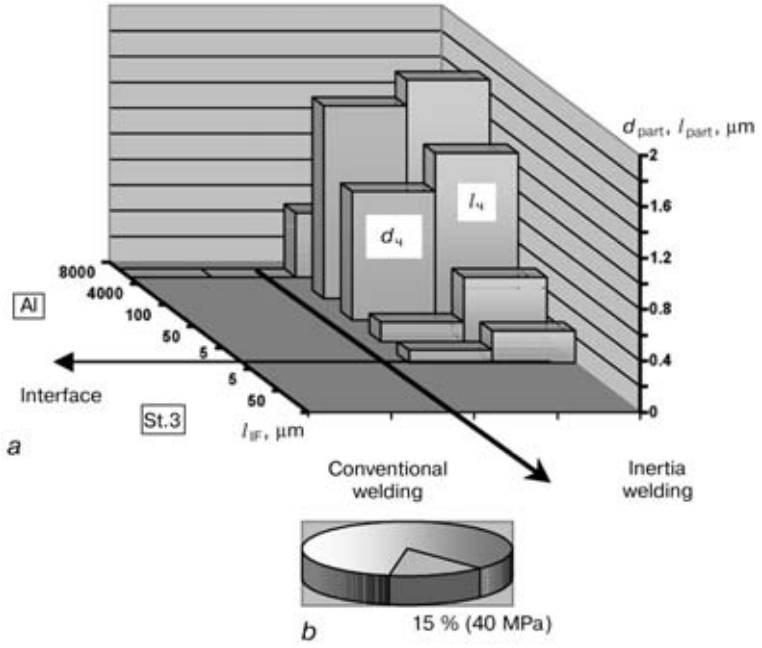

Figure 3. Change in sizes of inner-volume dispersed particles of phase precipitations in aluminium d_{part} and distance between them l_{part} in the zone of contact of St.3 + aluminium joints made by conventional welding (*a*), and also contribution of these parameters to a total strengthening in inertia welding (*b*)

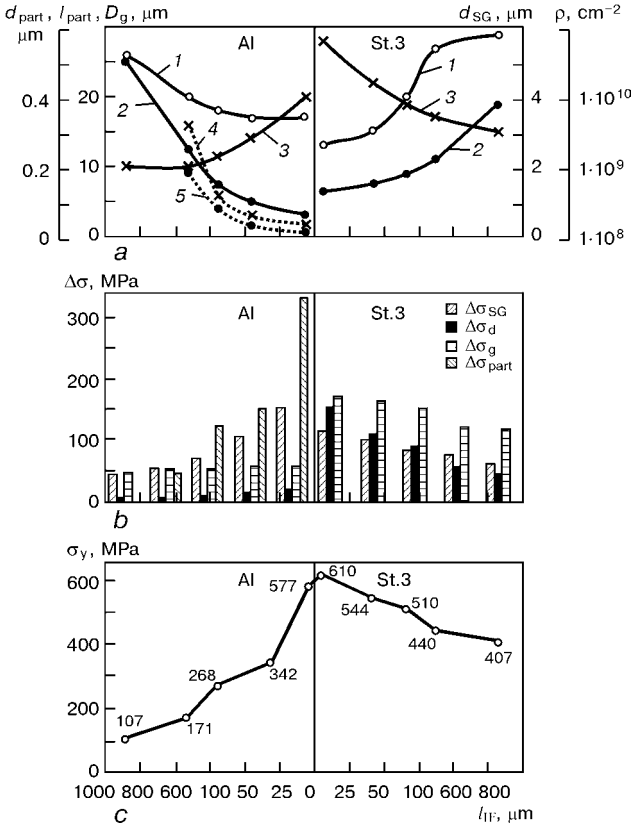

Figure 4. Change in structure and strength properties in St.3 + aluminium joints made by explosion welding at different distance from interface l_{IF}: *a* — distribution of main structural parameters of welding zone (*1* — D_g; *2* — d_{SG}; *3* — ρ; *4* — l_{part}; *5* — d_{part}); *b* — contribution of separate structural parameters in strengthening of different zones of the joint; *c* — total strengthening stipulated by the structure of the welded joint metal

gure 4, *c*) reflects the total strengthening. The Table shows results of calculation of contribution of each of structure parameters to the strengthening of metal of different zones of the welded St.3 + aluminium joint in explosion welding.

Analysis of experimental and calculated data showed that in explosion welding there is no gradient of mechanical properties directly along the interface which is observed usually in welding dissimilar metals. Moreover, the total increase in strength properties occurs both from the steel side and also from the aluminium side, which is manifested more clearly.

It should be noted that the increase in strength of the welded joint from the steel side is provided mainly due to the increase in a total density of dislocations and refining of the grain structure and substructure (Figure 5, *a, c*). From the aluminium side a significant increase in yield strength in the contact zone occurs mainly due to the formation of dispersed new phases, distributed in volumes of grains (Figure 5, *e*) and also refining of substructure (Figure 5, *b, d*). Thus, it can be concluded by analyzing the dynamics of changing properties of each of materials welded in the zone of welding that the main contribution into the strengthening of the welded joint from the aluminium side (with respect to strength of the parent metal) is made by refining of grain and subgrain structures, i.e. 58 MPa (52.7 %) and 151 MPa (137.3 %), respectively, formation of the new dispersed intermetallic phases, i.e. 332 MPa (301.8 %) and also increase in density of dislocations, i.e 20 MPa (18.2 %). The total strengthening in this, as a rule, weakened zone of the welded joint is 577 MPa, that approximately 5 times exceeds the strength of as-initial aluminium.

It is important to outline again the role of the new phase formations in the change of properties directly in the zone of interaction from the side of the least strong metal (aluminium in this case). As was shown earlier, the particles of phase precipitations, dispersed and uniformly distributed in inner volumes of the aluminium grains (Figure 5, *e*), have a ternary effect on the strengthening nature. Firstly, particles promote the formation of a fine-grain structure, and the effect of phase precipitations on increment of yield strength in this case is realized by the known mechanism of Hall–Petch [6, 7]; secondly, it is a barrier influence of forming particles in the zone of welding that preserves a high level of density of dislocations that is reflected in the increase of a component of dislocation strengthening [8, 10]; thirdly, the strengthening is provided by the particles proper, whose effect is determined usually by the known relationship of Orowan [11, 12].

Calculated evaluated of yield strength (MPa) of metal regions of welded joints at different distance from interface

Mechanism of strengthening	*Distance from interface, μm*									
	Aluminium					*St.3*				
	1000	*500*	*100*	*50*	*5*	*5*	*50*	*100*	*500*	*1000*
Friction stress of lattice	6	6	6	6	6	30	30	30	30	30
Solid-solution	8	8	8	8	10	70	70	70	70	70
Subgrain	42	54	70	106	151	115	100	83	75	60
Grain-boundary	45	52	54	57	58	169	163	150	121	115
Dislocation	6	6	9	14	20	154	109	89	56	44
Dispersion	–	45	121	151	332	–	–	–	–	–
Structural (pearlite formation)	–	–	–	–	–	72	72	88	88	88
Total (calculated) strengthening, MPa	107	171	268	342	577	610	544	510	440	407

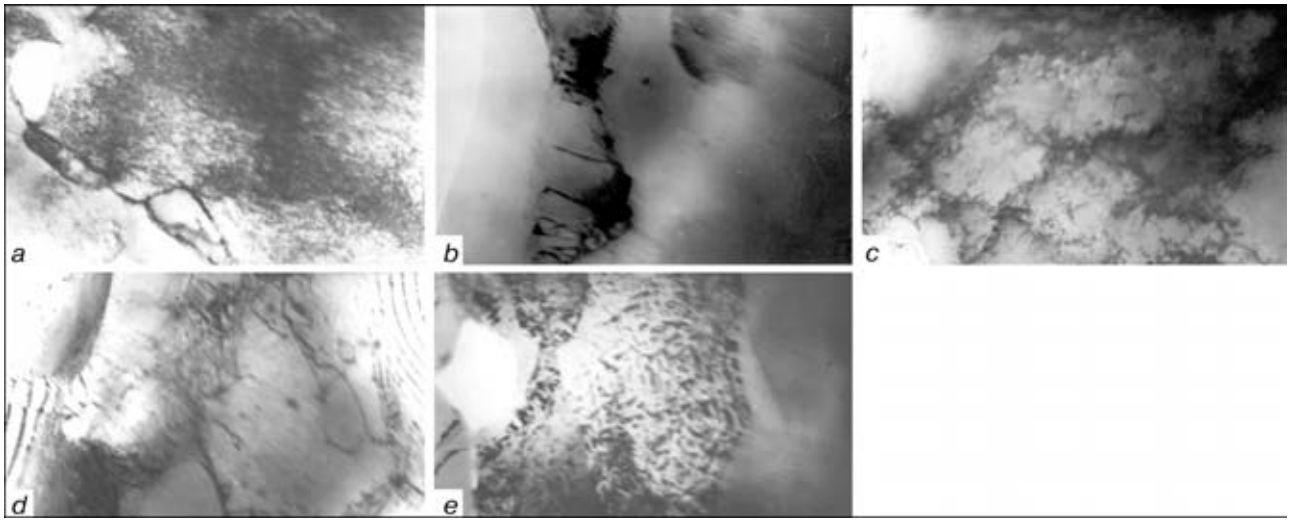

Figure 5. Fine structure of phase formation in St.3 + aluminium joints in the conditions of explosion welding: *a, b* — parent metal St.3 and aluminium, respectively (×20000); *c, d* — refining of grain and subgrain structures in the zone of contact, respectively, from the steel side (*c*) (×20000) and aluminium (*d*) (×37000); *e* — intravolume distribution of phases in aluminium (×30000)

Thus, at certain welding conditions, appropriate temperature intervals of polygonization (this is observed both in the conditions of inertia friction welding and explosion welding) the formation of the dispersed new phases uniformly distributed in inner volumes of grains in the transition zone of a less strong metal (aluminium) from the pair welded leads to a more gradual change in mechanical properties in the zone of contact of dissimilar metals (from stronger to less strong metal). This is provided by a significant strengthening of the welded joint from the side of aluminium (see Figure 4, *c*), as the aluminium represents an almost new metal by structure-phase state, which differs greatly from the initial aluminium. Structure of this, quite new aluminium, saturated with dispersed particles of phase precipitations, is similar to the structure of composite.

CONCLUSIONS

1. The optimum structure-phase state of metal of the contact zone for the conditions of welding dissimilar metals, characterized by a limited mutual solubility, is formed at definite (limited) temperature conditions of welding. This range of temperatures corresponds to temperature intervals of polygonization and provided by conditions of the inertia friction welding.

2. For optimum structure of the most soft material (aluminium) of metals welded at the temperature corresponding to the interval of polygonization, the formation of a specific structure state of a quasi-composite type is characteristic, for which the formation of dispersed intermetallic phases that promote refining of structure and increase in a total density of dislocation is typical.

3. The forming structure of a quasi-composite results in a significant (up to 260–577 MPa) strengthening of aluminium in the contact zone due to the dispersion strengthening with particles of forming phase precipitations, and also dislocation, grain-boundary and subgrain strengthening. This makes it possible to level an abrupt gradient of properties (more than 250 MPa) observed directly in the zone of contact of St.3 + aluminium welded joints.

1. Markashova, L.I., Grigorenko, G.M., Arsenyuk, V.V. et al. (1998) On relationship between structure and properties of steel-aluminium joints produced by friction welding. *Avtomatich. Svarka*, **8**, 7–14.
2. Suzuki, H. (1967) On yield stress of polycrystalline metals and alloys. In: *Structure and mechanical properties of metals*. Moscow: Metallurgiya.
3. Ashby, M.F. (1972) *On Orowan stress. In: Physics of strength and plasticity*. Moscow: Metallurgia.
4. Goldshtejn, M.I., Litvinov, V.S., Bronfin, B.M. (1986) *Metallophysics of high-strength alloys*. Moscow: Metallurgiya.
5. Konrad, G. (1973) Model of strain hardening to explain influence of grain size on flow metals stress. In: *Ultrafine grain in metals*. Moscow: Metallurgiya.
6. Armstrong, R.V. (1973) Strength properties of ultrafine grain metals. *Ibid*.
7. Petch, N.J. (1953) The cleavage strength of polycrystalline. *J. Iron and Steel Inst.*, **1**, 25–28.
8. Itoh, Y., Shindoh, T., Saitoh, M. et al. (1998) Characteristics of behaviour of diffusion in the transition zone of a copper aluminium joint during friction welding. *Transact. Jap. Soc. Mech. Eng. A.*, **618**, 494–499.
9. Orowan, E. (1954) *Dislocation in metals*. New York: AIME.
10. Ashby, M.F. (1983) Mechanisms of deformation and fracture. *Adv. Appl. Mech.*, **23**, 118–177.
11. Kelly, A., Nickolson, R. (1966) *Dispersion hardening*. Moscow: Metallurgiya.
12. Ebelling, R., Ashby, M.F. (1966) Yielding and flow of two phase copper alloys. *Phil. Mag.*, **7**, 805–809.

FUSIBILITY CURVES FOR ALLOYS OF THE Sn–Zn–Bi SYSTEM

V.F. KHORUNOV[1], V.I. SHVETS[1], T.G. TARANOVA[1] and G.F. KOBZENKO[2]
[1]The E.O. Paton Electric Welding Institute, NASU, Kyiv, Ukraine
[2]G.V. Kurdyumov Institute of Metal Physics, NASU, Kyiv, Ukraine

Fusibility curves and structural peculiarities of alloys of the Sn–Zn–Ni systems in a range of Sn-rich compositions were studied using differential thermal analysis. The resulting data can be employed for development of commercial Pb-free solders for soldering parts used in radio electronics.

Key words: *lead-free solder, alloy of the Sn-Zn-Bi system, fusibility curve, microstructure, electronics*

Alloys of the Sn–Pb system are the basic type of solders used in electronics. Lead is known to be a toxic element. One of the most important tasks of modern radio electronics is to make environmentally clean Pb-free solders. This task is difficult, because it is necessary to take into account a unique physical nature of solders of the Sn–Pb system and a wide field of their application.

As evidenced by literature data, owing to close melting temperatures, alloys of the Sn–Zn–Bi system can successfully substitute for the Sn–Pb system solders widely applied in electronics.

Phase transition temperature of alloys of the Sn–Zn–Bi system

Alloy series No.	*Alloy No.*	*Alloy composition*	T_b^{eu}, °C	T_e^{eu}, °C	T_e^{al}, °C
I	10	Sn–9Zn	194	200	–
	1	Sn–9Zn–2Bi	182	197	–
	2	Sn–9Zn–5Bi	171	196	–
	3	Sn–9Zn–10Bi	154	192	–
	4	Sn–9Zn–15Bi	147	186	–
II	9	Sn–1Zn	195*	200*	–
	5	Sn–1Zn–1Bi	189	195	226.0
	6	Sn–1Zn–3Bi	172	190	224.5
	7	Sn–1Zn–5Bi	167	185	221.0
	8	Sn–1Zn–7Bi	158	181	218.0
	11	Sn–1Zn–10Bi	156	183	216.0
	12	Sn–1Zn–13Bi	151	169	212.0
III	13	Sn–7Bi	180*	222*	–
	8	Sn–7Bi–1Zn	158	181	218.0
	14	Sn–7Bi–3Zn	167	190	208.0
	15	Sn–7Bi–5Zn	161	193	206.0

Notes. T_b^{eu} and T_e^{eu} are the temperatures of the beginning and end of melting of eutectic, respectively; T_e^{al} is the temperature of the end of melting of an alloy; the asterisk marks the temperature of the beginning and end of solidification of solid solution.

One study on alloys of the Sn–Zn–Bi system is known from the book «Constitutional Diagrams of Metal Systems» [1], which provides the most comprehensive information on the subject. This study presents calculation lines for the liquidus surface. The liquid temperatures range approximately from 150 to 400 °C.

The MSI database on the constitutional diagrams by 2001 had included 13 publications on investigations of alloys of the Sn–Zn–Bi system, including those additionally alloyed with cadmium, indium and lead. Unfortunately, now the access to a more comprehensive information on the subject is difficult.

The purpose of this study was to experimentally investigate the fusibility curves and structural peculiarities of alloys of the given system as the most important characteristics required for development of solders.

Polythermal profiles of the constitutional diagrams of alloys with a constant zinc content of 9 and 1 % (Sn–9Zn–...Bi, Sn–1Zn–...Bi) and bismuth content of 7 % (Sn–7Bi–...Zn) were considered in a range of compositions rich in tin.

The charge compositions of the alloys are shown in the Table. These alloys were melted in argon in a furnace with induction heating using alundum cruci-

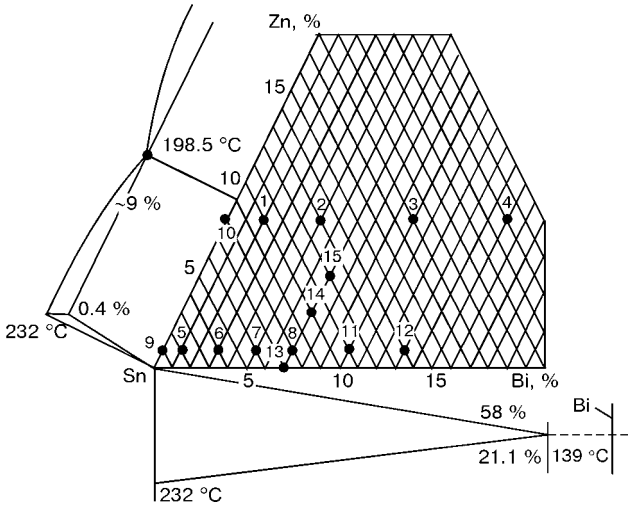

Figure 1. Position of figurative points (*1–13*) of alloys being analysed on a plane of the concentration triangle

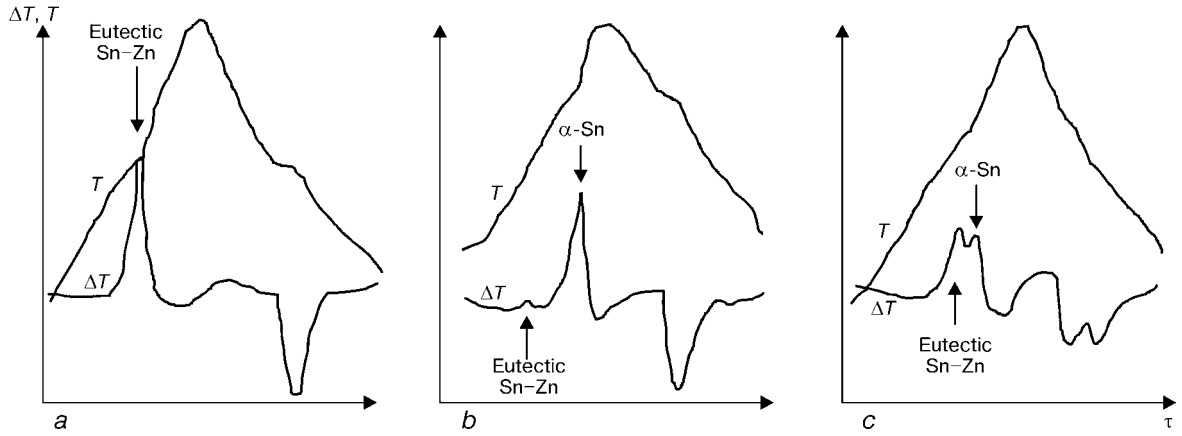

Figure 2. Characteristic thermal curves ($T = f(\tau)$, $\Delta T = f(T, \tau)$) of alloys of the Sn–Zn–Bi system: *a* — Sn–9Zn–5Bi; *b* — Sn–1Zn–3Bi; *c* — Sn–7Bi–3Zn

bles. The source materials were tin OVCh-000, bismuth Vu0 and zinc TsVCh. A total number of alloys melted was 15 (Figure 1).

Binary metal systems have been studied in detail up to now. It is known that tin combines with zinc and bismuth to form eutectic systems of two limited solid solutions with the eutectic point at a tin content of about 9 and 42 % and temperature of 198 and 139 °C, respectively [2].

As follows from the constitutional diagram of the Bi–Zn system, eutectic is formed between a solid solution of zinc in bismuth and zinc in a range of alloys rich in bismuth [3]. Here the eutectic point corresponds to a zinc content of 2.7 wt.% and temperature of 254.5 °C. Zinc and bismuth have a limited solubility not only in solid but also in liquid state, and at 416 °C they form a system with a monotectic equilibrium and a monotectic point corresponding to a zinc content of 98.1 %.

Therefore, the Sn–Zn–Bi system is limited to three binary systems of the eutectic type, and is likely to be the system with a ternary eutectic.

Data of this study were generated using differential thermal analysis, metallography and X-ray microanalysis.

Phase transition temperatures were determined using the Q-1500D derivatograph in helium. The involved crucibles with covers were made from aluminium oxide. The heating rate was 5 K/min. Cooling rate was not specified. Based on position of the curves of the $T = f(\tau)$ dependence (Figure 2), it equals approximately 5 K/min.

As thermal analysis was carried out in a heating mode using a non-controlled heat flow, ranges of phase transition temperatures turned out to be widened as a result of shift of the temperature of the end of melting of the eutectic towards higher temperatures. Consequently, the experimental data were corrected (see the dashed curve in Figure 3, *a, b*) by a value revealed by analysis of melting of pure metals, i.e. tin and bismuth. In a region corresponding to the zinc content of 0–1 % (Figure 3, *c*), the dashed line shows the shape of the curve predicted by the authors.

Microstructure of alloys was examined in the cast state and after thermal analysis using the scanning

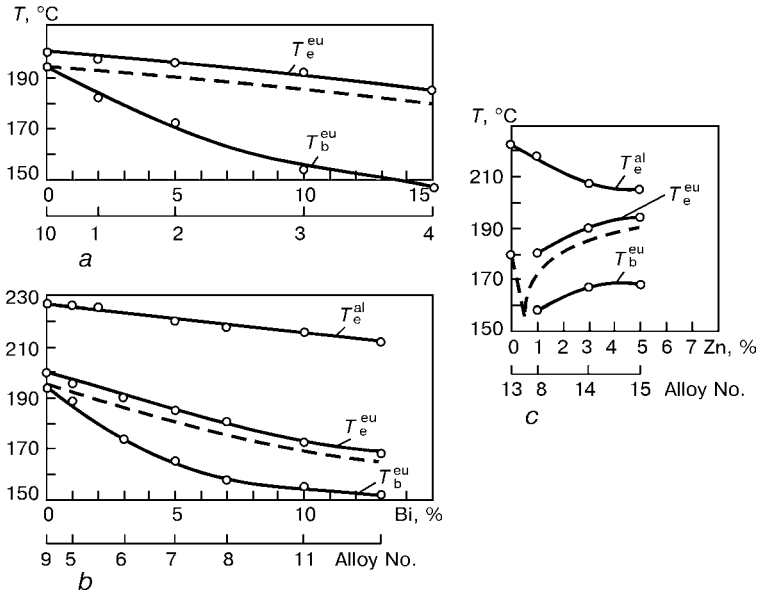

Figure 3. Polythermal profiles of the fusibility curves of alloys of the Sn–Zn–Bi system: *a* — Sn–9Zn–...Bi (alloy of series I); *b* — Sn–1Zn–...Bi (alloy of series II); *c* — Sn–7Bi–...Zn (alloy of series III)

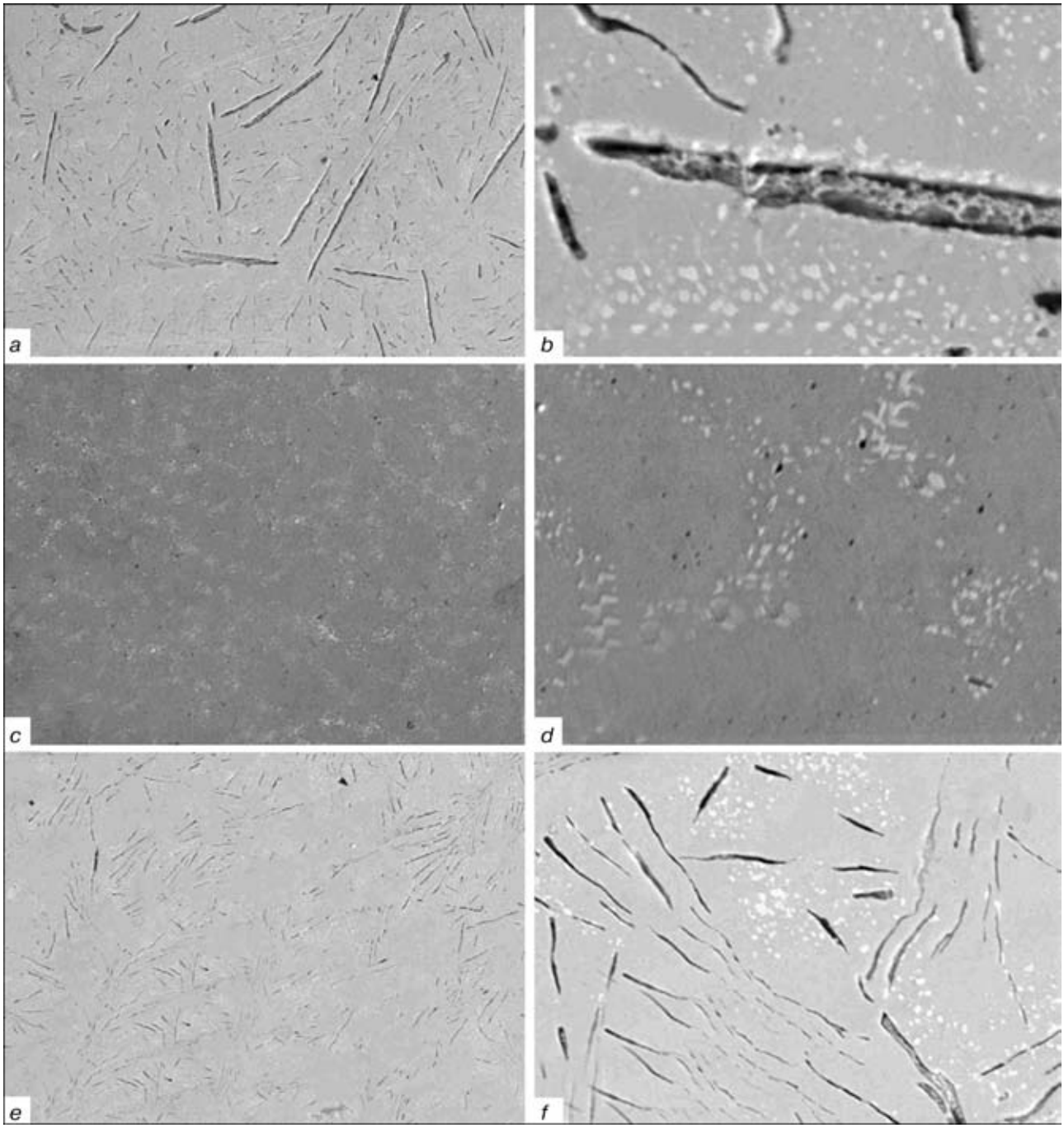

Figure 4. Characteristic microstructures of alloys of the Sn–9Zn–...Bi system (alloy Sn–9Zn–5Bi of series I) (*a*), Sn–1Zn–...Bi (alloy Sn–1Zn–5Bi of series II) (*c*), and Sn–7Bi–...Zn (alloy Sn–7Bi–5Zn of series III) (*e*): *a*, *c*, *e* — general view (×100); *b* — (×1000); *d*, *f* — fragments at higher magnification (×500)

electron microscope ISM-840 with the microanalyser «Link-Systems». The data obtained from X-ray microanalysis were used to identify structural components of the alloys in accordance with the binary constitutional diagrams of hypothetical solid solutions based on tin, bismuth and zinc.

Thermograms of the alloys, based on polythermal profile of the constitutional diagram of the Sn–Zn–Bi system with a constant content of zinc equal to 9 wt.% (series I) show one peak (Figure 2, *a*). Increase in the bismuth content is accompanied by a shift of the peak towards lower temperatures. This also involves decrease in temperatures of the beginning and end of phase transition (Figure 3, *a*, and the Table).

Microstructure of the analysed alloys of series I (Figure 4, *a*, *b*) is a tin matrix with acicular inclusions of the Zn-based phase and spherical fine inclusions of the Bi-based phase (the latter are absent in the Sn–9Zn alloy).

It is likely that the peak observed in the thermograms is caused by a heat effect of melting (solidification) of binary eutectic Sn–Zn, and the Bi-based inclusions are the redundant phase formed in solid state as a result of a substantial decrease in solubility of bismuth in the α-Sn phase during cooling. Precipitation of zinc should be similar in nature. The latter is likely to deposit on the Zn-based eutectic crystals.

Thermograms of alloys of the polythermal profile with a constant zinc content of 1 % (series II) show two peaks (see Figure 2, *b*). Increase in the bismuth content is also accompanied by a shift of both peaks to a region of lower temperatures. In this case the low-temperature peak remains insignificant compared with the high-temperature one. Dependence of temperatures of the beginning and end of the corresponding phase transitions upon the bismuth content is shown in Figure 3, *b*, while the numeric values are given in the Table.

Microstructure of this series of the alloys (Figure 4, *c, d*) contains grains of the Sn-based phase framed by the Bi-based phase inclusions. The Zn-based phase inclusions are distributed in the bulk of the matrix.

Comparison of the metallography and thermal analysis results suggests that the low-temperature peak is caused by a thermal effect of melting (solidification) of the binary eutectic Sn–Zn, whereas the high-temperature one is caused by that of primary crystals α-Sn. The α-Bi phase is redundant. Increased density of precipitates of this phase along the boundaries of grains of the α-Sn phase results from segregation heterogeneity of primary crystals. The presence of an insignificant amount of the Zn-based phase inclusions is determined by a small volume fraction of binary eutectic Sn–Zn.

Thermograms of alloys of the polythermal profile with a constant bismuth content of 7 % (series III) show two peaks (see Figure 2, *c*). It should be noted that increase in the zinc content leads to a substantial enhancement of the low-temperature effect. This causes the temperatures of the beginning and end of phase transition to increase. The range of the phase transition temperatures causes formation of the high-temperature effect, which is attributable to increase in temperature of the beginning of phase transformation and decrease in temperature of the end of phase transformation (see Figure 3, *c*, and the Table).

Microstructure of the alloys (see Figure 4, *e, f*) is similar to that of the alloys with a constant zinc content of 9 %. It is likely that the high-temperature heat effect is also caused by solidification of primary crystals α-Sn, and the low-temperature one is caused by binary eutectic Sn–Zn. Increase in the zinc content leads to increase in volume fraction of the eutectic.

It can be assumed that the ternary eutectic may also exist, proceeding from character and temperatures of phase transitions in the Sn–Zn, Sn–Bi and Bi–Zn systems and results of investigation of ternary alloys of the Sn–Zn–Bi system.

Investigations of alloys with a higher bismuth and zinc contents (Sn–20Zn–60Bi) proved the presence of the four-phase eutectic equilibrium L ↔ α-Sn + + α-Zn + α-Bi (here L is the liquid) at a temperature of 108 °C.

Therefore, the experimental data obtained are in agreement with the theoretical postulates, according to which solidification of the alloys considered begins from precipitation of primary crystals α-Sn, then follows formation of binary eutectic Sn–Zn. An exception is possible for a narrow range of compositions of alloys adjoining the Sn–Bi side of the concentration triangle (see Figure 1), which solidify as solid solution.

The data obtained on the ranges of melting and structure of alloys of the Sn–Zn–Bi system allow a conclusion that alloys of this system are promising for the use as substitutes for the Sn–Pb solders.

The E.O. Paton Electric Welding Institute has all necessary capabilities to produce solders of an optimal composition to meet the needs of interested companies.

1. (1977) *Constitutional diagrams of metallic systems published in 1977*. USSR State Committee on Science and Technology of USSR AS. Issue XXIII. Moscow: VINITI
2. (1996) *Constitutional diagrams of binary metallic systems*. Refer. Book. Vol. 3. Ed. by N.P. Lyakishev. Moscow: Mashinostroenie.
3. (1996) *Ibid.* Vol. 1.

WEAR-RESISTANT COMPOSITE COATINGS WITH FILLERS OF Fe–B–C SYSTEM

I.M. SPIRIDONOVA, E.V. SUKHOVAYA and **S.B. PILYAEVA**
Dnepropetrovsk National University, Dnepropetrovsk, Ukraine

Structure and abrasive wear resistance of composite coatings with a brass binder and fillers, made from alloys (Fe–B–C), containing 0–9 % B, 0–4 % C, Fe being the balance, deposited on steel components, are studied. The effect of structural and phase composition of the filler on structure and width of zones of a contact interaction forming at the interfaces of composite coatings is shown. Optimum sizes and structural composition of zones of interaction are determined which provide the higher wear resistance of the composite coatings.

Key words: *composite material, coating, impregnation, interphase interaction, dissolution, abrasive wear resistance*

During the recent years the composite materials find the wide application as coatings to protect and to restore the quick-worn parts of the equipment. These materials represent a heterogeneous system which is characterized by a thermodynamic instability due to the presence of developed internal interfaces. The instability results in an interphase interaction of components in the process of producing and service of composite coatings, which can lead to the formation of new undesirable phases at the interfaces, thus deteriorating the service characteristics.

Therefore, the effect of structural and phase composition of composite coatings with fillers of Fe–B–C system (0–9 % B, 0–4 % C, Fe being the balance) on their wear resistance was studied (Table 1). Brass L62 was used as an alloy-binder. Composite coatings were produced using the method of furnace impregnation. For this purpose, the filler granules of 0.5–2.0 mm sizes were poured and packed in the mould, which resembles the surface of a steel part with a gap equal to the thickness of the composite coating being deposited. At the top, the lumps of an alloy-binder were located. After the mould sealing the billet was put into a furnace heated up to 1050 °C temperature. Isothermal soaking in the furnace, required for a uniform heating of the billet, was 30 min. Then, the billet was cooled together with a furnace at the 0.2 °C/s rate. After impregnation completion the mould was removed by a mechanical treatment (cutting and grinding).

The produced composite coatings were examined using the metallographic, X-ray diffraction and X-ray microanalysis. Wear resistance in the conditions of the abrasive wear was examined in the unit which can estimate the decrease in a sample mass during grinding with an emery paper at 413 m path. Samples were of 16×6×16 mm sizes. Experiments were performed at temperature 20 ± 2 °C and relative humidity of air 60 ± 5 %. Accuracy in determination of mass losses was 0.0002 g in scales VLA-200M. Sample from steel 70KhL was used as a reference.

Structure of the examined composite coatings is characterized by the presence of the filler particles of irregular or spherical shape, distributed uniformly in matrix and occupying 55–60 % of volume. Structural and phase composition of the filler is changed completely only in alloy No.1. After impregnation the crystals of ferrite and flaky graphite are observed instead of initial ledeburite structure (Table 1), which proves about proceeding of process of a cementite decay in the filler (Figure 1, *a*).

Table 1. Chemical and structural composition of alloys-fillers of Fe–B–C system

Alloy No.	*Chemical composition, %*		*Cooling rate, °C/s*	*Shape of particle*	*Structural composition*
	B	*C*			
1	–	4.0	1000	Spherical	Eutectic Fe–Fe_3C
2	0.5	4.0	100	Irregular	Fe_3(C, B), eutectic Fe–Fe_3(C, B)
3	5.0	–	100	Same	Fe_2B, eutectic Fe–Fe_2B (30 %)
4	4.7	1.5	100	»	Fe_2(C, B), Fe_3(C, B), eutectic Fe–Fe_3(C, B)
5	9.0	–	100	»	Fe_2B, eutectic Fe–Fe_2B (5 %)
6	9.0	0.2	100	»	Fe_2(B, C), eutectic Fe–Fe_2(B, C) (5 %)
7	9.0	0.2	1000	Spherical	Fe_2(B, C), eutectic Fe–Fe_2(B, C) (12 %)
8	9.0	2.0	100	Irregular	Fe_2(B, C), eutectic C–Fe_2(B, C)

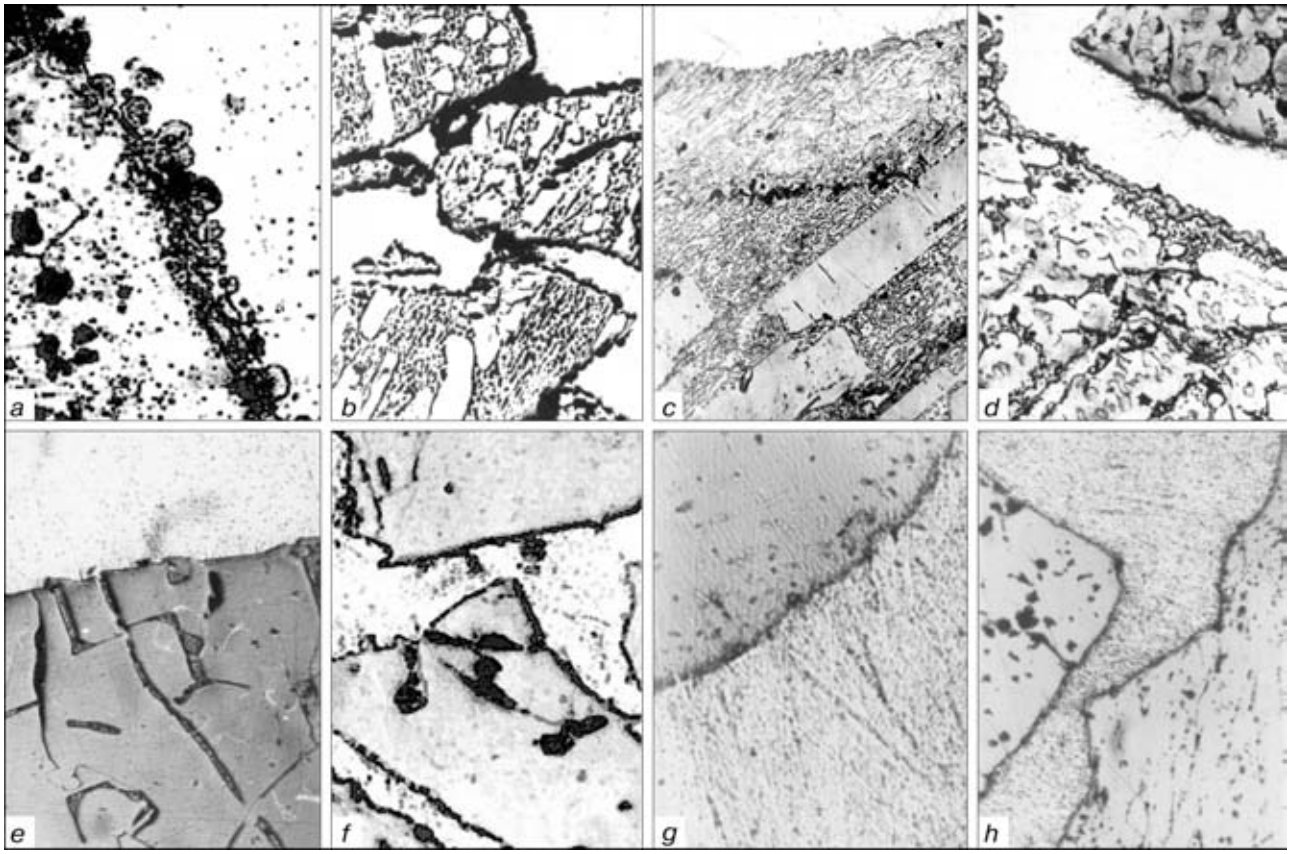

Figure 1. Microstructure of composite coatings with fillers of Fe–B–C system (×200): *a–h* — number of alloy according to Tables 1 and 2

In all the samples at the interface with a brass from the side of a matrix a continuous row of solid solutions Cu–Fe–Zn–C–B is formed (Figure 2). From the filler side a layer of recrystallization is formed. In sample No.1 a continuous crown or separate crystals of a globular shape with a pearlite structure, alloyed with zinc and copper a little, are appeared near the interface (Figures 1, *a*, and 2). When 0.5 % B is added into the composition of the filler Fe–4 % C (alloy No.2) the processes of graphitization are suppressed and the primary crystals $Fe_3(C, B)$ and ledeburite alloyed with boron are observed again in the filler structure after impregnation (Table 2). Morphology of eutectic colonies is changed due to proceeding of processes of a high-temperature coalescence. At the interface, the composition of austenite in eutectic is changed as a result of zinc and copper dissolution in it. In addition, crystals of globular pearlite are appeared here additionally (Figure 1, *b*). Width of zones of contact interaction in sample No.2 is preserved as compared with sample No.1 (see Table 2). In sample with a filler made from alloy No.3 a conglomerate of phases consisting of a solid solution on the base of iron, pearlite and Fe_2B is formed at the interface with a brass instead of the initial eutectic Fe–Fe_2B (Figure 1, *c*). The zones of contact interaction forming at the interface between the filler and matrix have a maximum width in this sample.

The initial structure of alloy-filler No.4 remains unchanged after impregnation and includes the primary crystals $Fe_2(C, B)$, peritectic phase $Fe_3(C, B)$ and eutectic Fe–$Fe_3(C, B)$ (see Table 1). The degree of completion of a peritectic reaction $L + Fe_2(C, B) \rightarrow$ $\rightarrow Fe_3(C, B)$ in the filler is not changed. From the side of the filler the crystals with a pearlite structure are formed additionally in the structure of the interaction zone (Figure 1, *d*).

With increase in boron content in the filler No.5 up to 9 % as compared with 5 % B in the sample No.3 the content of the primary phase Fe_2B in the structure

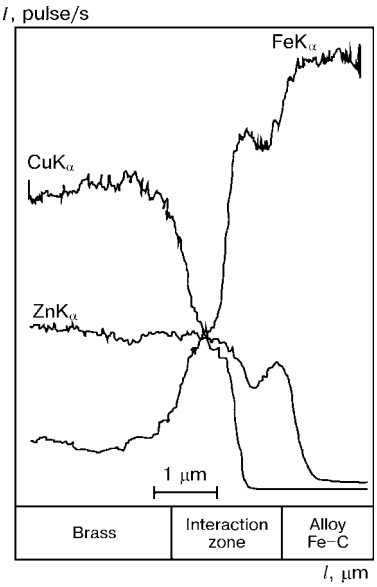

Figure 2. Diagram of distribution of intensity of radiation of elements in the probe passing through the region of interface (Fe–4 % C)/L62

Table 2. Structural composition and width of zones of a contact interaction at the interfaces between the filler of Fe–B–C system and matrix of composite coatings

Alloy No.	*Structural composition of zones of interaction from the filler side**	*Width of zones of interaction, μm*
1	Pearlite, ferrite, graphite	15–30
2	Pearlite, $Fe_3(C, B)$, eutectic Fe–$Fe_3(C, B)$	15–30
3	Fe, Fe_2B, pearlite, eutectic Fe–Fe_2B	100–120
4	Pearlite, $Fe_2(C, B)$, $Fe_3(C, B)$, eutectic Fe–$Fe_3(C, B)$	20–40
5	Solid solution on Fe_2B base, conglomerate of phases Fe and Fe_2B	10–15
6	Solid solution on $Fe_2(B, C)$ base, conglomerate of phases $Fe_2(B, C)$ and solid solution on Fe base	10–15
7	Solid solution on $Fe_2(B, C)$ base, conglomerate of phases $Fe_2(B, C)$ and solid solution on Fe base	15–25
8	Solid solution on $Fe_2(B, C)$ base, eutectic C–$Fe_2(B, C)$	< 5 μm

*A continuous row of solid solutions Cu–Fe–Zn–C–B is formed from the matrix side.

is increased, and the eutectic Fe–Fe_2B is decreased (see Table 1). Morphology of eutectic Fe–Fe_2B after impregnation is changed and a coarse conglomerate of phases consisting of solid solutions on the base of Fe and Fe_2B is formed along the boundaries of grains Fe_2B (Figure 1, *e*). Additional alloying with 0.2 % C of alloy No.6 leads to the appearance of a phase $Fe_2(B, C)$ in the filler structure and to the formation of a coarse conglomerate of solid solutions on the base of Fe and Fe_2B (Figure 1, *f*). Volumetric ratio of structural components in the filler is not changed. The increase in cooling rate of the alloy of Fe–9 % B–0.2 % C system (alloy No.6) from 10^2 to 10^3 °C/s (alloy No.7) leads to the growth of a volume content of the above-mentioned conglomerate of phases γ and $Fe_2(B, C)$ in structure from 5 to 12 vol.% (Figure 1, *g*). With increase in carbon content in alloy No.8 up to 2 % in the filler structure instead of conglomerate of phases γ and $Fe_2(B, C)$ the eutectic C–$Fe_2(B, C)$, having a globular fine-dispersed structure, is appeared (Figure 1, *h*).

Structure of interface from the side of filler in samples No.5–7 is characterized by the formation of a recrystallization layer having an increased content of iron as compared to the initial phase Fe_2B or $Fe_2(B, C)$ and alloyed with zinc and copper (Figure 1, *e–g*). Proceeding of processes of a high-temperature coalescence in these samples leads to larger distribution of phases of the coarse conglomerate and only austenite alloyed with zinc and copper is available at the interfaces of phase Fe_2B or $Fe_2(B, C)$ after impregnation. In sample No.6 this phenomenon is observed along the entire section of the filler particle, and in sample 7 — only at the interface. Unlike the samples No.5–7 the width of recrystallization layer from the side of the filler does not exceed 5 μm in the structure of sample No.8 (see Table 2). Structure changes at the interface in this sample are not observed (Figure 1, *h*). At the interface of the composite coating (Fe–B–C)/L62 with steel a decarburized layer is also formed from the side of the latter. The formation of a viscous ferrite layer, alloyed with zinc (Figure 3) has a favourable effect on the mechanical properties of the bimetal joint. A large amount of crystals with a pearlite structure are appeared from the side of coating near the interface with steel (Figure 3, *a*).

Results of determination of coefficients of a relative abrasive wear resistance of examined composite

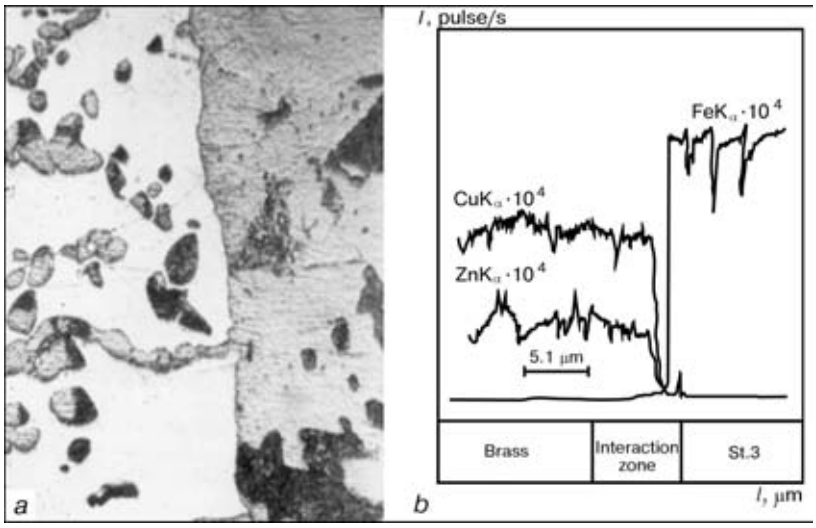

Figure 3. Microstructure (*a*) and diagram of distribution of intensity of radiation of elements in the probe passing through the region of interface L62/St.3 of composite coating with a filler of Fe–B–C system (*b*) (×200)

coatings are given in Table 3. Maximum wear resistance is typical of sample No.2, while the minimum — of sample No.8. Composite coatings, whose filler has eutectic Fe–Fe_2(C, B) in structure are characterized by the higher wear resistance (samples No.2 and 4). Then, composite coatings characterized by the presence of eutectics Fe–Fe_2B or Fe–Fe_2(B, C) in the filler structure are followed (samples No.3 and 7). With decrease in content of these eutectics in samples No.5 and 6 to 5 vol.% the wear resistance is decreased, respectively, 2 and 1.7 times. The wear resistance of sample No.8 is much lower than this characteristic in samples No.2 and 4.

The results obtained can be explained by the fact that to attain the higher wear resistance of composite coatings it is necessary to form a strong relation between the filler and matrix, and also between the composite coating and the steel part. This relation is provided owing to proceeding processes of a contact interaction at the interfaces (Fe–B–C)/L62 and L62/St.3 in composite coatings.

These processes include the following stages: wetting, dissolution of structure components of the filler and steel in the molten brass, recrystallization and solid-phase diffusion. It can be concluded on the basis of analysis of structural composition of interaction zones, forming at the interfaces, that during impregnation the phases on the austenite base are dissolved in the first turn.

The offered mechanism of a contact interaction explains the appearance of layers of recrystallization close by composition to the alloy of a limited saturation at the solid surfaces of the filler and/or steel. Austenite included into the composition of eutectics Fe–Fe_3C and Fe–Fe_3(C, B) (samples No.1, 2, 4) is dissolved to a less degree than the austenite in eutectic Fe–Fe_2B (sample No.3) that is confirmed by the results of determination of width of zones of contact interaction. This is due to a large extension of phase interfaces and increased content of iron in eutectic Fe–Fe_2B. Then, separate crystals or a continuous layer with a pearlite structure are formed at subsequent cooling at the expense of components of austenite dissolved in the brass. Composition of austenite in eutectics Fe–Fe_2B, Fe–Fe_2(C, B), Fe–Fe_3C and Fe–Fe_3(C, B) is also changed in recrystallization. As the carbide, boride and carbide-boride phases of eutectic are dissolved in impregnation with brass much slower, the recrystallization layer is characterized by a phase composition on the iron base and inherits the morphology of the initial eutectics with a coarser differentiation. Phases Fe_2B and Fe_2(B, C) in the places of contact with the molten brass are also dissolved (samples No.5–8). Except this, the austenite in samples No.5–7, included into the composition of a conglomerate of phases which form Fe_2B and Fe_2(B, C) at the grain boundaries, is dissolved. This is explained by the appearance of composite materials of a recrystallization layer with an increased iron content from the filler side at the interfaces.

Table 3. Coefficients of relative wear resistance (ε) in composite coatings with fillers of Fe–B–C system*

Alloy No.	ε_1	ε_2	ε_{av}
1	9.32	7.48	8.40 ± 0.92
2	18.48	20.56	19.52 ± 1.04
3	11.72	14.60	13.16 ± 1.44
4	12.28	14.28	13.28 ± 1.00
5	6.68	6.76	6.72 ± 0.04
6	6.76	6.72	6.74 ± 0.02
7	10.08	12.88	11.48 ± 1.40
8	5.76	5.04	5.40 ± 0.36

*Reference sample is made from steel of 70KhL grade.

Taking into account the offered mechanism of structure formation and results of determination of coefficients of a relative abrasive wear resistance of composite coatings it can be concluded that the optimum structure of the interface is formed in samples whose filler contains eutectic Fe–Fe_3(C, B). The decrease in wear resistance of composite coatings, whose filler is characterized by the presence of eutectic Fe–Fe_3C in the structure is explained by proceeding of processes of graphitizing in a non-dissolved volume of the filler during impregnation. The presence of filler Fe–5 % B of eutectic Fe–Fe_2B in the structure causes the intensification of processes of dissolution of the filler in the molten brass. This results in decrease of the wear resistance of the composite coatings.

The decrease in content of eutectic Fe–Fe_2B in filler Fe–9 % B does not lead to the increase in wear resistance of composite coatings as in this case the proceeding of processes of a contact interaction does not provide the formation of a reliable link between the filler and matrix.

Increase in wear resistance of the samples, strengthened by the filler of a similar composition, but cooled in solidification at a higher rate is associated with the increase in content of eutectic Fe–Fe_2B in structure and, consequently, with intensification of processes of contact interaction and formation of stronger interfaces between the filler and matrix in the composite coatings. The lowest wear resistance of samples with a filler Fe–9 % B–2 % C is explained by the absence of austenitic phases in its structure. The processes of dissolution of the phase Fe_2(B, C) at the interface of this composite coating are proceeding slowly and, consequently, the link between the filler and matrix is insufficient to attain the optimum strength of the material.

Thus, it is possible to control the processes of a contact interaction proceeding at the interface of composite materials used to produce coatings on steel parts by a proper selection of structural and phase composition of the fillers of Fe–B–C system. Owing to this, a reliable link of filler and matrix, required to attain the high wear resistance of composite coatings is provided in the conditions of the abrasive wear.

NEW DOCUMENTS FOR MANUFACTURE AND REPAIR OF POWER GENERATION EQUIPMENT

K.A. YUSHCHENKO[1], L.V. CHEKOTILO[1], A.K. TSARYUK[1], V.D. IVANENKO[1], T.M. STARUSHCHENKO[1], A.V. KUZHEL[1], Yu.A. LYSOV[2], N.V. KRAVCHENKO[3], V.I. ULIANOV[3] and V.A. GORDIENKO[3]

[1]The E.O. Paton Electric Welding Institute, NASU, Kyiv, Ukraine
[2]Open Joint Stock Company «Energomontazhproekt»
[3]Joint Stock Company «Kyivenergo»

The list of technological instructions and process flow sheets for welding operations to be used as a guideline in manufacture, assembly and repair of power generation equipment is given.

Key words: *heat power station, thermoelectric plant, steam plant, heating boiler plant, heating system, distribution systems, gas pipelines, pipelines, pipes, welding, heat treatment, welded joints, inspection of welded joints, technological documents*

Thermal power generation plays the major role in production of heat and electric power in Ukraine. Heat power stations (TES) and thermoelectric plants (TETs) produce about 67 %, nuclear power stations — about 24.5 % and hydroelectric stations — about 8.5 % of the electric power in the country. Ukraine has 14 heat power stations* in operation, comprising 104 units of a different capacity (6 units for 150 MW, 43 units for 200 MW, 5 units for 250 MW, 42 units for 300 MW and 8 units for 800 MW), more than 20 thermoelectric and steam plants belonging to the Ministry of Power Generation, as well as power workshops operating at enterprises.** All the cities have heating boiler plants of a different capacity. In all the cases heat is supplied through heating and distribution systems.

Table 1. Characteristics of pipelines used in heat and power units

Category	*Group*	*Working medium parameters*	
		Temperature, °C	*Pressure, MPa (kgf/cm²)*
I	1	Above 560	Unlimited
	2	Above 520–560	Same
	3	Above 450–520	»
	4	Up to 450	More than 8.0 (80)
II	1	Above 350–450	Up to 8.0 (80)
	2	Up to 350	More than 4.0 (40) Up to 8.0 (80)
III	1	Above 250–350	Up to 4.0 (40)
	2	Up to 250	More than 1.6 (16) Up to 4.0 (40)
IV	1	Above 115–250	More than 0.07 (0.7) Up to 1.6 (16)

Thermal power generation is a major industry of the country. Heat power stations of Ukraine are primarily equipped with units having a capacity from 150 to 800 MW, while thermoelectric plants (and some heat power stations) incorporate units of a lower capacity, i.e. from 25 to 100 MW. The trend is to construction of higher-capacity units at thermoelectric plants. For example, a unit with a capacity of 300 MW is constructed at TETs-6 in Kyiv.

The most typical units operating at heat power stations and thermoelectric plants of Ukraine have capacity of up to 300 MW. Large power units of a high capacity (800 MW each) were put into operation in 1980–1990 at the Uglegorskaya (3 units), Zaporozhskaya (3 units) and Slavyanskaya (2 units) heat power stations.

Thermal power facilities are classed with those of an increased hazard. Almost all equipment at heat power stations, thermoelectric and steam plants, other thermal facilities, heating boiler plants, heating and distribution systems, as well as part of the auxiliary equipment (gas distribution, steam and residual fuel oil lines, pipeline hangers and supports, feed water supply lines, etc.) are subject to requirements of state legislation to ensure safe operation of heat and power units, as well as safety of attending personnel [1–10, etc.]. Scopes and complexity of welding operations employed in manufacture, assembly and repair of process equipment of heat power stations, thermoelectric and steam plants, as well as other thermal facilities, are very high. First of all, this is associated with wide ranges of steels used, billets, parts, sections and operation conditions (spatial position of pipelines and other assemblies). Manufacture, assembly and repair operations are performed using pipes, plates, forgings, structural shapes and castings from general-applica-

*Zaporozhskaya, Pridneprovskaya, Krivorozhskaya, Zuevskaya, Kurakhovskaya, Luganskaya, Slavyanskaya, Starobeshevskaya, Burshtinskaya, Dobrotvorskaya, Ladyzhinskaya, Uglegorskaya, Zmievskaya, Tripolskaya.

**TETs-2, TETs-3, TETs-4, TETs-5, TETs-6 (Kyiv), TETs-2 «Eskhar», TETs-3, TETs-4 (Kharkiv), Sevastopolskaya, Lisichanskaya, Kramatorskaya, Cherkasskaya, Severodonetskaya, Energodarskaya, TES of the Zaporizhya Aluminium Production Works, Open Joint Stock Company «Azovstal» and Ilyich Metallurgical Works (Mariupol), Open Joint Stock Company «Krivorozhstal» and Eastern Mining Facility (Zheltye Vody), etc.

Table 2. Modules of Technological Instructions (TI) and Process Flow Sheets (PFS) for welding, heat treatment and inspection of welded joints in process equipment of heat power stations, thermoelectric plants, steam plants, heating boiler plants, heating and distribution systems and gas pipelines

Index of TI and PFS	*Designation of TI and PFS*
	Preparation of production and improvement of skill of workers performing assembly, welding and inspection of welded joints
009	Instruction for qualification of work places of welders, flaw detection specialists and fitters
023	Technology for manufacture of backing rings
025	TI for feeding argon inside a pipe for welding power unit pipelines*
011	TI for preliminary inspection of welding consumables and shielding gases
	Welding of pipelines and process equipment
001	TI for manual arc welding of carbon and low-alloy steel station pipelines for heat and power units*
002	TI for manual arc welding of high-temperature pearlitic steel station pipelines for heat and power units*
003	TI for manual argon-arc and combined welding of pearlitic steel pipelines from 20 to 100 mm in diameter for heat and power units*
004	TI for welding of gas pipelines from gas distribution substations to boilers and main pipelines*
005	TI for welding of austenitic steel pipelines for power units*
006	TI for welding dissimilar steel pipelines for power units*
007	TI for welding of austenitic steel nozzle branch pipes for power units*
012	TI for manual arc welding of steam and hot water pipelines (categories III and IV) and inside a boiler*
013	TI for manual arc welding and inspection of welded joints in reheat pipelines of low-alloy high-temperature pearlitic steels at heat and power units*
014	TI for welding and inspection of welded joints of supports and hangers to pipelines*
015	TI for welding of pearlitic steel nozzle branch pipes*
018	TI for manual arc welding of heating main pipelines (from 76 to 1020 mm in diameter) and distribution systems*
020	TI for welding of load-carrying and enclosure metal structures for heat and power units*
022	TI for welding of pipelines on a backing ring*
026	TI for welding of plate structures for manufacture and assembly of large-size vessels (tanks)
028	TI for butt welding of oil and steam-residual fuel oil pipelines*
029	TI for welding in manufacture of section branch pipes*
	Repair of elements of equipment and welded joints
008	TI for repair of sections of pipelines after transportation and reshipment*
017	TI for repair of defects of welded joints in pipelines*
019	TI for repair of typical damages in medium- and high-pressure steam lines during operation*
021	TI for repair of pipe systems of steam and water-heating boilers*
	Equipment and technology for preheating and heat treatment of welded joints
027	TI for preheating of edges in welding and heat treatment of welded joints**
	Inspection of welding consumables and welded joints
011	TI for preliminary inspection of welding consumables and shielding gases
016	TI for radiographic inspection of welded joints in nozzle branch pipes of pipelines
024	TI for preliminary inspection and monitoring during welding
	In-process inspection of welding and heat treatment of welded joints
010	PFS for the technological process of welding of pearlitic steel pipelines
030	PFS for the technological process of welding of austenitic steel pipelines
031	PFS for the technological process of welding of dissimilar steel pipelines
032	PFS for the technological process of heat treatment in welding of power unit pipelines

*With flow charts.
**To be considered together with instructions 001, 002, 003, 005, 007, 008, 012, 013, 015, 017, 018, 019, 021, 022, 026, 028, 029.

tion carbon steels (all modifications of St.3), high-quality carbon steels of pearlitic grades (St.10, St.20), low- and medium-alloyed steels (of the Mn–Si, Cr–Mo and Cr–Mo–V systems), high-temperature steels of pearlitic grades (12KhM, 12Kh1MF, 15Kh1M1F, etc.), other high-alloy chromium steels of the 12Kh11V2MF grade and chrome-nickel austenitic steels of the 12Kh18N12T, 12Kh18N10T, 08Kh18N10T and other grades. One-third of heat and power units consists of pipelines of four categories and nine groups (Table 1) of the above steel grades. Welding of pipelines with a diameter of less than 800 mm involves much difficulties, as in this case there is no way of welding the weld root from inside of a pipe.

All the available fusion welding methods are employed for manufacture of process equipment for heat and power units, whereas repair is carried out using covered-electrode welding, TIG welding in argon atmosphere with and without a filler wire and combined welding. In the latter case the weld root (1–2 beads) is welded in argon and groove is filled using covered electrodes. At negative temperatures all the assemblies are welded with preheating, while those of carbon steels with a carbon content of more than 0.18 % and of low- and medium-alloyed steels, independently of the ambient temperature, are welded with preheating plus mandatory heat treatment of welded joints.

All the operations associated with welding, heat treatment and inspection of pipelines of categories III and IV operating under extreme temperature and pressure conditions are performed with special care.

Inspection of welded joints is a difficult element of a welding technology.

Specialists should take into account many state regulatory documents, including standard RD 34 15.027–89 (RTM-1S–93) «Welding, Heat Treatment and Control of Pipe Systems of Boilers and Pipelines in Assembly and Repair of Electric Power Station Equipment», to perform assembly, welding, heat treatment and inspection of welded joints in pipelines, pipe systems of boilers, auxiliary equipment, heat and distribution systems, gas pipelines and other equipment operating at heat power stations, thermoelectric plants and other thermal facilities. All such documents were prepared in a general form, this making them difficult to use. There are cases where some important requirements are not met during welding. In view of this fact, the E.O. Paton Electric Welding Institute, in collaboration with the Open Joint Stock Company «Energomontazhproekt» and Joint Stock Company «Kyivenergo», developed modules of Technological Instructions (TI) with flow charts and Process Flow Sheets (PFS) (32 items in total) for welding, heat treatment and inspection of specific assemblies of heat power stations, thermoelectric plants and other thermal facilities (Table 2).

The TI and PFS developed have been examined, agreed upon with the State Department of the Ministry of Health and Safety (Gosnadzorokhrantruda) of Ukraine and enacted since 2000–2001. These documents give a detailed description of all the stages of a technological process for welding specific assemblies of heat power stations, thermoelectric plants and other thermal facilities and systems, starting from acceptance of initial billets, factory made sections, their repair in a case of damage during transportation and handling, and ending with acceptance of finished weldments by technical inspection bodies. Also, they give recommendations on repair of assemblies with typical damage, application of welding consumables, welding and heat treatment equipment, parameters of all the preparatory operations for welding, preheating (cooling), heat treatment and inspection of welded joints. Process Flow Sheets include data on in-process monitoring by the managing- and executive-level technical and engineering employees.

Technological Instructions and Process Flow Sheets developed for welding of boiler parts, distribution systems, industrial reheat pipelines (categories III and IV) cover heat and power units with a capacity of up to 300 MW. The rest of TI and PFS can be used independently of the capacity of units available at heat power stations and thermoelectric plants.

If necessary, specialists of the E.O. Paton Electric Welding Institute can provide a specific field development of TI and PFS to meet the needs of a customer for specific heat and power units, and perform an appropriate examination and coordination with the authorities of the Gosnadzorokhrantruda of Ukraine.

Application of the documents suggested will make it possible to increase the level of preparation and performance of welding operations, improve the skill, technological discipline and responsibility of workers (operators and technical and engineering employees) involved in manufacture, assembly and repair of heat and power unit equipment, avoid mistakes in development of technologies and, consequently, provide high quality and operational reliability of equipment used at heat power stations, thermoelectric and steam plants, heating boiler plants, heat systems and gas pipelines.

The new documents are applied by Company «Kyivenergo» for construction of power unit with a capacity of 300 MW at the Kyiv TETs-6. It is planned to use them for repair and reconstruction of power units at heat power stations and thermoelectric plants.

1. *DNAOP 0.00-1.11–98*. Rules of arrangement and safe operation of steam and hot water pipings. Appr. 08.09.98. Kyiv.
2. *DNAOP 0.00-1.08–94*. Rules of arrangement and safe operation of steam and hot-water boilers. Appr. 26.05.94. Kyiv.
3. *DNAOP 0.00-1.07–94*. Rules of arrangement and safe operation of pressure vessels. Appr. 18.10.94. Kyiv.
4. *SNiP 3.05.03–85*. Heating systems. Intr. 01.06.85.
5. *SNiP 2.04.07–86*. Heating systems. Intr. 01.05.85.
6. *SNiP 3.03.01–87*. Load-carrying structures and enclosures. Intr. 01.07.88.
7. *DNAOP 0.00-1.20–98*. Safety rules for gas supply systems. Intr. 01.09.98.
8. *SNiP 3.05.02–88*. Gas supply. Rules of production and acceptance of work. Interior equipment. Exterior systems and installations. Intr. 01.06.88.
9. *SNiP 3.05.05–84*. Building codes and rules. Manufacturing equipment and industrial pipelines. Intr. 01.06.84.
10. (1997) *Current regulatory documents on protection of labour and fire safety mandatory for fulfillment by enterprises and organisations of Minenergo of Ukraine*. Kyiv: NDI Energetyky.

FEATURES OF DIRECT CURRENT STRAIGHT POLARITY WELDING OF ALUMINIUM ALLOYS

V.P. BUDNIK
The E.O. Paton Electric Welding Institute, NASU, Kyiv, Ukraine

Papers dedicated to the process of direct polarity current welding of aluminium alloys developed by the E.O. Paton Electric Welding Institute and its commercial application are reviewed. The application field of this process has been identified, the related problems are listed and advantages are shown.

Key words: *arc welding, aluminium alloys, non-consumable electrode, straight polarity, oxide film*

Development of leading industrial sectors, in particular, welding fabrication, is closely connected with development and introduction of new highly efficient technologies and equipment. In 1960–70s in FSU advanced structures were developed in space, aircraft, ship-building and other sectors of engineering with a wide scope of application of aluminium alloys. Development of «Buran» space system was started. Advanced high-strength weldable aluminium alloys were being developed and used at the same time, for instance, a number of alloys of 1915, D20, D21, 1201 type of Al–Zn–Mg and Al–Cu–Mn alloying systems. The need arose to perform single-pass welding of 10–15 mm thick metal at minimal heat input. The available welding processes did not permit satisfying these requirements. At that time the PWI started performing investigations to develop and improve advanced highly efficient processes of welding aluminium alloys, namely electron beam and helium-arc welding (HAW) at direct current of straight polarity (DCSP) [1].

Based on the data, published in foreign journals [2, 3], the non-consumable electrode straight polarity HAW process was promising. However, the information given in them mostly was of promotional nature. For successful application of HAW the industry had to solve a number of theoretical and experimental problems. The most urgent of them included investigation of the process of oxide film disruption, studying the energy characteristics, development of industrial technology, defining requirements to special equipment and its development, and studying the properties of joints in high-strength alloys.

Work on HAW investigation and introduction was conducted by a team, led by Prof. Daniil M. Rabkin. The core of the team was made up by O.N. Ivanova, V.P. Budnik, B.A. Steblovsky.

During discussion of the arising issues Prof. Rabkin emphasized more than once that solution of the posed problems depends on identifying and defining more precisely the processes, proceeding in the arc at DCSP, including those, which influence disruption of aluminium oxide film.

It was believed for a long time that cathode sputtering is the main process, promoting disruption of the oxide film in welding of aluminium alloys [4]. From this view point, it was impossible to account for the ability of producing sound welds in straight polarity welding. Work [5] suggested the possibility of an energy-based process of oxide disruption occurring in welding.

A series of experiments were conducted at the PWI, providing a reply to this question [6]. Mass-spectrometry investigations of pairs of aluminium samples revealed ion currents, corresponding to molecules of aluminium and Al_2O. Thermodynamic calculation of the possible chemical reactions in the weld pool showed the most probable type of interaction of the oxide film with molten aluminium:

$$Al_2O_3(\text{solid}) + 4Al(\text{liquid}) \leftrightarrow 3Al_2O(\text{gas phase}).$$

These experiments allowed establishing the possibility of a chemical reaction, proceeding in molten aluminium, as well as disruption of oxides in the weld pool.

Thermodynamic calculation and experimental data yielded the sought values of the equilibrium temperature of this reaction: 2300 K (theoretical) and 2130 K (at recalculation of experimental data).

Thus, it was established that disruption of oxide film in aluminium welding proceeds at high temperatures of molten metal. Therefore, development of a chemical reaction in the entire volume of the weld pool is unlikely.

Temperature conditions during welding were studied by taking measurements with tungsten-rhenium thermocouples [7]. Experiments were conducted in helium and argon. When helium was used, a temperature rise by 200–300 K was found across the entire depth of the pool, compared to welding in argon. In HAW the measured temperature directly under the arc of the liquid metal is 2000–2100 K. It is obvious that the bulk of the oxide film disintegrates directly in the near-electrode layer. These experiments also provide an explanation for insufficient disruption of the oxides, when using argon, and impossibility of its application for welding by this process.

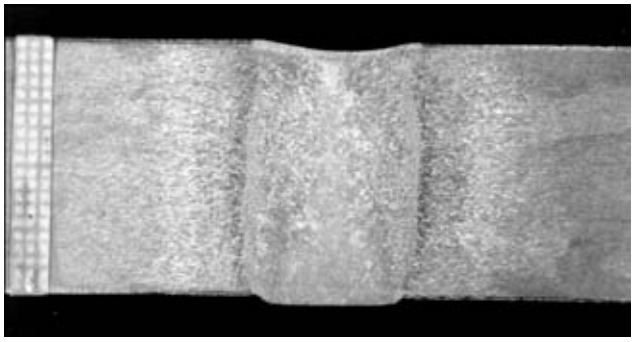

Figure 1. Macrosection of a joint of alloy 1201 20 mm thick, produced in single-pass HAW (I_w = 550 A, v_w = 6 m/h)

A sound weld surface can be obtained at a high concentration of the arc energy, which is achieved in HAW. Disruption of the oxide film is also registered in argon-arc welding but with an arc gap, close to a short-circuit in its length, and at a significantly shallower penetration. HAW also requires a short arc, but this requirement is less stringent than when argon is used. This feature of the process, as well as the need to apply expensive helium, can be regarded as the disadvantages of the above welding process.

Establishing the sequence of aluminium oxide disruption in the weld pool allowed investigation of the features of the process of DC welding. HAW advantages were studied. Process efficiency can be up to 85 %, which leads to a greater depth of penetration at smaller current (compared to other arc processes).

A high penetrability of the process permits making welds on thick metal in one pass [8]. Up to 20 mm thick joints may be produced (Figure 1). It is impossible to weld parts of such or similar thickness by single-pass argon-arc welding (AAW).

High concentration of thermal energy, high rates of heating and cooling of the base metal, lead to a narrower HAZ of the joint, exposed to high temperatures. As a result, in HAW the HAZ and weld width are 1.5 to 2 times smaller than in AC welding in argon (Figure 2) [9]. Such an advantage is particularly important in welding of heat-hardenable high-strength alloys.

It is established that in HAW it is possible to produce joints at much higher speeds than at AAW. So, a joint of metal 3 mm thick was performed at welding speed of 100 m/h without disturbing of weld formation.

The features of HAW process further include the influence of the high temperature of weld pool on the behaviour of alloying components of the metal. Evaporation of overheated interlayer from the near-anode spot is enhanced. This is particularly noticeable in welding of aluminium alloys with alloying elements (zinc, manganese, lithium), having a low boiling temperature of 907, 1107 and 1342 °C, respectively. In aluminium this index is 2520 °C. Such elements evaporate rather intensively, leaving a dark residue on the surface of the weld and the joint, which is easily removed, and does not in any way affect the joint properties. Such a residue is not formed in welding of alloys, not containing elements with a low boiling temperature. The appearance of the surface of a HAW weld on alloy 1201, is shown in Figure 3.

Process automation and development of special equipment became necessary to maintain a short arc gap in HAW. A system of automatic adjustment of arc voltage (AAAV) was developed, based on the dependence, existing between arc voltage and length. One of the components of this system is the welding torch (A-1736 type) with a mobile electrode, developed in the PWI Design Bureau. Torch control to maintain an arc gap with an error of ± 0.1 mm was performed with OB-2041 module.

The process of welding with application of AAAV system has greatly improved the stability of weld formation. The other welding equipment used may be batch-produced, without additional retrofitting.

Further development of the process of DCSP welding of aluminium alloys is aimed at increasing the level of automation with controlling the depth of penetration of the joints.

A rigid connection between the drop of the voltage of the arc and arc gap was used for development of the process of gravity welding. This allowed stabilizing the depth of penetration, maintaining it at a constant level by automatic variation of current.

A number of investigations had been conducted, and their results were used to develop a block to control the power source for adjustment of welding current. Technological experiments demonstrated the ability to produce welded joints of aluminium alloys without supporting the molten metal by backing elements.

Technology of manual HAW was developed. Impossibility of automatically controlling the arc gap makes it more difficult to conduct such a process. Nonetheless, a skilled welder can perform repair welding of various joints, particularly on thick metal. In this case, all the advantages of HAW process are

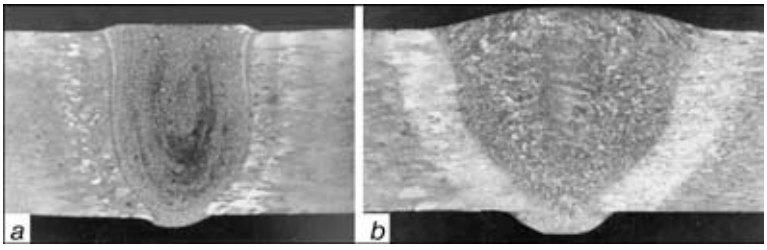

Figure 2. Macrosections of joints of alloy 1201 12 mm thick: *a* — in single-pass HAW (I_w = 430 A, v_w = 14 m/h); *b* — in AAW (I_w = = 600 A, v_w = 8 m/h)

preserved, namely a high penetrability, small HAZ, and no heating required to achieve deeper penetration.

When the technology of DCSP welding aluminium alloys was developed, requirements to the shape of the working tip of non-consumable electrode, base metal preparation and joint fit-up were defined. Technological factors, responsible for weld quality, were studied in detail, and conditions were established, providing optimal results in welding.

Performed research allowed establishing the possibility of applying DCSP welding of aluminium alloys for fabrication of critical structures. HAW process was introduced in space and aircraft industries of FSU (in fabrication of «Energiya» rocket fuel tanks and components of the flight deck of «Buran» space shuttle), as well as for a number of other critical structures.

CONCLUSIONS

1. DCSP welding of aluminium alloys has the advantages of high penetrability, being 1.5–2 times greater, compared to AAW, which allows performing single-pass welding of thick metal; 1.5–2 times lower heat input than in AAW, HAZ reduction, ability to perform high-speed welding.

2. The disadvantages of the process include the need to perform welding with a short arc gap, which requires application of automatic control, need for a thorough preparation of the metal for welding and of the joint-fit up to meet higher requirements than in AAW. In addition, use of helium as the shielding medium makes the welding process more expensive.

3. It is rational to apply HAW process for welding critical structures of high-strength heat-hardenable and work-hardened alloys.

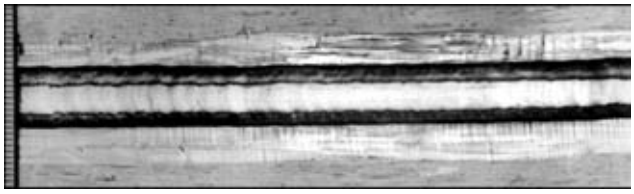

Figure 3. Appearance of a weld in HAW of alloy 1201 10 mm thick (I_w = 300 A, v_w = 12 m/h)

1. Rabkin, D.M., Ivanova, O.N., Steblovsky, B.A. et al. (1971) Welding of aluminium alloys at direct current of straight polarity. *Avtomatich. Svarka*, **3**, 71–72.
2. Liptak, J.A. (1965) Gas tungsten-arc welding heavy aluminium plate. *Welding J.*, **6**, 276–281.
3. Agnew, S.A., Anderson, N.E., Felmley, C.R. et al. (1964) Welding aluminum space launch vehicles. *Ibid.*, **11**, 932–936.
4. Brodsky, A.Ya. (1956) *Tungsten-electrode argon-arc welding*. Moscow: Mashgiz.
5. Yusufova, Z.A., Leskov, G.I. (1970) On mechanism of disruption of oxide films during inert-gas shielded welding of aluminium alloys. *Svarochn. Proizvodstvo*, **7**, 57–58.
6. Budnik, V.P., Rabkin, D.M., Smiyan, O.D. et al. (1975) Thermal disruption of oxide film during welding of aluminium. *Avtomatich. Svarka*, **10**, 74–75.
7. Budnik, V.P. (1994) Influence of inert gas type on temperature of pool and disruption of oxide film during welding of aluminium. *Ibid.*, **12**, 23–25.
8. Budnik, V.P., Steblovsky, B.A., Butsko, M.G. et al. (1982) Penetrability of DC and AC arc. *Ibid.*, **8**, 68–70.
9. Ivanova, O.N., Lozovskaya, A.V., Rabkin, D.M. et al. (1973) Properties of aluminium alloy welded joints produced by DCSP welding. *Ibid.*, **3**, 8–11.

LASER WELDING OF THIN-SHEET STEELS USING SPECIAL APPROACHES

V.D. SHELYAGIN, V.Yu. KHASKIN, A.V. SIORA, A.V. SAKHARNOV and **E.I. GONCHARENKO**

The E.O. Paton Electric Welding Institute, NASU, Kyiv, Ukraine

Advantages of laser welding using various technological approaches, including an additional feed of a filler wire, deposition of thin layers of flux on base metal, decrease in focal distance of the lens and application of periodic-pulse modulation of the laser beam, are considered.

Key words: *laser welding, thin-sheet steels, special approaches, flux, filler wires, focal distance, continuous and periodic-pulse radiation, welding speed, microstructure, microhardness*

Laser welding [1], and laser welding of thin-sheet (up to 1.5–2.0 mm) steels in particular, finds an increasingly wide application in industrialised countries. For example, laser welding is applied for joining tailored blanks of steels of different grades and thickness for forming of car bodies [2]. The domestic industry also has areas where it is necessary to weld large-size parts of thin-sheet stainless and carbon steels by avoiding their thermal distortions. For example, this applies to welding of large-size conical diffusers of stainless steel with thickness of δ = 0.8 mm for food processing industry, 3D structures for interior designs of shops etc. It is either impossible or very difficult to solve such problems by traditional welding methods.

One of the methods which allows the problems that may arise to be handled is laser welding. However, it imposes certain requirements to aligning of edges welded [3] (especially in the case of welding thin-sheet parts). In addition, conventional laser welding may involve such phenomena as thinning of a weld, formation of pores and internal cavities, un-

dercuts, blistering of metal in the upper part of the weld (especially in high-speed welding of rimming and non-oxidised steels). An example may be a butt joint (Figure 1) made by laser welding at a speed of 340 m/h (beam power is 3 kW and focal distance of the lens is 300 mm). A welding production engineer needs to use different technological approaches to make performance of preparatory welding operations easier, simplify design of process fixtures and reliably avoid the above defects of the welds.

The required fixture was designed for laser welding of thin-sheet steels, and special technological approaches were developed to improve weld formation, provide mechanical properties of the welds as close as possible to those of the base metal, relieve stringent requirements for preparation of the weld edges, decrease the laser beam power and increase the welding speed. Such approaches include those traditionally related to welding (application of fluxes and filler wires), those associated with peculiarities of laser radiation as a heat source (use of various focusing lenses, periodic-pulse laser beam modulation), as well as a combination of laser heating with plasma, arc or high-frequency heating (hybrid and combined welding methods). The latter group is very promising, as it allows the laser beam power to be partially replaced by power of cheaper heat sources (e.g. electric arc ones) at comparatively negligible variations in quality of the process [3]. This article considers only the first two groups of special approaches.

Investigations of laser welding of thin-sheet steels were conducted using a technological laser LT-104 (with a power of up to 10 kW) [4]. Welding was carried out using «flying» optics installed on a two-axis manipulator. Samples 300×100 mm in size were fixed in a special clamp. They were made from low-carbon rimming (St.05kp, St.08kp, St.3kp) and stainless (08Kh12N9Y2, 12Kh18N10T) steels with δ = 0.1, 0.8, 1.0, 1.25, 1.5 and 2.0 mm. Welding was performed by the butt and overlap methods using a one-component flux (TiO_2) without and with filler wires of the Sv-08G2S and 12Kh18N10T grades (δ = = 0.8 mm) (Figure 2). Carbon dioxide was used as a shielding gas for welding low-carbon steels, and argon — as a shielding gas for welding stainless steels. A special welding head was made for welding using a filler wire (Figure 2). In all the cases power of a continuous CO_2 laser beam focused on a workpiece was about 3 kW. The optimal filler wire feed speed was found to range from 90 to 100 m/h for almost all the cases tried. The use of a filler wire leads to a substantial decrease in requirements to alignment of edges to be joined: gaps of up to 30–50 % δ and warping of up to 50 % are permitted [5] (the latter parameter should preferably be eliminated from an aesthetic standpoint).

Two types of the one-element lens were used for focusing of the laser beam: with a focal distance of F = 300 and 200 mm. Caustic necking was located at a half-thickness of the sample. The welding speed of

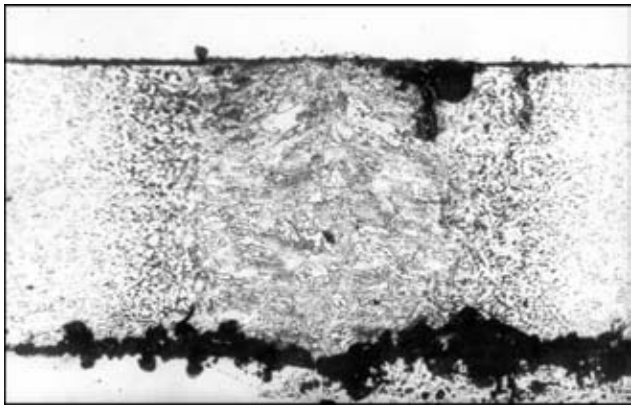

Figure 1. Microstructure of a welded joint in steel St.08kp (rimming) made by laser welding using no additional approaches (×63)

v_w = 360 m/h (δ = 0.8 mm) and 120 m/h (δ = = 1.5 mm) was achieved with the lens having a focal distance of F = 300 mm. In the case of using a filler wire v_w was up to 240 m/h (δ = 0.8 mm). The lens with F = 200 mm made it possible to achieve v_w = = 600 m/h (δ = 0.8 mm) and 300–320 m/h (δ = = 1.5 mm). In the case of using a filler wire v_w was up to 400 m/h (δ = 0.8 mm).

It should be noted that with an increased thickness of the sample ($\delta \geq 3$ mm) the use of short-focus lenses prevents any further increase in the welding speed. Welds made by using such lenses are much wider than those made with longer-focus ones. This is attributable to decrease in length of the caustic neck with decrease in the focal distance [6].

The necessity of applying fluxes is caused by the fact that a very high welding speed (400–600 m/h)

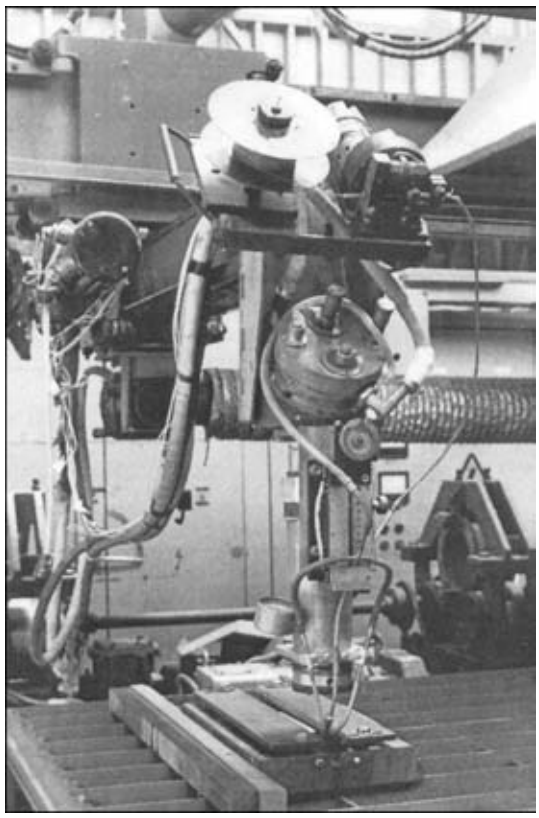

Figure 2. General view of the welding head for laser welding using filler wire

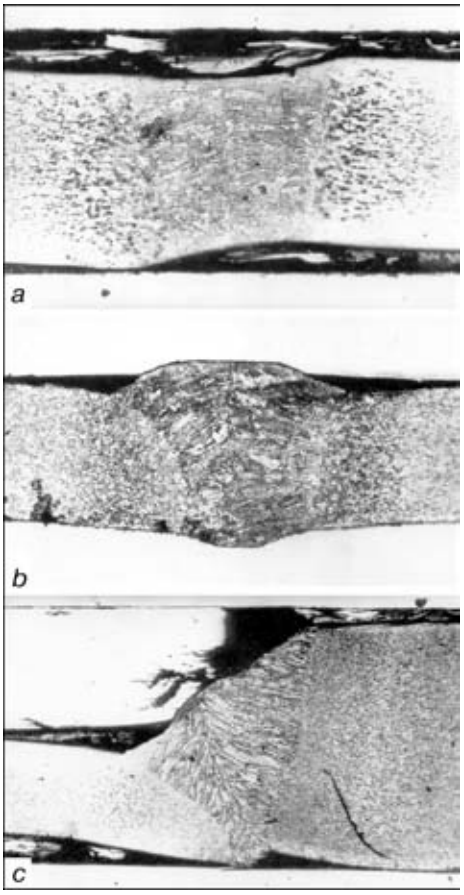

Figure 3. Microstructure of laser welded joints in low-carbon steels (×63): *a* — v_w = 540 m/h, δ = 0.8 mm; *b* — using filler wire Sv-08G2S (v_w = 420 m/h, δ = 0.8 mm); *c* — butt welding of sheets of a different thickness using filler wire (v_w = 240 m/h, δ = 0.8 and 2.0 mm) (×32)

gives no time for the weld pool to be fully degassed, thus leading to formation of pores in the upper part of the weld. Welding fluxes slow down cooling of the tailing edge of the weld pool, alloy it (deoxidise) and allow the sound welds to be produced. The use of a flux for high-speed welding is justifiable if it is applied in a very thin layer (< 0.1 mm) strongly adhering to the sample. If the layer is relatively thick and loosely adheres to the sample, the beam power is absorbed in the flux and fails to be transferred to

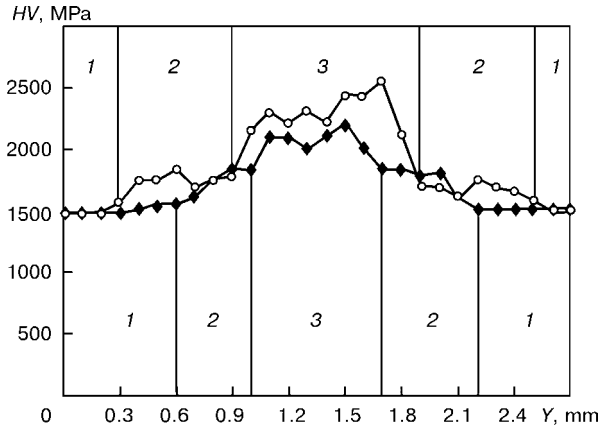

Figure 4. Distribution of microhardness *HV* in direction *Y* normal to the plane of a butt welded joint, at the centre of the sample for a case of high-speed laser welding (◆) and laser welding using a filler wire (○): *1* — base metal; *2* — HAZ metal; *3* — weld metal. Thus, the flux (TiO_2 based) and a binding component, i.e. glue «Supertsement» (a layer of about 0.5 mm thick), are deposited on samples (St.5kp and St.08kp) to provide a reliable deoxidation of the weld pool and avoid porosity. With a lens of F = 200 mm v_w = 420 m/h for δ = 0.8 mm and v_w = 300 m/h for δ = 1.25 mm.

It is possible to eliminate porosity in high-speed laser welding not only through using fluxes, but also through alloying the weld pool from filler wires. It is reasonable to use them for welding low-carbon steels (v_w > 400 m/h) and for a case of unavoidable gaps present between the edges being aligned. The main disadvantage of using filler wires is the need to increase the power of laser radiation to achive a higher welding speed. In this connection, it is of interest to use an extra power source in the form of the metal-electrode arc combined with the laser beam.

It is advisable to perform welding of super-thin steels using a periodic-pulse laser beam. In this case the HAZ is substantially decreased in size, stability of the process is improved and the risk of burns-through is avoided [7]. So, the following process conditions could be recommended for welding stainless foil with δ = 0.1 mm: shielding — axial argon feeding, focal distance of the lens F = 300 mm, diameter of the radiation spot on the workpiece surface 0.6 mm, mean power of the beam 190–200 W, peak power of the beam 500–600 W, pulse frequency 200 Hz, relative pulse duration 2.5–3.0, and v_w = 360 m/h.

Metallography of the weld and HAZ metals was conducted on microsections using the optical microscope «Neophot-32» (×25–600) and LECO hardness meter M-400 MVK-E under loading of 0.01–10 N. Mictrostructure of welds in low-carbon steels was revealed by cold chemical etching in a 4 % alcohol solution of nitric acid, and that in stainless steel was revealed by electrolytic etching in a chromic acid solution. Processing of the results of welding steel St.05kp (δ = 0.8 mm) showed the following.

In laser welding using no special approaches (v_w = = 540 m/h) the resulting weld is 0.705 mm wide and the HAZ metal is 0.214–0.277 mm wide. Structure of the weld metal is a mixture of ferrite (*HV* 1850 MPa) and pearlite (*HV* 2200 MPa). A small portion of ferrite has a Widmanstätten structure. The HAZ metal has a ferritic-pearlitic structure. The amount of pearlite is substantial, which is probably associated with high cooling rates during laser welding (high-rate cooling leads to formation of a pseudoeutectoid containing less carbon than pearlite formed in slow cooling) [8]. Index of the ferrite grain is 7–8, according to GOST 5639–82.

In laser welding using the Sv-08G2S filler wire (δ = 0.8 mm) v_w = 420 m/h, the weld width is 0.882 mm and the HAZ metal width is 0.441–0.567 mm. Structure of the weld metal is ferritic-pearlitic (*HV* 1680 MPa — ferrite, and *HV* 1850–2010 MPa — pearlite). Also, there are regions of ferrite with a Widmanstätten structure, as well as

regions with an acicular structure, probably bainitic (*HV* 2240–2290 MPa). The HAZ metal has a ferritic-pearlitic structure. Here the content of pearlite is a bit higher, compared with the previous sample. Index of the ferrite grain is 7–8.

Transverse distribution of microhardness in the central part of the welds shown in Figure 3, *a, b*, is presented in Figure 4. The result of using filler wire is shown in Figure 3, *b, c*. As seen from comparison of Figure 3, *a* and *b*, the filler wire leads to elimination of sag of the welds and forms the required reinforcement of the upper bead. A small bend of edges in the weld area results from the effect of guillotine shears used to make the samples (no additional edge preparation was done). Structure of the welds in stainless steel with $\delta = 0.1$ mm is shown in Figure 5.

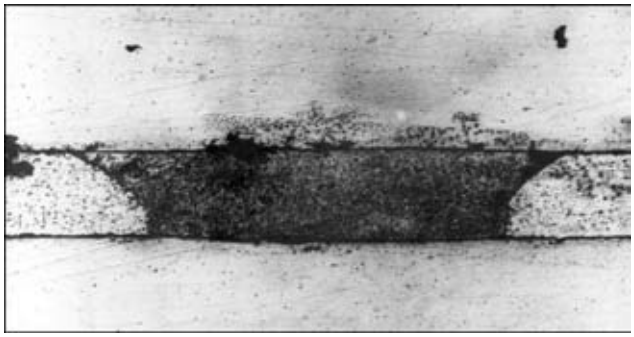

Figure 5. Microstructure of the weld in stainless steel ($\delta = 0.1$ mm) made by periodic-pulse laser welding (×156)

CONCLUSIONS

1. Technological peculiarities of laser welding of thin-sheet ($\delta \leq 2$ mm) low-carbon and stainless steels were studied:

- feeding of a filler wire at a speed of 90–100 m/h allows the weld metal to be alloyed, porosity and undercuts to be avoided, and requirements to alignment of weld edges to be considerably decreased; the filler wire metal forms the required reinforcement;
- use of fluxes deposited in dense thin layers leads to deoxidation of the weld metal, slows down cooling of the tailing part of the weld pool, eliminates porosity and improves formation of the upper reinforcement bead;
- decrease in focal distance of the lens from 300 to 200 mm allows the speed of welding thin-sheet steels to be reduced 1.5–3 times (this relationship is lost at $\delta = 3$ mm);
- use of periodic-pulse modulation of the laser beam leads to formation of narrow and finely dispersed welds with a small HAZ, which can be beneficial for welding of foils.

2. As shown by metallography, laser welding of thin-sheet steels using special approaches (like conventional laser welding) provides sufficiently strong and ductile joints with a finely dispersed equiaxed ferritic-pearlitic structure in the case of a low (up to 0.3 %) carbon content of both base and filler metal.

3. A drawback of laser welding using a filler wire is the need to spend an additional laser beam power (10–30 %) to melt this wire.

1. Kovalenko, V.S. (2001) Laser technology at a new stage of development. *The Paton Welding J.*, **12**, 3–8.
2. Schneider, C., Prange, W. (1992) Tailored Blanks — ein Werkstoff für neue Formen der Konstruktion. *Thyssen Technische Berichte*, **1**, 97–106.
3. Shelyagin, V.D., Khaskin, V.Yu. (2002) Tendencies in development of laser-arc welding (Review). *The Paton Welding J.*, **6**, 25–28.
4. Garashchuk, V.P., Shelyagin, V.D., Nazarenko, O.K. et al. (1997) CO_2 technological laser LT 104 of 10 kW power. *Avtomatich. Svarka*, **1**, 36–39.
5. Grigoriants, A.T., Shiganov, I.N. (1998) *Laser equipment and technologies*. Book 5. Laser welding of metals. Moscow: Vysshaya Shkola.
6. Landsberg, G.S. (1976) *Optics*. Moscow: Nauka.
7. Khaskin, V.Yu., Pavlovsky, S.Yu., Garashchuk, V.P. et al. (2001) Peculiarities of welding thin-sheet low-carbon steels using a pulsed-periodic radiation of CO_2 laser. *The Paton Welding J.*, **2**, 42–45.
8. Grabin, V.F. (1982) *Physical metallurgy of fusion welding*. Kyiv: Naukova Dumka.

THERMAL CYCLES IN PLASMA-MIG SURFACING

N.A. MAKARENKO[1] and **V.A. NEVIDOMSKY**[2]
[1]Priazovsky State Technical University, Mariupol, Ukraine
[2]Novo-Kramatorsk Machine-Building Works, Novo-Kramatorsk, Ukraine

Drawbacks of the technology for flux-cored wire submerged-arc surfacing of metallurgical equipment parts operating under thermal loading conditions are noted. Non-uniform distribution of alloying elements across the deposited bead section leads to decrease in strength of the roll-type continuous casting machines. Peculiarities of heat input in plasma-MIG surfacing provide uniform distribution of the surfacing alloy components in the first layer.

Key words: *arc surfacing, plasma-MIG surfacing, repair technology, metallurgical equipment, heat input, thermal cycle, element distribution*

Methods of plasma surfacing, applied in industry, feature a number of technological advantages, and in many cases provide a rather high quality of the deposited metal. Nonetheless, flux-cored wire arc surfacing is exactly the process, which allows producing deposited metal of the specified calculated composition and providing high performance of items, exposed to metal, which is liquid and heated up to high temperatures, to high thermocyclic loads, etc. [1].

Possibilities of flux-cored wire surfacing can be used to the utmost in plasma-MIG process, allowing separate regulation of current, as well as heat input from an arc, formed by a circular electrode, and central arc of the consumable electrode [2–4]. This study was aimed at determination of the total action of temperature fields from both heat sources and ability to control the thermal cycles in the HAZ.

Experiments were conducted in surfacing of 50×100×400 mm plates of 38KhMN steel, which was performed with NM-4 plasmatron with a copper circular non-consumable electrode with inner diameter of 8 mm and ring width of 2 mm. Such parameters allow maintaining up to 20 A/mm current density [5].

In the first stage the possibility was considered of replacement of the total preheating (up to T = 400 °C) by local preheating in the surfacing zone, characteristic of plasma-MIG process with an external arc, formed by a circular electrode.

Thermal cycles were determined by the data, obtained by measurement with chromel-alumel thermocouples, arranged as follows: three — in the direction of displacement along the sample axis at 5 mm distance from each other (thermocouple junctions were buried in the drilled channels at 2, 5 and 10 mm distance from the processed surface), and three — in the transverse section, normal to sample axis at 4 mm distance from each other at 2 mm depth from sample surface (Figure 1, *7a, 7b, 7c* and *7a, 7d, 7e*).

Zone of measurement (thermocouple arrangement) was located in a section, equal to 2/3 of plate length, which ensured experiment performance in a steady-state heat mode. Parameters of surfacing mode were as follows: plasma arc current I_{PA} = 150–200 A; plasma arc voltage U_{PA} = 44 V; consumable electrode current I_{CE} = 280 A; consumable electrode arc voltage U_{CE} = 22–25 V; deposition rate v_d = 22 m/h; flow rate of plasma (central) gas Q_{pl} = 5–7 l/min; shielding gas flow rate Q_{sh} = 10–15 l/min.

Three series of experiments were conducted with variation of I_{PA} (Figure 2), Q_{pl} and Q_{sh}. Other parameters remained unchanged. The above three series of experiments were conducted twice: without consumable electrode arc (I_{CE} = 0) and with simultaneous

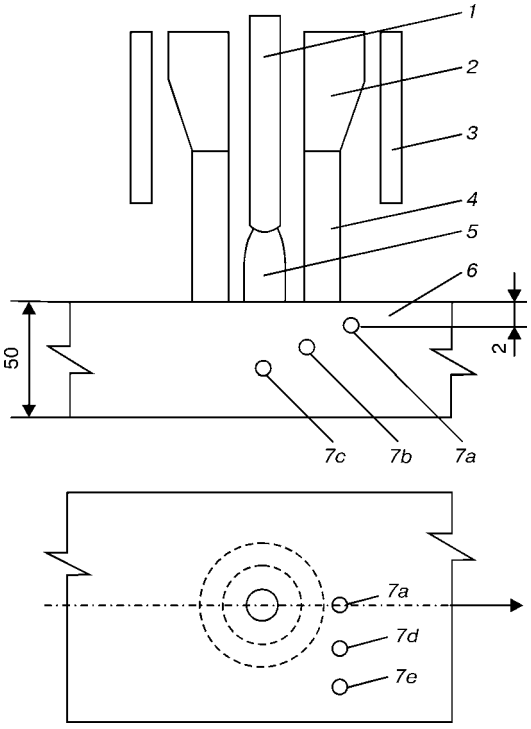

Figure 1. Schematic of an experiment to determine the thermal cycles: *1* — consumable electrode; *2* — non-consumable electrode; *3* — protective nozzle; *4* — arc, formed by a circular cathode; *5* — consumable electrode arc; *6* — item; *7a, 7b, 7c* and *7a, 7d, 7e* — thermocouples, located along the line of electrode displacement along sample axis and in the transverse section, normal to sample axis, respectively

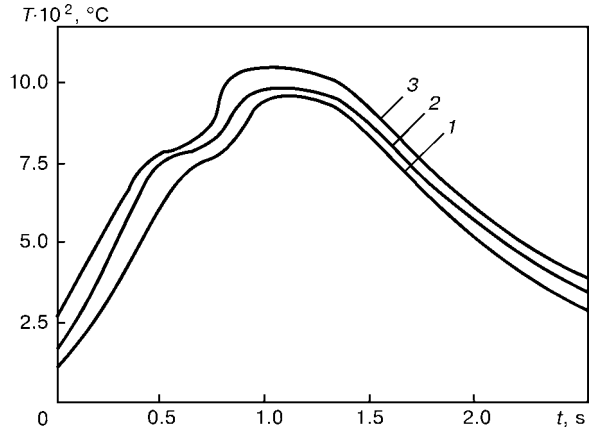

Figure 2. Isotherms in point *7a*, located along the line of plasmatron displacement with variation of I_{PA}: *1* — 150; *2* — 180; *3* — 200 A; Q_{pl} = 6 l/min; Q_{sh} = 10 l/min

running of two arcs with formation of the weld pool and bead.

Figure 2 shows the isotherms, registered by thermocouple *7a* (see Figure 1), located along the line of displacement of the plasmatron axis, at change of current of the plasma arc, formed by the circular electrode (150, 180, 200 A — without consumable electrode arc). Start of the isotherm corresponds to the moment of contact with the heat spot from the arc, formed by a circular electrode.

Investigations showed that increase of the flow rate of plasma gas Q_{pl} promotes a minor increase of the temperature peak and a certain decrease of the heating temperature in a section, close to the moment of plasmatron passage to thermocouple *7a*. Furtheron the temperature is equalized, and isotherm lines merge into one, which is indicative of the fact, that plasma gas flow rate does not influence the heat input with the other mode parameters unchanged.

Experiments on heating the plate surface showed that the heat flow from the arc, formed by a circular electrode, is uniformly distributed over a width, equal to the diameter of the non-consumable copper electrode at the moment, when the leading front of the pool, formed under the impact of the consumable electrode, passes through the zone of heating by the plasma arc.

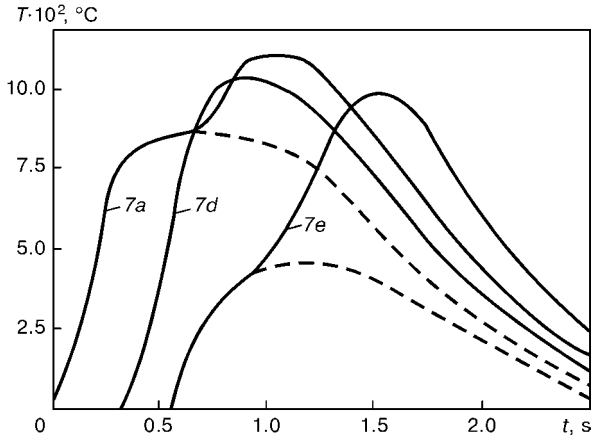

Figure 3. Thermal cycle of the process of plasma-MIG surfacing (isotherms of heating by a consumable electrode arc): *7a, 7d, 7e* — thermocouples, noted in Figure 1

Of greatest interest is the thermal condition of the studied section at the moment of heating by both arcs and heat of molten electrode metal.

Preliminary determination of the base metal fusion zone, made on macrosections, showed the following:

- depth of base metal melting by just the arc, formed by the circular electrode, is equal to 0.2–0.4 mm;
- at complete running of the surfacing process, the penetration depth is equal to 0.4–0.6 mm (on bead axis). Isotherms for points, located at the depth of 2 mm from the processed surface (Figure 1, thermocouples *7a, 7d, 7e*) indicate that heating in a point, located in the plane of bead axis (*7a*) reaches the value of 850–900 °C 0.4–0.5 s after the reference time (Figure 3). Reference time was selected to be the moment, when the leading front of the heat spot from the arc, formed by a circular electrode, has reached a point on the sample surface, under which thermocouple *7a* is located.

Furtheron (after half a second) the values of temperature of 1000–1050 °C are recorded by thermocouple *7d*, which corresponds to the moment of direct heating of this section by a shifted plasma arc. At the same moment (Figure 3) the axis of the consumable electrode is above thermocouple *7a*, and thermocouple readings are increased up to 1100–1200 °C. Thus, the conducted research shows that the drop of electrode metal penetrates into a shallow pool of initially partially melted base metal.

As in surfacing in the above range of modes the thermal cycles vary only slightly, additional studies were conducted at a lower value of current of the plasma arc (I_{PA} = 100–120 A) and increased speed of displacement (v_d = 30 m/h), i.e. heat input into the item from the arc, formed by a circular electrode was thus reduced.

Thermograms and calculations showed that the regularity of temperature distribution, characteristic of this process, is preserved. However, temperature values in the surfacing zone decreased, compared to a similar previous experiment and were equal to 400–500 °C. Therefore, plasma-MIG process allows regulation of the preheating temperature of the item being surfaced by varying the current of the arc, formed by a circular electrode.

Intensity of the flow of energy, applied by each of the sources, was determined by the data of measurement of temperature, area of active spots and electric parameters of the arcs. Areas of application of heat (energy) were taken to be as follows:

- for plasma arc — equal to the area of the circular electrode;
- for consumable electrode — by the data of high-speed filming.

It should be noted that in the latter case the diameter of the active spot changed during the drop formation from the size, equal to electrode diameter, to a diameter, exceeding the initial one 2 times, and

was taken to be on average equal to 1.5 diameters of the consumable electrode.

Investigation results show that the heat input into the item consists of the sum of energy flows from the plasma arc and consumable electrode arc. A dependence was derived of the density of heat flow q in different points of the heat spot, from which is follows that q of the plasma arc reaches its maximum value of 400 W/cm^2 at distance r = 3.5 mm from the point of projection of the consumable electrode axis on the sample (Figure 4, curve *1*).

Value of q, depending on current of the consumable electrode arc, reaches the maximum value (about 1000 W/cm^2) at r = 0 (Figure 4, curve *2*). Dependencies were derived in the following modes of deposition: I_{PA} = 180 A; U_{PA} = 44 V; I_{CE} = 280 A; U_{CE} = = 23 V; v_d = 21 m/h; Q_{pl} = 6 l/min; Q_{sh} = 14 l/min (Figure 4, curve *2*). A total dependence of the densities of heat flows from the plasma arc and consumable electrode arc (Figure 4, curve *3*) was determined for regulation of the heat input into the item by selection of the surfacing mode parameters, required for optimal preheating of the surface.

CONCLUSIONS

1. In plasma-MIG surfacing in the range of working parameters the isotherm of heating by the arc, formed by a circular electrode, in a point, located at 2 mm distance from the surface, reaches a maximum at the moment of the consumable electrode arc axis being in this point. Depth of melting by an arc, formed by a circular electrode, is 0.2–0.4 mm, temperature of heating in the measured section (at the depth of 2 mm from the surface) is up to 1000 °C.

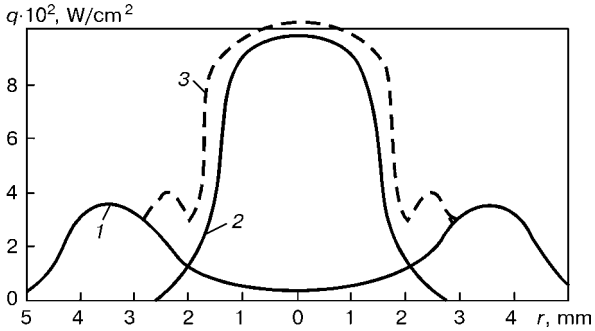

Figure 4. Distribution of density of the vapour flow

2. Radius of the heat spot from the arc, formed by a circular electrode, is only slightly greater than the electrode diameter. Heat energy is applied to the item around the periphery of the spot and depends on current, voltage and speed of displacement.

3. Process of plasma-MIG surfacing allows regulation of the heat input by changing the main parameters of surfacing in a sufficiently broad range.

1. Frumin, I.I. (1961) *Automatic electric-arc surfacing*. Kharkov: Metallurgizdat.
2. Makarenko, N.A., Granovsky, A.V., Kondrashov, K.A. (2001) Improvement of technological characteristics of plasma-MIG surfacing using flux-cored wire. *The Paton Welding J.*, **6**, 43–45.
3. Chigarev, V.V., Makarenko, N.A., Kondrashov, K.A. et al. (2001) Features of electrode wire melting in surfacing by plasma-MIG process. *Ibid.*, **8**, 10–12.
4. Chigarev, V.V., Makarenko, N.A., Kondrashov, K.A. (2000) Peculiarities of development of technology for production of press molds resisting thermocyclic loadings. In: *Improvement of processes and equipment for pressure treatment used in metallurgy and mechanical engineering*. Kramatorsk: DDMA.
5. Kondrashov, K.A., Chigarev, V.V., Makarenko, N.A. (2000) Investigation of energy and technological peculiarities of plasma-MIG surfacing. In: *Proc. of 7th Regional Sci.-Tech. Conf.* Mariupol: PGTU.

SANITARY-HYGIENIC CHARACTERISTIC OF PROCESS OF CONSUMABLE ELECTRODE INERT-GAS WELDING OF AMg6 ALUMINIUM ALLOY

O.G. LEVCHENKO and **V.S. MASHIN**
The E.O. Paton Electric Welding Institute, NASU, Kyiv, Ukraine

Results of investigation of the content of harmful elements in air in inert-gas welding of aluminium alloys are presented. Recommendation are given on protection of welders' respiratory organs.

Key words: *arc welding, aluminium alloy, welding aerosols, labour conditions, local ventilation, protection means*

MIG welding of aluminium alloys as compared with TIG welding provides the higher efficiency of the process, decrease in the HAZ and reduction in the level of residual deformations of products. MIG welding makes it possible to fulfil multilayer welds into a narrow groove and is indispensable in manufacture of T- and overlap joints. In addition, the economical characteristics of the process are improved with increase in thickness of the metal being welded.

Disadvantages of the MIG welding in argon are the increased porosity of welds, large losses of easily-evaporating alloying elements from the electrode metal and high evolutions of harmful elements in the form of a welding aerosol (WA) into a working zone air, that requires the use of special devices of local ventilation, and also (in some cases) the means of an individual protection of the welders' respiratory organs.

The higher quality of the welds is attained in welding in helium or helium-argon mixture. The application of He-based shielding gases in welding at high currents (when the temperature of electrode wire drops reaches the boiling temperature of metal) leads (as compared with argon welding) to the drop of a mean temperature of electrode droplets by 100–200 °C, decrease in evaporation of easily-boiling alloying elements and, consequently, to the reduction of evolution of arc burning products into the surrounding atmosphere.

The aim of the work is to perform the comparative investigations of sanitary-hygienic conditions of labour of operators in MIG and TIG welding at increased currents of thick-plate aluminium alloy of AMg6 grade and to work out recommendations on protection from WA.

Table 1. Chemical composition of metal being welded and electrode (filler) wire

Object of examination	*Elements, wt.%*						
	Mg	*Mn*	*Si*	*Fe*	*Ti*	*Cu*	*Zn*
Alloy AMg6	6.23	0.60	0.20	0.28	0.10	0.03	0.01
Wire Sv-AMg6	6.55	0.62	0.15	0.25	0.10	0.01	0.01

For experiments on WA sampling the AMg6 alloy plates (GOST 4784–74) of 25 mm thickness, welding wire Sv-AMg6 (GOST 7871–75) of 2.5 and 3.15 mm diameter, high-grade argon (GOST 10157–79) and helium of grade B (TS 51-940–80) were used. Chemical composition of metal being welded and electrode wire is given in Table 1. Plates and wire were cleaned in solutions of alkali and nitrogen acid. Edges were subjected to scraping before welding.

Single-sided TIG welding was performed using equipment PRS-630 at the following conditions: I_w = = 460–480 A; U_a = 13–15 V; v_f = 50 m/h; v_w = = 6 m/h; d_{el} = 8 mm; d_{wire} = 2.5 mm; Q_{Ar} = 35 l/min. Width of groove with a curvilinear bevel of two edges was 26 mm, blunting — 5 mm.

Single-sided MIG welding in helium-argon mixture (50 % He) was performed using A1431 machine supplied from VDU-1201 power source at the following conditions: I_w = 480–500 A; U_a = 32–33 V; v_f = = 280 m/h; v_w = 30 m/h; d_{wire} = 3.15 mm; Q_{mix} = = 70 l/min. Width of opening of edges with a curvilinear bevel was 12 mm, blunting — 5 mm.

Joints were subjected to X-ray control, metallographic examination and mechanical tests.

Condition of air medium was evaluated by air sampling in the welding zone at the 20 cm distance from the arc. To provide validity of results six samples at least were taken. During determination of content of harmful elements in air, contaminated with WA, the air was aspirated using an electric aspirator of model 822 through preliminary weighted filters AFA-VP-20 at the rate of 5–15 l/min [1, 2].

Amount of a hard component of WA (HCWA) in air of the working zone was determined by a gravimetric method [1]. Content of HCWA components (compounds of aluminium, manganese, iron, titanium, copper) was determined using the procedure described in [2].

Concentration of components of a gaseous component of WA (GCWA) (ozone, carbon monoxide, nitrogen oxide and dioxide) was determined in unit GKh-4 using colorimetric methods [2].

Table 2. Content of harmful elements in air during welding

Place of WA sampling	*Description of WA components*	*Number of determinations*	*Concentration of WA components, mg/m³*	
			Range of values	*Mean value*
		MIG method		
0.20 m from arc	HCWA	10	126.3–740.6	318.9 ± 65.41
	Al_2O_3	10	69.3–329.9	169.7 ± 27.8
	MgO	10	5.6–44.8	21.4 ± 4.17
	MnO_2	10	2.0–3.17	2.42 ± 0.13
	Fe_2O_3	10	2.0–5.0	3.5 ± 0.32
	O_3	6	0.13–0.22	0.17 ± 0.016
	CO	6	6.25–6.25	6.25 ± 0
	NO	6	6.7–10.0	8.9 ± 0.58
4.0 m from arc	HCWA	4	1.0–1.4	1.3 ± 0.12
	Al_2O_3	4	1.2–1.6	1.4 ± 0.12
	MgO	4	0.27–0.35	0.32 ± 0.002
	O_3	4	0.03–0.05	0.04 ± 0.006
		TIG method		
0.2 m from arc	HCWA	6	1.4–4.1	2.5 ± 0.47
	O_3	6	0.010–0.026	0.016 ± 0.003
	CO	6	12.5–12.5	12.5 ± 0
	NO	6	2.7–4.7	3.7 ± 0.35

Condition of air medium in the industrial room was evaluated in accordance with requirements of GOST 12.1.005–88.

To provide validity of obtained data, the methods of a mathematical statistics were used [3]. 114 air samples were taken from the operator's respiratory zone, 120 chemical analyses and 78 express-analyses were made.

Results of X-ray examination of a linear length of 1.6 m of multipass welds showed that in MIG welding single pores of 0.5–2.5 mm diameter, tungsten inclusions of 0.5–1.5 mm and oxide films of 5–12 mm length were revealed in them. In TIG welding only single pores of 0.5–1.5 mm diameter were observed.

Values of strength of weld metals and welded joints produced by MIG and TIG welding are on average at the same level (in both cases the samples were cut from defect-free regions). Strength factor of TIG and MIG welded joints was 0.91–0.92 and 0.94–0.95, respectively, of strength of as-delivered parent metal (σ_t = 338 MPa).

Results of determination of concentration of harmful elements in the operator's respiratory zone (at 20 cm distance from welding arc) and in a neutral point (at 4 m distance from arc) are given in Table 2. As is follows from data of the Table, when the consumable electrode is used the concentration of HCWA in the operator's respiratory zone is much higher than in use of the non-consumable electrode. This is explained by that the main source of HCWA formation is the evaporations from the consumable electrode end, which have the higher temperature as compared with that of the parent metal [4]. As the non-consumable (tungsten) electrode does not contribute to the HCWA formation, and the efficiency of melting of a filler wire is much lower, then the amount of metal evaporated in this process is smaller than that in use of the consumable electrode.

The main toxic component of HCWA is manganese. Chemical analysis HCWA samples (see Table 2) proves that average concentration of this component was 2.42 ± 0.13 mg/m³, that is approximately 8 times higher than the limiting admissible concentration (LAC).

As to the compounds of aluminium and magnesium, then their concentration exceeded LAC by 85 and 24 times, respectively. Concentration of iron oxides did not exceed the established standards. Compounds of titanium and copper were not observed in any sample.

Among the toxic GCWA, forming in MIG welding of aluminium, ozone is most hazardous, whose concentration exceeded LAC by 1.7 times. Toxic nitrogen dioxide was not revealed, while the nitrogen oxide concentration exceeded the standard by 1.8 times. Concentration of carbon monoxide did not exceed LAC.

Results of evaluation of air medium condition at the 4 m distance from the arc showed that in the course of removing from it the HCWA concentration is decreased drastically (250 times). Naturally, the concentration of components included into its composition are also decreased (in this case lower than LAC), while iron, manganese, titanium and copper in samples are absent. Only ozone in the amount, not exceeding LAC, was revealed among the gaseous components (see Table 2).

It was established during examination of air medium composition of the welders' respiratory zone in use of the tungsten electrode that this process is accompanied by much lower evolutions of HCWA and gases (see Table 2). Due to a negligible contamination of air with a dust, it was not possible to determine the content of components included in the composition of AMg6 alloy (compounds of aluminium, manganese, titanium, iron and copper). In the composition of gases, evolving during welding, oxides of carbon and nitrogen, as well as ozone were revealed in small amounts not exceeding LAC.

Thus, it was stated that in MIG welding of Al–Mg alloy AMg6 the air of the working zone is contaminated with WA of a complex chemical composition containing some toxic components in the composition of a hard component (up to 50 % aluminium oxide, 6.3 % magnesium oxide, 0.7 % manganese dioxide, about 1 % iron oxides) and gaseous component (ozone, carbon monoxide and nitrogen oxide).

One of the simplest hygienic recommendations in automatic MIG welding is the increase in distance from the welding arc where the concentration of harmful elements is lower.

The most effective means of protection of the respiratory organs are the devices of a local exhaust ventilation which are capable to trap WA directly near the source of their evolution [5]. It is recommended for MIG welding to use mobile or stationary ventilation or filtering-ventilation units of efficiency of not less than 1000 m^3/h [6]. To provide the maximum localizing of the evolving flame of WA the air-receiving funnels of these units with flexible air conduits should be mounted directly on the welding heads of the machines or near them at a minimum distance from the arc. In filtering-ventilation units the use of filters is necessary to purify the air, removed from the place of welding, not only from HCWA, but also from GCWA (ozone, carbon monoxide and nitrogen oxide) [7].

In case when the use of the offered means of a local ventilation is impossible or a low-efficient ventilation is used, i.e exceeding LAC, the means of an individual protection of respiratory organs, filtering respirators with appropriate filters should be used [7, 8].

1. *MU 1924–78*. Hygienic estimation of consumables and processes of welding, surfacing and cutting of metals. Moscow: Minzdrav SSSR.
2. *MU 4945–88*. Methodological guidelines on definition of harmful substances in welding aerosol (hard phase and gases). Moscow: Minzdraw SSSR.
3. Charykov, A.K. (1984) *Mathematical processing of chemical analysis results*. Leningrad: Khimiya.
4. Kobayashi, M., Maki, S., Hashimoto, V. et al. (1979) Quelques considerations sur le mecanisme de formation des fumees de soudage. *Soudage et Techniques Connexes*, **3/4**, 124–131.
5. Levchenko, O.G., Metlitsky, V.A. (1995) Current means of ventilation during welding (Review). *Avtomatich. Svarka*, **3**, 40–48.
6. Levchenko, O.G., Metlitsky, V.A. (2001) *Current means of welders protection*. Kyiv: Ekotekhnologiya.
7. Levchenko, O.G. (1999) Classification of welding aerosols and selection of methods of their neutralisation. *Avtomatich. Svarka*, **6**, 38–41.
8. Rakitskaya, T.L., Ennan, A.A., Bandurko, A.Yu. (1995) Carbon fiber materials for respirator «Snezhok GP-ozon». *Ibid.*, **7**, 62–64.

SYSTEM OF WELDING TORCH FOLLOWING ALONG THE BUTT USING A TV SENSOR

F.N. KISELEVSKY, S.I. PRITULA and **V.V. DOLINENKO**
The E.O. Paton Electric Welding Institute, NASU, Kyiv, Ukraine

Architecture of system for the butt following using a laser-TV sensor is considered. Hardware components of a pilot model of this system are described and their technical characteristics are given.

Key words: *automatic system, butt following, object-oriented designing, laser-TV sensor, luminous section, geometric and technical adaptation*

Systems of butt following are widely used both abroad and at domestic welding enterprises where the automatic welding of butts of different configurations is used [1–3]. These systems allow to be positioned automatically at a preset point before the beginning of welding, enable us to direct the torch along the weld at a preset set-up of shifting as regards to the butt axis and to complete the welding process properly by an operation of «crater filling». As the following system is complicated from the technical point of view, it is rational to use an object-oriented approach during its development which will make it possible to transform an external complexity of designing problem into an internal simplicity of architecture and a program code. The object-oriented approach gives an opportunity to the developers to use the definite formal rules of designing and to apply the standardized software-hardware solutions [4, 5].

Continuing the designing of following systems with TV sensors, a radically new system of the butt following has been developed on the basis of the object-oriented approach. As a result of the analysis the following classes of objects of the following system are distinguished:

- subsystem of TV sensor (laser-TV unit (LTU) and a module of measuring a contour of a luminous section of butt/weld),
- subsystem of a geometric adaptation (a module of evaluating the weld butt parameters, mathematical model of weld butt and module of torch position control),
- subsystem of a technological adaptation.

In accordance with a conception of open systems, a local information network Ethernet 10Base-T serves a system-forming element (Figure 1). Selection of type of the information network used and protocols of exchange (TCP/IP, NetBIOS, IPX/SPX, etc.) can be specified in technical assignment.

The following system is a digital system of the automatic control, therefore, the behaviour of its constituent objects is realized in the form of machine programs (except LTU), which operate in a real time.

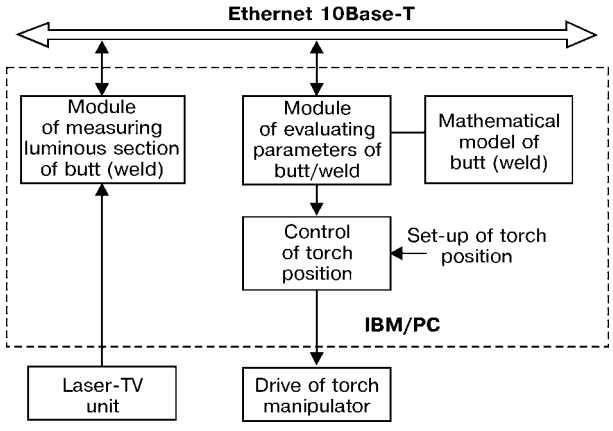

Figure 1. Schematic diagram of open system of butt following

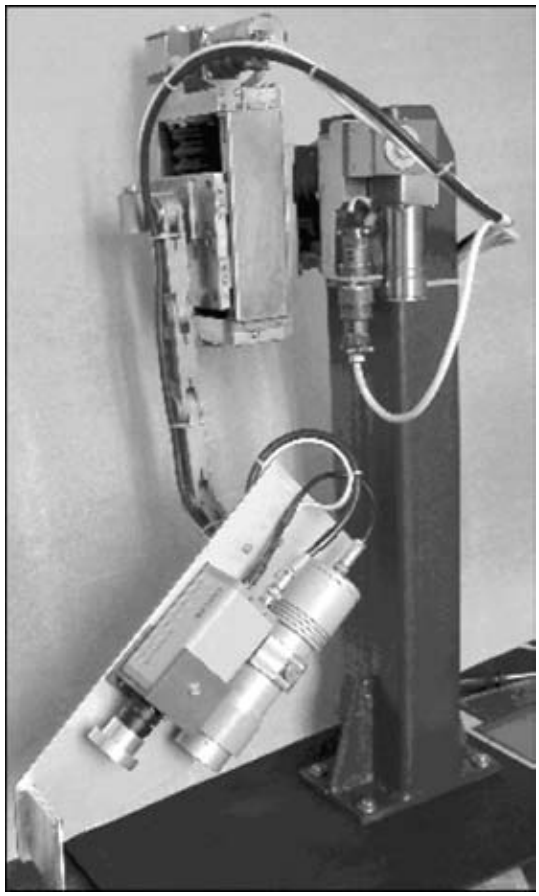

Figure 2. General view of a manipulator with a laser-TV unit (protective housing is removed) of open system of butt following

To realize the following system, both one controller of IBM/PC type and also several these units, removed at an arbitrary distance from each other can be used.

In exhibition «Welding–Ukraine 200'2» (Kyiv) a pilot model of the system of butt following with LTU, manufactured at the E.O. Paton Electric Welding Institute, was exhibited (Figure 2). The unit operates by a principle of a luminous section and corresponds by design to the variant with a reflecting mirror in an optical axis of the video-camera. The system is equipped with a two-coordinate manipulator of torch (mechanism of correction) of TD164.12.10 type and DC electrical drives of PC-14 type developed by Company «Duga» (the PWI). The system includes a control computer IBM/PC-Pentium-III-800, having a board of a videocapture with a video processor Bt-878 and a module of output of analog signals PCI-1710 (Advantech Co., Ltd.) which serves for control of the torch manipulator drives. The parameters of weld can be evaluated both from the model with a weld reinforcement and weakening. The reliable weld following is guaranteed in the presence of tacks and different damages of the surfaces welded. The main parameters of the device are given below:

error in following across the butt, mm	± 0.25
error in following in distance, mm	± 0.22
error in determination of a gap value, mm	± 0.16
error in determination of value of displacement of edges, mm	± 0.16
dynamics of compensation of butt deviation, mm/s	≤ 2
working range of measuring of gap width, mm	0.16–5.00
recommended distance to workpiece surface H_0, mm	20
working range of measuring distance H, mm	$H_0 \pm 15$
LTU mass, kg	≤ 2
dimensions of LTU, mm	410×135×80

1. Paton, V.E., Moshkin, V.F., Pritula, S.I. et al. (1990) Prospects of development of arc welding equipment. In: *Problems of Welding and Special Electrome-tallurgy*. Kyiv: Naukova Dumka.
2. Sakalo, N.N. (1990) Experience of creation of following systems for welded structures automatic production. *Ibid*.
3. Nazarenko, O.K. (1998) Secondary electron servosystem with electromechanical drive. *Avtomatich. Svarka*, **12**, 47–50.
4. Kisilevsky, F.N., Dolinenko, V.V. (2001) Object-oriented programming of systems of welding technological process control. *The Paton Welding J.*, **6**, 40–42.
5. Kisilevsky, F.N., Butakov, G.A., Dolinenko, V.V. et al. (2001) Increase in quality of seam tracking on the base of technical vision. In: *Proc. of Int. Sci.-Pract. Conf. and Exhibition on Problems of Quality Maintenance in Welding Production*. Kyiv.

MULTIFUNCTIONAL WELDING INVERTER MADE BY TWO-MODULE DESIGN

A.E. KOROTYNSKY

The E.O. Paton Electric Welding Institute, NASU, Kyiv, Ukraine

Design of a multifunctional welding inverter is described which is based on a two-module scheme. A module based on a single-step bridge converter was selected as the inverter core. Several design variants for MMA, TIG and MIG/MAG welding are described, as well as for air-plasma cutting, based on a two-module structure.

Key words: *arc welding, inverter, module, control devices*

This class of welding equipment is based on a self-contained power module (*PM*) designed on a base of a high-frequency single-cycle bridge transistor converter, whose output characteristic is formed with the help of a control unit (*CU*). Thus, its external characteristic is defined by time parameters of *CU* and output choke (Figure 1).

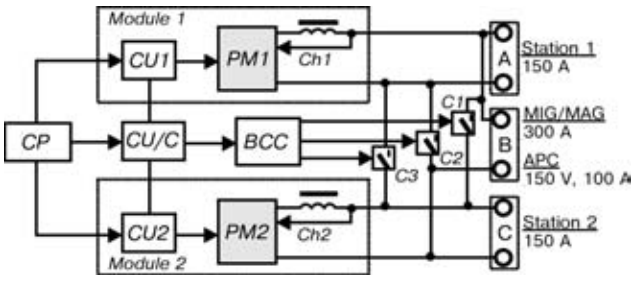

Figure 1. Schematic diagram of a two-module multifunctional welding source with a reconfigurable structure

Methods of input and output connection of modules can be distinguished depending on the technological task to be solved. If their input parameters correspond to 220 V, 50 Hz, then they can be connected in parallel to a single-phase mains (1×220 V). Surely, if the number of modules is divisible by 3, then the three-phase connection is preferable (3×220 V), their connection to mains 2×220 V is also admissible. At the absence of the three-phase mains it is always easy to transfer to a single-phase supply of input circuits that is, undoubtedly, advantage of these power sources.

Output terminals of modules are connected in parallel almost in all the methods of arc welding, while a series connection is used in air-plasma cutting (APC) and periodically in definite intervals of time in realization of AC condition of welding.

Let us consider more comprehensively the specifics of design and operation of a two-module device on

Table 1

Variant of schematic diagram	*Condition of commutators*	*Condition of outputs*	*Variant of technological application*
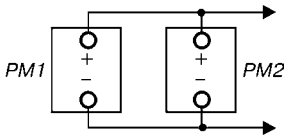	*C1:1* *C2:1* *C3:0*	A:0 B:1 C:0	*Parallel connection* Used in MMA welding and mechanized MIG/MAG welding at current conditions 10–300 A
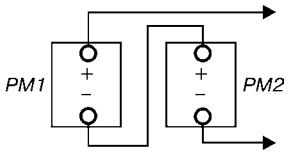	*C1:0* *C2:0* *C3:1*	A:0 B:1 C:0	*Series connection* Used in air-plasma cutting at conditions of 150 V, 100 A
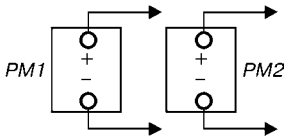	*C1:0* *C2:0* *C3:0*	A:1 B:0 C:1	*Separate connection* Used in two-station MMA welding and mechanized MIG/MAG welding at current conditions 5–150 A

Note. The given parameters correspond to the module with parameters $U_{0.x} = 75$ V, $I = 150$ A.

Table 2

Type of unit	*Functional purpose*	*Delivery set*
«Koral-301/1»	DC welding, 300 A condition	–
«Koral-301/2»	DC welding, 300 A condition, two-station condition 2×150 A	–
«Koral-301/3»	DC welding, 300 A condition, two-station condition 2×150 A, air-plasma cutting (120 V/100 A condition)	–
«Koral-301/4»	DC and AC welding, 300 A condition	Torch for TIG welding
«Koral-301/5»	DC and AC welding, 300 A condition, two-station DC condition 2×150 A	Same
«Koral-301/pa»	DC welding, 300 A condition, mechanized welding with a self-shielding wire, and also in CO_2	Feeding mechanism

whose base it is possible to design the different in configuration schematic diagrams of power sources of the required technological purpose. Table 1 gives a schematic representation of separate structures and also variants of their technological application are indicated. All the technological conditions, shown in the Table, are realized in practice using a scheme of a two-module multifunctional source (Figure 1). The device includes two identical power modules *PM1* and *PM2* with control units *CU1* and *CU2*. The latter are capable to operate both in a self-contained condition and also by the commands of a common control unit *CU/C*, forming control signals for the block of commutation of conditions (*BCC*). From its commands, which determine the condition of power commutating elements (commutators) *C1*, *C2* and *C3*, a necessary technological condition is preset from the control panel (*CP*). When all the commutators are open, the mentioned device can operate in the condition of a two-station welding with a complete isolation of welding circuits. When commutator *C3* is closed the device is transferred into the condition of air-plasma cutting at which current up to 100 A is provided.

Some difficulties occur in the condition of a parallel connection of modules, because in this case it is necessary in the wide ranges of adjustment to keep the equality of values of their output voltages with an error of not worse than ≤ 5 %. This is attained by an action of a scheme of comparison included into

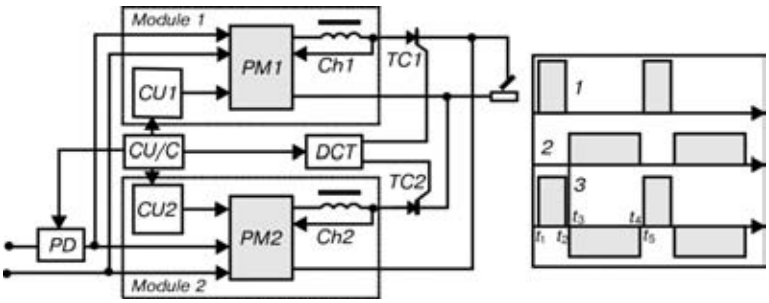

Figure 2. Variant of structure of welding power source in the condition of alternating current (*a*) and time diagrams of its operation (*b*): *1* — pulse of *PM1*; *2* — pulse of *CM2*; *3* — output current of power source

Figure 3. Multifunctional welding unit «Koral-301/2»

CU/C design. The mean-square values of voltages, available at *Ch1* and *Ch2* are used as feedback signals.

The described device can be used for AC welding at a negligible modification. Variant of structure of welding source with an indicated functional purpose is shown in Figure 2. Device for control of thyristors (*DCT*) and two power commutators *TC1* and *TC2* are included into it additionally. Each commutator operates, respectively, in formation of pulses of positive and negative half-waves of welding current.

Algorithm of operation of the device will be explained using time diagrams presented in Figure 2, *b*. At the moment t_1 from command of *CU1* a module *PM1* is energized and a thyristor commutator *TC1* is open simultaneously. The pulse of welding current of a positive polarity is beginning to be formed at the device output. At the moment t_2 *PM2* is first switched off and then *TC1* is closed. Within the time interval (t_2–t_3) there is no welding current at the power source output. This interval is selected from the condition of a necessary time for damping of transition processes connected with commutation of power elements of the welding power source. At the moment t_3 the phase of formation of a pulse of current of a negative polarity is beginning. Successively, *PM2* is energized and commutator *TC2* is open. Negative pulse of welding current is interrupted at the moment t_4. Further, the processes are repeated with a periodicity which is preset by the operator. Time intervals t_1–t_2 and t_3–t_4 are preset from the *CP* and can be set in the range of 5–500 ms. Amplitudes of pulses of current of both positive and negative polarity are set independently within the 5–150 A. Thus, the described device represents a sufficiently convenient tool for welding aluminium alloys and other non-ferrous metals.

Taking into account the modern requirements to a electromagnetic compatibility the power source is equipped with a protection device (*PD*) of mains which represents a combined filter of lower and upper frequencies. The first filter suppresses the low-frequency commutating disturbances, while the second filter suppresses disturbances created by high-frequency converters of power modules. The experimental check-out showed that as to the electromagnetic compatibility the device meets the requirements of the European standard EN 50199–95.

The appearance of the multifunctional welding unit «Koral-301/2», developed at the E.O. Paton Electric Welding Institute of the NAS of Ukraine, is given in Figure 3.

Table 2 presents different variants of welding inverters which can be realized on the base of a two-module design of the power unit, and also their delivery sets are given.

Development of the PWI

DEVICE «PATON PPR-200» FOR AIR-PLASMA CUTTING OF METALS

In view of the fact that most metal structures are made from metals of small and medium thickness, the «Paton PPR-200» device (Figure) commercially produced by the PWI Pilot Plant for Welding Equipment has found wide application for blanking operations in machine building, for cutting and spraying in food and chemical industries, repair of heat and water distribution pipes in public utilities, repair of gas-pumping stations and oil and gas pipelines, as well as for disposal of metal structures (wagons, ships, planes, bridge girders and other facilities that exhausted their service life).

«Paton PPR-200» specifications

Mains voltage (50 Hz), V	380
Rated welding current, A	200
Power consumption, kV·A	60
Duty cycle, %	60
Open-circuit voltage, V	300
Range of operating voltages, V	150–200
Plasma gas flow rate, m^3/h	2.0–2.5
Plasmatron type	VPR-11, VPR-200
Thickness of metal cut, mm:	
steel	3–50
copper	2–25
aluminium	2–50
Arc ignition	oscillation
Cooling	water
Overall dimensions, mm	1300×800×950
Weight, kg	350

The power supply is made on the base of a special three-phase power transformer with two groups of secondary windings. Each group is connected to its rectifying unit. The rectifying units are connected to each other in series. Connection of two groups of secondary windings of the power transformer provided a vector diagram with a shift of phases of currents and voltages of one group relative to the other. The volt-ampere characteristic resulting from the sum of currents and voltages at the rectifying bridges is

determined by the configuration of the plasma generation chamber.

The value of pulsations of the rectified plasmatron current is decreased, which allowed a smoothing choke to be avoided, provided the stable arc and extended the life of electrode and nozzle.

The device can be optionally fitted with the independent cooling unit «Paton BAO-421» operating with water or antifreezing agent. The unit provides efficient cooling of the welding tool. It is cost effective and mobile.

The «Paton PPR-200» semi-automatic device is advantageous owing to its high operational reliability. It is simple to maintain and beneficial in terms of weight and overall dimensions.

For more information please contact:
Tel.: (380 44) 226-27-20, 294-78-00
Fax: (380 44) 269-12-56, 252-84-10
E-mail: ozspaton@ukrnet.net

WELDING MOBILE COMPLEX KSM 005

The complex is designed for the field continuous flash-butt welding of rails of cross-section area from 6500 up to 10000 mm^2 with a flash removal directly after welding. The complex is completed with a welding head K 920-1.

The KSM 005 type is manufactured on the base of automobile chassis MAZ-6303-040 and has a combined travel for movement on the railway track that allows it to arrive at the site of construction and repair of the railway in short periods of time. In the automobile body are arranged: electric station, welding machine, pumping station, control cabinet, hoist and other auxiliary equipment.

Technical characteristics of welding mobile complex KSM 005

Electric station ADZ-360, kV·A	360
Rated voltage of electric station, V	400
Frequency, Hz	50
Time of welding one weld, min	not more than 3
Angle of hoist rotation with a welding head in horizontal position, deg	90
Hoist boom extension from the track axis, mm	3915
Maximum extension of section with a welding head, mm	860
Movement speed along the railway track, km/h	25
Dimensions, mm	not more than 10000×2500×3850
Mass of furnished complex, kg	25800
Rated long-time secondary current, kA	21.5
Highest secondary current, kA	67
Highest short-circuit power, kV·A	500
Rated upsetting force at 21 MPa pressure in hydrosystem, kN	1000
Capacity at 40 % duty cycle, kV·A	236
Maximum upsetting rate, mm/s	20

КЗЭСО

Kakhovka Plant of Electric Welding Equipment
109, Pushkin str.,
Kherson region, Kakhovka city,
74800, Ukraine.
Tel.: (38 05536) 33285, 35967; Fax: (38 05536) 42590
E-mail: info@kzeso.com